Analytica Chimica Acta 1037 (2018) 63–74

Contents lists available at ScienceDirect

Analytica Chimica Acta

journal homepage: www.elsevier.com/locate/aca

Development of an LC-ESI(-)-MS/MS method for the simultaneous quantification of 35 isoprostanes and isofurans derived from the major n3- and n6-PUFAs

Katharina M. Rund [a], Annika I. Ostermann [a, d], Laura Kutzner [a], Jean-Marie Galano [b], Camille Oger [b], Claire Vigor [b], Sabine Wecklein [c], Nina Seiwert [c], Thierry Durand [b], Nils Helge Schebb [a, d, *]

[a] Institute for Food Toxicology, University of Veterinary Medicine Hannover, Bischofsholer Damm 15, 30173 Hannover, Germany
[b] Institut des Biomolécules Max Mousseron (IBMM), UMR 5247 CNRS, Université de Montpellier, ENSCM, France
[c] Department of Toxicology, University Medical Center Mainz, Obere Zahlbacher Str. 67, 55131 Mainz, Germany
[d] Chair of Food Chemistry, Faculty of Mathematics and Natural Sciences, University of Wuppertal, Gaußstraße 20, 42119 Wuppertal, Germany

GRAPHICAL ABSTRACT

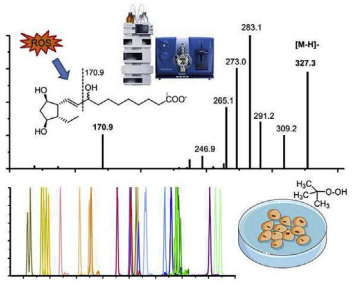

ARTICLE INFO

Article history:
Received 14 July 2017
Received in revised form
18 October 2017
Accepted 1 November 2017
Available online 14 November 2017

ABSTRACT

Misregulation of oxidative and antioxidative processes in the organism – oxidative stress – contributes to the pathogenesis of different diseases, e.g. inflammatory or neurodegenerative diseases. Oxidative stress leads to autoxidation of polyunsaturated fatty acids giving rise to prostaglandin-like isoprostanes (IsoP) and isofurans (IsoF). On the one hand they could serve as biomarker of oxidative stress and on the other hand may act as lipid mediators, similarly as the enzymatically formed oxylipins. In the present paper we describe the development of an LC-ESI(-)-MS/MS method allowing the parallel quantification of 27 IsoP and 8 IsoF derived from 6 different PUFA (ALA, ARA, EPA, AdA, n6-DPA, DHA) within 12 min. The chromatographic separation was carried out on an RP-C18 column (2.1 × 150 mm, 1.8 μm) yielding narrow peaks with an average width at half maximum of 3.3–4.2 s. Detection was carried out on a triple quadrupole mass spectrometer operating in selected reaction monitoring mode allowing the selective detection of regioisomers. The limit of detection ranged between 0.1 and 1 nM allowing in combination with solid phase extraction the detection of IsoP and IsoF at subnanomolar concentrations in biological samples. The method was validated for human plasma showing high accuracy and precision. Application of the approach on the investigation of oxidative stress in cultured cells indicated a distinct pattern of IsoP and IsoF in response to reactive oxygen species which warrants further investigation.

* Corresponding author. Chair of Food Chemistry, Faculty of Mathematics and Natural Sciences, University of Wuppertal, Gaußstraße 20, 42119 Wuppertal, Germany.
E-mail address: nils@schebb-web.de (N.H. Schebb).

https://doi.org/10.1016/j.aca.2017.11.002

The described method is not only the most comprehensive approach for the simultaneous quantification of IsoP and IsoF, but it was also integrated in a targeted metabolomics method (Ostermann et al. (2015) Anal Bioanal Chem) allowing the quantification of in total 164 oxylipins formed enzymatically and non-enzymatically within 30.5 min.

1. Introduction

Oxidative stress results from misregulation of oxidative and antioxidative mechanisms in the organism and is characterized by increased formation of reactive oxygen and nitrogen species [1–3]. These highly reactive molecules attack biomolecules, thereby e.g. modifying proteins as well as DNA and causing mutations [4]. Oxidative degradation of membrane lipids alters the function of membranes and gives rise to a multitude of reactive and stable products [5,6]. Oxidative stress, and thus autoxidation, is associated with the pathophysiology of several diseases including inflammatory, cardiovascular, respiratory and neurodegenerative diseases.

In order to evaluate oxidative stress in health and disease, several biomolecules affected by autoxidation (i.e. proteins, DNA, lipids), their degradation products (e.g. malondialdehyde (MDA)) or endogenous antioxidants (e.g. glutathione (GSH)/glutathione disulfide) are used as common biomarkers [7].

In a multi-laboratory comparison of different oxidative stress markers the measurement of 15-F_{2t}-IsoP, an isoprostane derived from arachidonic acid (C20:4 n6, ARA) was found to be promising for the evaluation of the oxidative stress status *in vivo* [8]. Isoprostanes (IsoP) are prostaglandin-like autoxidation products formed from free PUFA and under physiological conditions dominantly from PUFA esterified in phospholipids [9]. During non-enzymatic, free radical mediated autoxidation, PUFA are initially converted via radical abstraction of a bisallylic hydrogen and subsequent addition of molecular oxygen to hydroperoxy fatty acid radicals (Fig. 1). Depending on the position of the initial radical abstraction, different regioisomeric hydroperoxy radicals are formed. The primary formed hydroperoxy intermediates further undergo secondary reactions leading to a diverse product spectrum. For instance, a sequence of two 5-*exo*-cyclization steps of the hydroperoxy radicals followed by addition of molecular oxygen and reduction of the side chain hydroperoxide leads to prostaglandin-H-like bicyclic endoperoxide intermediates. These are under physiological conditions unstable and react in the presence of reducing agents like GSH to stable F-ring isoprostanes or, when reducing cellular agents are depleted, undergo isomerization to D- or E-ring isomers (Fig. 1) [10]. From ARA, 4 regioisomeric F_2-IsoPs can be formed each comprising 8 racemic diastereomers leading to a total of 64 possible isomers. However, the regioisomers are formed at different rates with the terminal 5- and 15-F_2-IsoP being more abundant compared to the 8- and 12-F_2-IsoP isomers [11,12]. Also, other PUFA can be converted by an analogous mechanism leading to F_1-PhytoP from α-linolenic acid (C18:3 n3, ALA) and F_3-IsoP from eicosapentaenoic acid (C20:5 n3, EPA). Adrenic acid (C22:4 n6, AdA) gives rise to F_2-dihomo-IsoP, docosahexaenoic acid (C22:6 n3, DHA) and docosapentaenoic acid (C22:5 n6, n6-DPA) to F_4-NeuroP and F_3-$NeuroP_{n6}$, respectively.

The product spectrum during autoxidation is directed by the oxygen content: with increasing oxygen concentration (i.e. partial pressure) the levels of IsoP increase, however, above 21% no further increase of IsoP occurs while the formation of another class of cyclic PUFA derivatives, the tetrahydrofuran substituted isofurans (IsoF), is significantly elevated *in vitro* [13]. Based on two proposed formation mechanisms – the cyclic peroxide cleavage pathway and the epoxide hydrolysis pathway – 8 regioisomeric isofurans comprising 32 stereoisomers are formed from ARA resulting in a total of 256 possible isomers [13]. Conversion of other PUFA by an analogous mechanism leads to PhytoF [14,15], dihomo-IsoF and NeuroF from ALA, AdA and DHA, respectively.

Moreover, depending on the tissue fatty acid composition a characteristic pattern of the formed isoprostanes results. For example, DHA and AdA are both found in the brain, however AdA is predominantly enriched in myelin which is part of the white matter, whereas DHA is enriched in neurons present in the grey matter [16]. Consequently, F_2-dihomo-IsoP are associated with oxidative stress of the white matter, whereas F_4-NeuroP are related to oxidative damage of the grey matter *in vitro* [17].

The analysis of isoprostanes in biological matrices is challenging because of their low concentration and the multitude of possible isomers formed from different PUFA. Several methods using gas chromatography (GC) and liquid chromatography (LC) coupled to mass-spectrometry (MS) as well as immunoassays are described for the analysis [18–38]. Immunoassays like ELISA which only allow the analysis of single isomers are easy to handle and enable high sample throughput. However, due to the multitude of structurally similar isoprostanes, ELISAs are susceptible to cross-reactivity leading to an overestimation compared to LC- and GC-MS methods [38,39]. In contrast, chromatographic methods coupled to MS allow the selective and sensitive parallel quantification of multiple isomers derived from a single as well as different PUFA. In addition to sample preparation steps, including extraction and purification, GC-MS requires derivatization of the analytes to volatile derivatives. Since this is more laborious, LC-MS has been predominantly used in the past years [26–34,40,41]. Most LC-MS methods cover only ARA derived F_2-IsoP, especially the prominent 15-F_{2t}-IsoP isomer [26–29,32,41] or are focused on IsoP derived from a single PUFA [31,34,40]. Only few methods have been described enabling the parallel quantification of IsoP derived from different PUFA [30,33,42].

However, keeping the tissue specific PUFA pattern in mind, the simultaneous analysis of a comprehensive set of IsoP and IsoF from all biolocially relevant PUFA is crucial for the evaluation of oxidative stress *in vivo* independent of the origin of the analyzed biological specimen. Therefore, we developed in the present study a new, sensitive LC-ESI(-)-MS/MS method covering a comprehensive set of IsoP and IsoF from 6 biologically relevant PUFA that was integrated in an established method covering enzymatically formed oxylipins. The mass-spectrometric and chromatographic parameters were optimized and the method performance was thoroughly characterized. Finally, the method was applied on the investigation of the formation of IsoP and IsoF in response to *tert*-butyl hydroperoxide (*t*-BOOH) induced oxidative stress in HCT116 cells.

2. Materials and methods

2.1. Chemicals

The isoprostane standard 15-F_{2t}-IsoP as well as the deuterated

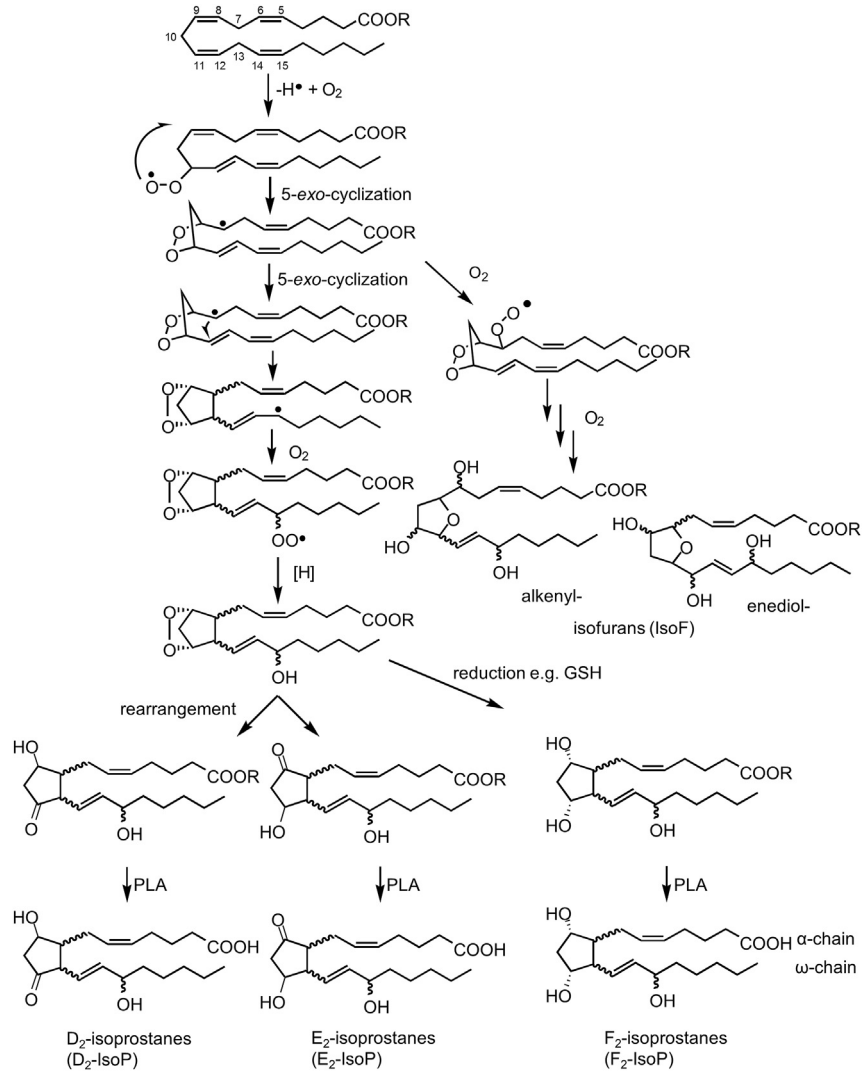

Fig. 1. Simplified mechanism of isoprostane (IsoP) and isofuran (IsoF) formation from arachidonic acid bound in phospholipids (R) depending on O_2 concentration. The bicyclic endoperoxide intermediate is under physiological conditions unstable and in the presence of reducing agents like GSH reduced to stable F-ring isoprostanes. When reducing cellular agents are depleted it undergoes isomerization to D- or E-ring isomers. Finally the free oxylipins can be released by phospholipase (PLA).

internal standards (IS) $^2H_4$-15-F_{2t}-IsoP ($^2H_4$-8-*iso*-$PGF_{2\alpha}$) and $^2H_{11}$-5(*R,S*)-5-F_{2t}-IsoP ($^2H_{11}$-5-iP$F_{2\alpha}$-VI) were purchased from Cayman Chemicals (local distributor: Biomol, Hamburg, Germany). All other IsoP and IsoF standards, i.e. ARA derived 5-F_{2t}-IsoP, 5-*epi*-5-F_{2t}-IsoP, 2,3-dinor-15-F_{2t}-IsoP, 15-*epi*-2,3-dinor-15-F_{2t}-IsoP, EPA derived 5-F_{3t}-IsoP, 5-*epi*-5-F_{3t}-IsoP, 8-F_{3t}-IsoP, 8-*epi*-8-F_{3t}-IsoP, DHA derived 4(*R,S*)-4-F_{4t}-NeuroP, 10-F_{4t}-NeuroP, 10-*epi*-10-F_{4t}-NeuroP, 14(*R,S*)-14-F_{4t}-NeuroP, 4(*R,S*)-ST-Δ^5-8-NeuroF, AdA derived 17(*R,S*)-17-F_{2t}-dihomo-IsoP, *ent*-7(*R,S*)-7-F_{2t}-dihomo-IsoP, 17(*R,S*)-10-*epi*-SC-Δ^{15}-11-dihomo-IsoF, 7(*R,S*)-ST-Δ^8-11-dihomo-IsoF, n6-DPA derived 4-F_{3t}-$NeuroP_{n6}$, 4-*epi*-4-F_{3t}-$NeuroP_{n6}$, and ALA derived *ent*-9-F_{1t}-PhytoP, *ent*-9-*epi*-9-F_{1t}-PhytoP, *ent*-16-F_{1t}-PhytoP, *ent*-16-*epi*-16-F_{1t}-PhytoP, 16-B_1-PhytoP, 9-L_1-PhytoP, *ent*-16(*R,S*)-13-*epi*-ST-Δ^{14}-9-PhytoF as well as the unlabeled odd-chain IS C19-17-*epi*-17-F_{1t}-PhytoP and C21-15-F_{2t}-IsoP were synthesized, using our last strategy, as described [14,43,51]. 4(*R,S*)-4-F_{4t}-NeuroP, 14(*R,S*)-14-F_{4t}-NeuroP, 4(*R,S*)-ST-Δ^5-8-NeuroF, 17(*R,S*)-17-F_{2t}-dihomo-IsoP, *ent*-7(*R,S*)-7-F_{2t}-dihomo-IsoP, 17(*R,S*)-10-*epi*-SC-Δ^{15}-11-dihomo-IsoF, 7(*R,S*)-ST-Δ^8-11-dihomo-IsoF, *ent*-16(*R,S*)-13-*epi*-ST-Δ^{14}-9-PhytoF were only available as epimeric mixtures. LC-MS-grade methanol (MeOH), acetonitrile (ACN) and acetic acid were purchased from Fisher Scientific (Schwerte, Germany). *n*-Hexane (HPLC Grade) was obtained from Carl Roth (Karlsruhe, Germany). All other chemicals were purchased from Sigma Aldrich (Schnelldorf, Germany). Pooled human EDTA plasma was generated by centrifugation (10 min, 4 °C, 20,000×*g*) of EDTA blood, followed by mixing plasma from six healthy male and female volunteers aged between 25 and 38 years and immediately stored at −80 °C until analysis. All volunteers gave their written informed consent and all procedures were conducted according to the guidelines laid down in the Declaration of Helsinki and approved by the ethic committee at the medical chamber of Lower Saxony (Hannover, Germany).

2.2. Calibration and quantification of IsoP

For calibration, stock solutions of the individual analytes (in MeOH) were mixed and diluted in glass volumetric flasks (5–100 mL) with MeOH at 10 concentration levels (0.1, 0.25, 0.5, 1, 2, 5, 10, 20, 100 and 500 nM), each with 20 nM of the four internal standards. Calibration curves were calculated using linear least square regression (weighting: $1/x^2$). Analyte quantification was carried out based on the analyte to corresponding IS (Table 1) area

Table 1
Parameters of the LC-ESI(-)-MS/MS method for the quantification of isoprostanes and isofurans. Shown are the mass transitions for quantification in scheduled SRM mode, electronical MS parameters (declustering potential (DP), entrance potential (EP), collision energy (CE), collision cell exit potential (CXP)), the assigned internal standards (IS), retention time (t_R), peak width at half maximum (FWHM), limit of detection (LOD), the calibration range (lower limit of quantification (LLOQ), upper limit of quantification (ULOQ)), correlation coefficient (r) and the normalized slope of the calibration curve.

Analyte	Mass transition		MS parameters[a]				IS	t_R[b]	FWHM[c]	LOD[d]		Calibration range		r[g]	slope[h]
	Q1	Q3	DP	EP	CE	CXP		[min]	[sec]	[nM]	[pg on column]	LLOQ[e] [nM]	ULOQ[f] [nM]		
ent-16(*R,S*)-13-*epi*-ST-Δ^{14}-9-PhytoF 1 *)	343.1	200.9	−80	−10	−33	−8	C19-17-*epi*-17-F_{1t}-PhytoP	4.19	3.4	0.12	0.20	0.24	235	0.9993	0.91
ent-16(*R,S*)-13-*epi*-ST-Δ^{14}-9-PhytoF 2 *)	343.1	200.9	−80	−10	−33	−8	C19-17-*epi*-17-F_{1t}-PhytoP	4.30	3.4	0.13	0.23	0.26	265	0.9995	1.02
ent-16-*epi*-F_{1t}-PhytoP	327.3	225.0	−70	−10	−34	−8	C19-17-*epi*-17-F_{1t}-PhytoP	4.72	3.3	0.25	0.41	0.50	500	0.9983	0.78
ent-16-F_{1t}-PhytoP	327.3	225.0	−70	−10	−34	−8	C19-17-*epi*-17-F_{1t}-PhytoP	4.89	3.4	0.25	0.41	0.50	500	0.9997	0.73
ent-9-F_{1t}-PhytoP	327.3	170.9	−40	−10	−31	−8	C19-17-*epi*-17-F_{1t}-PhytoP	4.81	3.3	0.10	0.16	0.25	500	0.9991	1.44
ent-9-*epi*-F_{1t}-PhytoP	327.3	170.9	−40	−10	−31	−8	C19-17-*epi*-17-F_{1t}-PhytoP	4.98	3.3	0.25	0.41	0.50	500	0.9990	1.12
15(*R,S*)-2,3-dinor-15-F_{2t}-IsoP	325.2	237.0	−40	−10	−18	−8	C19-17-*epi*-17-F_{1t}-PhytoP	5.41	3.3	0.25	0.41	0.50	500	0.9995	1.79
8-F_{3t}-IsoP	351.1	155.0	−60	−10	−27	−8	C19-17-*epi*-17-F_{1t}-PhytoP	6.15	3.6	0.50	0.88	1.0	500	0.9980	0.70
8-*epi*-8-F_{3t}-IsoP	351.1	155.0	−60	−10	−27	−8	C19-17-*epi*-17-F_{1t}-PhytoP	6.51	3.3	0.50	0.88	1.0	500	0.9992	0.60
5(*R,S*)-5-F_{3t}-IsoP	351.2	114.9	−50	−10	−27	−8	C19-17-*epi*-17-F_{1t}-PhytoP	6.53	3.4	1.0	1.8	2.0	500	0.9962	0.07
15-F_{2t}-IsoP (8-*iso*-$PGF_{2\alpha}$)	353.1	193.1	−70	−6	−33	−8	$^2H_4$-15-F_{2t}-IsoP	7.56	3.7	0.25	0.44	0.50	500	0.9989	0.98
10-F_{4t}-NeuroP	377.2	153.0	−40	−10	−25	−8	$^2H_4$-15-F_{2t}-IsoP	8.04	3.3	0.25	0.47	0.50	500	0.9989	1.81
10-*epi*-10-F_{4t}-NeuroP	377.2	153.0	−40	−10	−25	−8	$^2H_4$-15-F_{2t}-IsoP	8.37	3.5	0.50	0.95	1.0	500	0.9990	0.88
5(*R,S*)-5-F_{2t}-IsoP	353.2	114.8	−60	−10	−26	−8	$^2H_{11}$-5(*R,S*)-5-F_{2t}-IsoP	8.07	3.5	0.25	0.44	0.50	500	0.9959	0.52
16-B_1-PhytoP	307.3	235.0	−60	−10	−27	−8	$^2H_{11}$-5(*R,S*)-5-F_{2t}-IsoP	8.26	3.7	0.10	0.15	0.25	500	0.9994	3.00
9-L_1-PhytoP	307.3	185.1	−60	−10	−27	−8	$^2H_{11}$-5(*R,S*)-5-F_{2t}-IsoP	8.33	3.7	0.10	0.15	0.25	500	0.9986	3.07
14(*R,S*)-14-F_{4t}-NeuroP	377.2	205.1	−50	−10	−27	−8	C21-15-F_{2t}-IsoP	8.62	6.5	10	19	20	500	0.9998	0.09
4(*R,S*)-4-F_{4t}-NeuroP	377.1	101.3	−60	−10	−26	−8	C21-15-F_{2t}-IsoP	9.35	3.6	0.50	0.95	1.0	500	0.9982	0.23
4(*R,S*)-ST-Δ^5-8-NeuroF	393.3	187.2	−40	−10	−29	−8	C21-15-F_{2t}-IsoP	9.59	4.2	20	39	40	500	0.9941	0.02
17(*R,S*)-17-F_{2t}-dihomo-IsoP 1 *)	381.3	263.2	−90	−10	−31	−8	C21-15-F_{2t}-IsoP	9.78	3.6	0.63	1.2	1.3	314	0.9967	0.31
17(*R,S*)-17-F_{2t}-dihomo-IsoP 2 *)	381.3	263.2	−90	−10	−31	−8	C21-15-F_{2t}-IsoP	9.95	3.2	0.37	0.71	0.75	186	0.9980	0.19
7(*R,S*)-ST-Δ^8-11-dihomo-IsoF	397.3	245.1	−50	−10	−31	−8	C21-15-F_{2t}-IsoP	9.81	8.9 #)	1.0	2.0	2.0	500	0.9993	0.42
ent-7(*R,S*)-7-F_{2t}-dihomo-IsoP	381.3	143.0	−50	−10	−31	−8	C21-15-F_{2t}-IsoP	9.86	5.7	0.25	0.48	0.50	500	0.9972	1.87
4(*R,S*)-4-F_{3t}-$NeuroP_{n6}$	379.2	101.0	−50	−10	−29	−8	C21-15-F_{2t}-IsoP	11.03	4.1	0.50	0.95	1.0	500	0.9971	0.59
17(*R,S*)-10-*epi*-SC-Δ^{15}-11-dihomo-IsoF 1 *)	397.1	221.0	−90	−10	−31	−8	C21-15-F_{2t}-IsoP	11.26	3.7	0.52	1.0	1.0	260	0.9992	0.41
17(*R,S*)-10-*epi*-SC-Δ^{15}-11-dihomo-IsoF 2 *)	397.1	221.0	−90	−10	−31	−8	C21-15-F_{2t}-IsoP	11.44	3.7	0.48	0.96	0.96	240	0.9982	0.38
C19-17-*epi*-17-F_{1t}-PhytoP	341.3	239.0	−70	−10	−35	−8	IS	6.02	3.3						
$^2H_4$-15-F_{2t}-IsoP	357.2	196.8	−50	−6	−33	−8	IS	7.54	3.6						
$^2H_{11}$-5(*R,S*)-5-F_{2t}-IsoP	364.3	115.2	−40	−10	−29	−10	IS	7.97	4.5						
C21-15-F_{2t}-IsoP	367.2	193.1	−60	−10	−35	−8	IS	9.18	3.8						

*) Isomers were provided as mixture of two diastereomers which were separated chromatographically; 1 and 2 indicate the two isomers (see Fig. 3). The individual concentration of each isomer was calculated based on the ratio in SIM.

[a] The collision cell exit potential (CXP) was for all analytes −8 V.

[b] Relative standard deviation of t_R within one batch was ≤0.18% (<0.01 min).

[c] Full peak width at half maximum (FWHM) was determined as mean width of standards with the concentrations LLOQ -100 nM, for 14(*R,S*)-F_{4t}-NeuroP and 4(*R,S*)-ST-Δ^5-8-NeuroF concentrations LLOQ - 500 nM were used; [#) for 7(*R,S*)-ST-Δ^8-11-dihomo-IsoF (incompletely separated) the FWHM was determined at the half maximal height of the smaller peak (see Fig. 3B(V))].

[d] LOD was set to the lowest concentration yielding a signal to noise ratio ≥ 3.

[e] LLOQ was set to the lowest calibration standard injected yielding a signal to noise ratio ≥ 5 and an accuracy in the calibration curve within ± 20%.

[f] ULOQ concentration does not represent the end of the dynamic range, but is the highest calibration standard injected.

[g] Calibration was performed as linear weighted least square regression using $1/x^2$ weighting.

[h] Slope of the calibration curve normalized for all analytes to 15-F_{2t}-IsoP × 10.

ratio using the obtained calibration curves.

2.3. In vitro assay

HCT116 human colorectal carcinoma cells were grown in 10 cm dishes (5×10^6 cells/dish) and incubated after 24 h with 50 μM and 200 μM of *t*-BOOH (Sigma Aldrich, Schnelldorf, Germany) for 30 min, 1 h and 2 h. The cells were then detached using trypsin and harvested by centrifugation (5 min, 4 °C, 300×*g*). After a washing step in cold PBS, the cells were centrifuged again (5 min, 4 °C, 300×*g*) and the supernatant was discarded. The remaining cell pellet was snap-frozen in liquid nitrogen and stored at −80 °C until analysis. The cytotoxicity of the used *t*-BOOH concentrations was assessed using the MTS assay, which is based on the reduction of the tetrazolium salt MTS (3-(4,5-dimethylthiazol-2-yl)-5-(3-carboxymethoxyphenyl)-2-(4-sulfophenyl)-2H-tetrazolium) by viable cells. To this end, HCT116 cells were seeded at a density of 2×10^4 per well and grown overnight. Cells were then incubated with 50 μM and 200 μM *t*-BOOH for 2 h and the viability was assessed as described [44].

2.4. Sample extraction

Human plasma was extracted using anion exchange Bond Elut Certify II SPE cartridges (200 mg, 3 mL, Agilent, Waldbronn, Germany) [45]. In brief, 10 μL of IS solution (containing 100 nM of $^2H_4$-15-F_{2t}-IsoP, $^2H_{11}$-5(*R,S*)-5-F_{2t}-IsoP, C19-17-*epi*-17-F_{1t}-PhytoP, C21-15-F_{2t}-IsoP and 13 isotope labeled internal standards used in the targeted metabolomics method [45], Table S2) and 10 μL of antioxidant solution (0.2 mg/mL BHT and EDTA, 100 μM indomethacin, 100 μM of the soluble epoxide hydrolase inhibitor *trans*-4-[4-(3-adamantan-1-yl-ureido)-cyclohexyloxy]-benzoic acid (*t*-AUCB) [46] in MeOH/water (50/50, *v/v*)) were added to 500 μL freshly thawed human plasma.

The proteins were precipitated by addition of 1400 μL ice cold MeOH and storage at −80 °C for at least 30 min. After centrifugation (10 min, 4 °C, 20,000×*g*) the supernatant was evaporated under a N_2-stream to a volume less than 1 mL and diluted with 2 mL of

0.1 M disodium hydrogen phosphate buffer adjusted to pH 5.5 with acetic acid, thus yielding a MeOH content of <17% (pH = 6).

The SPE cartridge was preconditioned with one column volume of each, ethyl acetate/*n*-hexane (75/25, *v/v*) containing 1% acetic acid, MeOH and 0.1 M disodium hydrogen phosphate adjusted to pH 6.0 with acetic acid in water/MeOH (95/5, *v/v*). After loading onto the preconditioned cartridge, the sample was washed with 3 mL water and 3 mL water/MeOH (50/50, *v/v*) and dried with excess pressure of N_2 for 1 min. The analytes were eluted with 2 mL of 75/25 *(v/v)* ethyl acetate/*n*-hexane with 1% acetic acid in tubes containing 6 μL of 30% glycerol in MeOH as trap solution for the analytes and evaporated until only the glycerol plug remained using a vacuum concentrator (1 mbar, 30 °C, 45–60 min; Christ, Osterode am Harz, Germany). The residue was resuspended in 50 μL MeOH containing 40 nM of 1-(1-(ethylsulfonyl)piperidin-4-yl)-3-(4-(trifluoromethoxy)phenyl)urea as IS2 for the calculation of the extraction efficiency of the IS, centrifuged (10 min, 4 °C, 20,000×*g*) and analyzed by LC-MS.

For the analysis of isoprostanes formed in cell incubations, 10 μL of antioxidant solution, 50 μL water and 300 μL MeOH were added to the cell pellets which contained about 1×10^7 cells. After homogenization in a ball mill (MM 400, Retsch, Haan, Germany) using two 3 mm stainless steel beads (10 min, 25 Hz), 600 μL MTBE was added and the homogenate was vigorously mixed. For separation of the aqueous and the organic layers 300 μL 0.15 M ammonium acetate solution was added. Following mixing and centrifugation (5 min, 4 °C, 3500×*g*), the upper organic layer was transferred to another tube and the aqueous phase was washed with 300 μL MTBE. The combined organic layers were evaporated using a vacuum concentrator (1 mbar, 30 °C, 90–120 min). To the residue 10 μL IS solution (100 nM, see above), 500 μL water/MeOH (50/50, *v/v*) and 300 μL 10 M NaOH were added and lipids were hydrolyzed for 30 min at 60 °C. After hydrolysis, the sample was immediately cooled, neutralized using acetic acid (50%) and mixed with 1900 μL 0.1 M disodium hydrogen phosphate buffer (pH = 6). SPE was conducted as described above.

2.5. Method characterization

The method was characterized and validated regarding linearity, sensitivity (limit of detection (LOD) and lower limit of quantification (LLOQ)), extraction efficiency, intra- and interday accuracy and precision based on criteria of the guideline on bioanalytical method validation of the European Medicines Agency [47]. Linearity was assessed using standard solutions covering a concentration range from 0.1 to 500 nM. The LOD was determined as the concentration yielding a signal to noise ratio (S/N) ≥ 3. The concentration with a S/N ≥ 5 and an accuracy and precision within the calibration curve of ± 20% was defined as LLOQ and set as the lowest concentration of the calibration curve.

The extraction efficiency at three different level of plasma volumes (200, 500 and 1000 μL human plasma) was determined as the recovery of the IS spiked to the sample prior extraction calculated using a calibration curve normalized to IS2 which is added in the last step of the analysis.

Intraday accuracy and precision (relative standard deviation, RSD) were evaluated in plasma samples spiked at four concentration levels (3 nM, 10 nM, 30 nM, 100 nM in vial) with IsoP and IsoF prior extraction. Four replicates of each level as well as unspiked plasma were analyzed. For interday accuracy and precision the samples were analyzed on 3 days. The accuracy was calculated by comparing the determined concentration with the added concentration. For IsoP isomers detected in unspiked plasma samples this concentration was substracted from the determined concentration following spiking.

2.6. LC-(ESI-)-MS/MS analysis

Samples (5 μL) were injected into the LC-MS system using a HTS xt-PAL autosampler (CTC Analytics, Switzerland, local distributor: Axel Semrau, Sprockhövel, Germany) equipped with a 100 μL syringe and a 20 μL sample loop. The sample rack was kept at 4 °C.

Liquid chromatography was performed using a 1290 Infinity LC System (Agilent, Waldbronn, Germany) composed of a binary pump and a column oven. Separation of the analytes was carried out on a Zorbax Eclipse Plus C18 reversed phase column (2.1 × 150 mm, particle size 1.8 μm; Agilent, Waldbronn, Germany) at 40 °C equipped upstream with an inline filter (3 μm, 1290 infinity II inline filter, Agilent, Waldbronn, Germany) and a SecurityGuard Ultra C18 cartridge as precolumn (2.1 × 2 mm, Phenomenex, Aschaffenburg, Germany). The mobile phase consisted of 0.1% acetic acid as solvent A and 800/150/1 (*v/v/v*) ACN/MeOH/acetic acid as solvent B. The chromatographic separation was achieved using the following binary gradient with a flow rate of 0.3 mL/min: 0–1.0 min isocratic 25% B, 1.0–1.5 min linear from 25% B to 30% B, 1.5–10.0 min linear from 35% B to 53% B, 10.0–19.5 min linear from 53% B to 68% B, 19.5–24.5 min linear from 68% B to 95% B, 24.5–27.0 min isocratic 95% B, 27.0–27.10 min linear from 95% B to 25% B followed by reconditioning for 3.40 min. During the first 2 min and the last 6 min of each run the LC flow was directed to waste using the 2-position-6-port valve integrated in the MS. Detection was carried out on a 6500 QTRAP mass-spectrometer (Sciex, Darmstadt, Germany) following negative electrospray ionization (ESI(-)) with the following source settings: ion-spray voltage −4500 V, curtain gas (N_2): 35 psi, nebulizer gas (gas 1, zero air): 60 psi generated with a zero air generator (UHP-300-ZA-S-E, Parker, Kaarst, Germany) and drying gas (gas 2, zero air): 60 psi at a temperature of 475 °C. The offset of the sprayer was 0.250 cm for the vertical axis and 0.550 cm for the horizontal axis, the electrode protrusion was approx. 1 mm.

The analytes were detected in scheduled selected reaction monitoring mode (SRM) using nitrogen as collision gas (set to "high", 12 psi) with a detection window of ±22.5 s around the expected retention time and a cycle time of 0.4 s. The compound specific parameters were optimized for each analyte and are summarized in Table 1. The LC-MS analysis of isoprostanes and related analytes from other PUFA was combined with an established multimethod for oxylipins [45,48,49]. A list of all covered analytes and their mass spectrometric parameters can be found in the supplementary information (SI, Table S1). For data acquisition and instrument control Analyst Software (version 1.6.2, Sciex) and for integration and quantification Multiquant (version 2.1.1, Sciex) was used.

3. Results and discussion

For selective and sensitive LC-MS analysis of the isoprostanes and related analytes the mass-spectrometric parameters were optimized for each compound individually and the chromatographic conditions were adjusted in order to yield good and rapid separation of the isobaric isomers.

3.1. Mass spectrometric detection

Isoprostanes are autoxidative derivatives of fatty acids containing a carboxylic moiety, thus ionization was carried out in ESI(-) mode leading to the formation of $[M-H]^-$ ions, whose dominating formation was confirmed in MS full scan experiments. For each compound the declustering potential (DP) was optimized in single ion monitoring mode of the $[M-H]^-$ ion to achieve an effective transmission of the ionized analytes from the source to the

entrance of the vacuum chamber with minimal in-source fragmentation. For selective detection of regioisomers specific fragment ions for selected reaction monitoring (SRM) were chosen from the product ion spectra (SI, Fig. S1) and the collision energy (CE) was optimized. The optimized MS parameters are shown in Table 1. The structure of F-IsoP is characterized by a prostanoid-like F-ring with two hydroxyl groups and one further hydroxyl group in one of the two side chains, either the α-chain (carboxy terminus) or the ω-chain (methyl terminus) (Fig. 1). Accordingly, for different regioisomers identical abundant fragments resulting from unspecific loss of H_2O or CO_2 as well as combinations of CO_2 and up to 3 fold H_2O loss were observed (Fig. 2A and B). Thus, for selective MS detection of different regioisomers the choice of specific fragment ions is crucial. Specific fragments result from backbone fragmentation and can be attributed to α-cleavage adjacent to the hydroxyl group in the side chain which is referred to as "α-hydroxy-β-ene-rearrangement", a common fragmentation for unsaturated hydroxy-fatty acids [50]. For the investigated F-IsoP the observed α-fragments comprise the carboxy-terminus with or without subsequent loss of CO_2 and/or H_2O. Depending on the side chain where the hydroxyl group is located, the predominantly observed α-fragments can be assigned to distinct cleavage sites relative to the hydroxyl group: F-IsoP with the hydroxyl group in the α-chain, e.g. *ent*-9-F_{1t}-PhytoP (Fig. 2A), showed an α-fragmentation which could be attributed to the cleavage on the methyl side of the hydroxyl group leading to a specific fragment containing the carboxyl- and the hydroxyl-moiety (*m/z* 170.9 for *ent*-9-F_{1t}-PhytoP). By contrast, the dominantly observed fragments of F-IsoP with the hydroxyl group in the ω-chain, e.g. *ent*-16-F_{1t}-PhytoP (Fig. 2B) could be assigned to the cleavage on the carboxyl side relative to the hydroxyl group and thus to a fragmentation segment carrying the carboxyl-moiety (*m/z* 269.1 for *ent*-16-F_{1t}-PhytoP). Interestingly, the DHA derived 10(*R,S*)-10-F_{4t}-NeuroP with the hydroxyl group in the α-chain and the 14(*R,S*)-14-F_{4t}-NeuroP with hydroxyl group in the ω-chain are exceptions, showing a reverse fragmentation behavior compared to the observed pattern for the other F-IsoP described above, i.e. forming predominantly charged fragments which can be assigned to the reverse α-cleavage site relative to the hydroxyl group (SI, Fig. S1 D(ii) + (iii)). The selected fragment ions are consistent with the transitions used in other SRM methods for almost all F-IsoP with exception of 16(*R,S*)-16-F_{1t}-PhytoP [31], 8(*R,S*)-8-F_{3t}-IsoP [32,33] and 17(*R,S*)-17-F_{2t}-dihomo-IsoP [30,33,51]. For those analytes different transitions compared to existing methods were selected which, however, could be ascribed to specific α-cleavages of the backbone of the molecule.

The investigated cyclopentenone PhytoP with B- (Fig. 2C) and L-ring structure (SI, Fig. S1 A(iv)) only gave rise to few abundant fragment ions. Based on this fragmentation pattern no suggestion for the site of fragmentation could be made. For structural elucidation of the formed fragments, further studies, e.g. using isotopically labeled standards are necessary. Nevertheless, the selected transitions were specific for these PhytoP and have been reported previously for their quantification [31,34].

The isofurans are structurally characterized by a furan-like 5-membered oxygen containing ring carrying a hydroxyl group and additionally two hydroxyl groups in the side chains located either in the same side chain as it is the case for enediol furans or in different side chains like in alkenyl furans (Fig. 1). For each of the investigated IsoF the fragmentation behavior is distinct: Compared to F-IsoP unspecific loss of H_2O and CO_2 is less pronounced and specific fragments resulting from backbone cleavage might be attributed either to fragmentation next to the furan ring (Fig. 2D) or adjacent to one of the side chain hydroxyl groups (as e.g. in 7(*R,S*)-ST-Δ^8-11-dihomo-IsoF, SI, Fig. S1 E(iii)). However, 4(*R,S*)-ST-Δ^5-8-NeuroF and 17(*R,S*)-10-*epi*-SC-Δ^8-11-dihomo-IsoF show a different fragmentation pattern (SI, Fig. S1 D(iv), E(iv)) and suggestions for the structure of the fragments and fragmentation sites cannot be made based on the data. For 17(*R,S*)-10-*epi*-SC-Δ^8-11-dihomo-IsoF

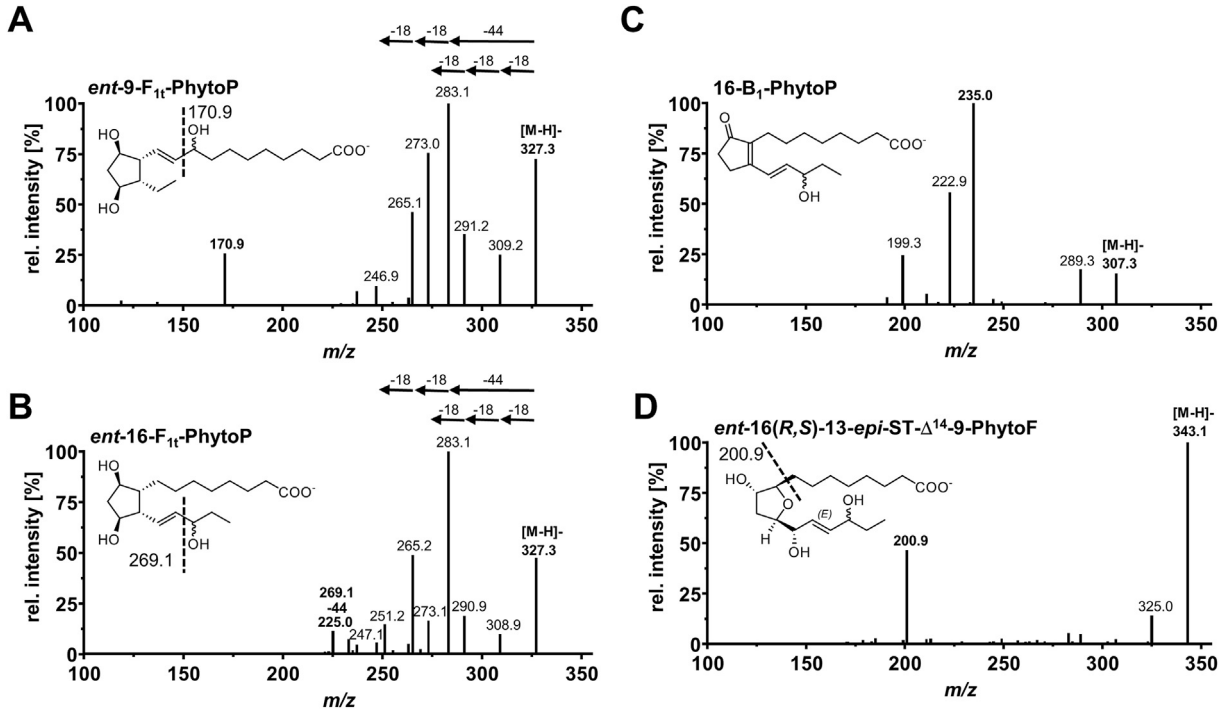

Fig. 2. Collision induced dissociation (CID) product ion spectra of $[M-H]^-$ ions of α-linolenic acid derived PhytoP and PhytoF. (**A**) *ent*-9-F_{1t}-PhytoP (F-ring-PhytoP carrying the hydroxyl group in the α-chain) (**B**) *ent*-16-F_{1t}-PhytoP (F-ring-PhytoP carrying the hydroxyl group in the ω-chain) (**C**) 16-B_1-PhytoP (cyclopentenone with B-ring structure) (**D**) *ent*-16-(*R,S*)-13-*epi*-ST-Δ^{14}-9-PhytoF (enediol-furan).

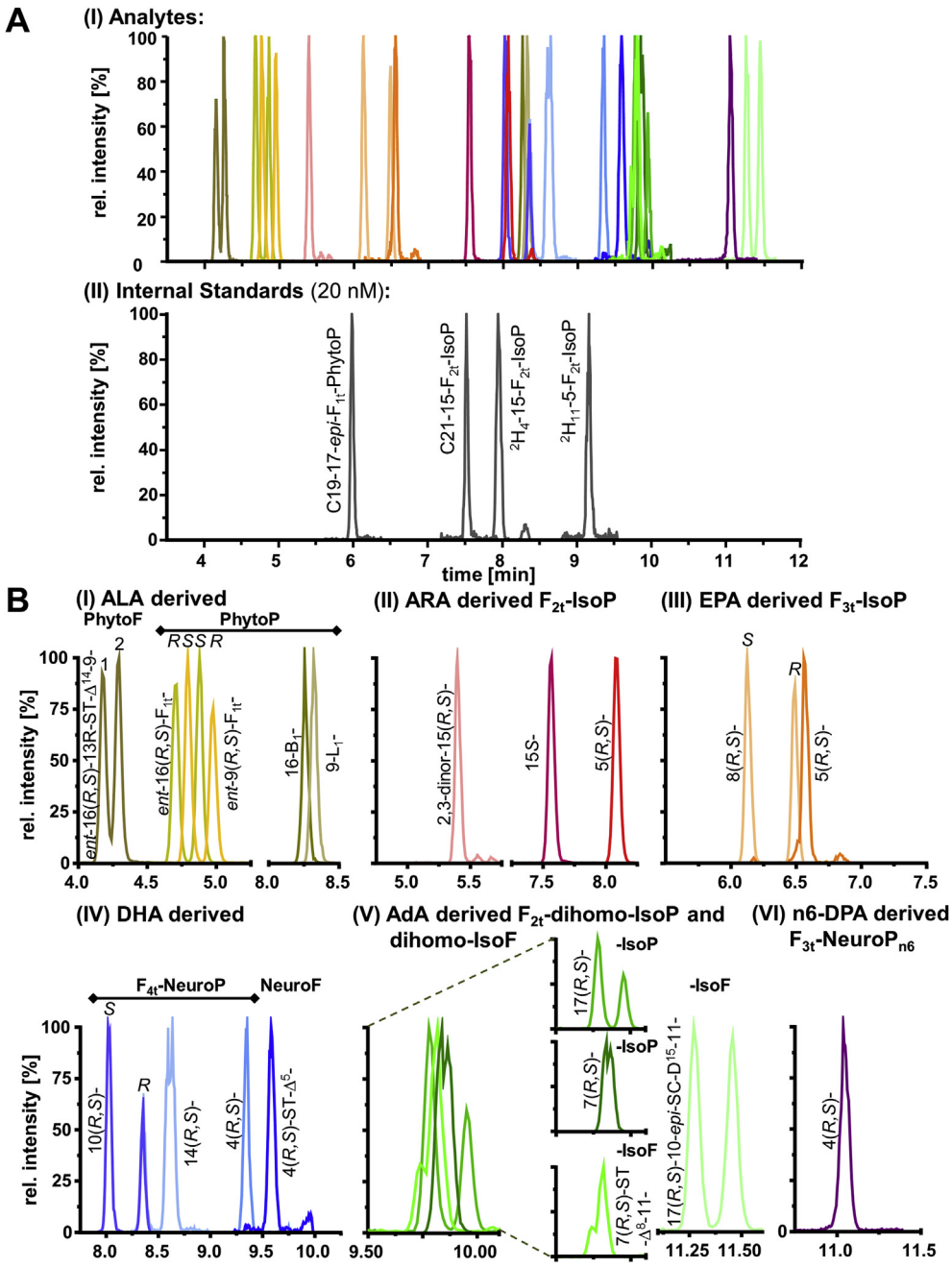

Fig. 3. A: Chromatographic separation of **(I)** 27 isoprostanes and 8 isofuranes derived from 6 different PUFA. Shown are the SRM signals used for quantification following injection of a multianalyte standard (100 nM; except 14(*R,S*)-14-F_{4t}-NeuroP, 4(*R,S*)-ST-Δ^5-8-NeuroF, *ent*-7(*R,S*)-7-F_{2t}-dihomo-IsoP, 17(*R,S*)-17-F_{2t}-dihomo-IsoP each 500 nM). **(II)** For the quantification 4 internal standards (20 nM) are used: 2 deuterated IS and 2 odd-chain IS.
B: Chromatographic separation efficiency of isoprostanoids covered by the method grouped by their precursor PUFA. Shown are the SRM signals used for quantification of
(I) α-linolenic acid (C18:3 n3, ALA) derived *ent*-16(*R,S*)-13-*epi*-ST-Δ^{14}-9-PhytoF, *ent*-16-F_{1t}-PhytoP, *ent*-16-*epi*-16-F_{1t}-PhytoP, *ent*-9-F_{1t}-PhytoP, *ent*-9-*epi*-F_{1t}-PhytoP, 16-B_1-PhytoP, 9-L_1-PhytoP.
(II) arachidonic acid (C20:4 n6, ARA) derived 15(*R,S*)-2,3-dinor-15-F_{2t}-IsoP, 15-F_{2t}-IsoP (= 8-*iso*-$PGF_{2\alpha}$), 5(*R,S*)-5-F_{2t}-IsoP.
(III) eicosapentaenoic acid (C20:5 n3, EPA) derived 8-F_{3t}-IsoP, 8-*epi*-8-F_{3t}-IsoP, 5(*R,S*)-5-F_{3t}-IsoP.
(IV) docosahexaenoic acid (C22:6 n3, DHA) derived 10-F_{4t}-NeuroP, 10-*epi*-10-F_{4t}-NeuroP, 14(*R,S*)-14-F_{4t}-NeuroP, 4(*R,S*)-4-F_{4t}-NeuroP, 4(*R,S*)-ST-Δ^5-8-NeuroF.
(V) adrenic acid (C22:4 n6, AdA) derived 7(*R,S*)-ST-Δ^8-11-dihomo-IsoF, *ent*-7(*R,S*)-7-F_{2t}-dihomo-IsoP, 17(*R,S*)-17-F_{2t}-dihomo-IsoP, 17(*R,S*)-10-epi-SC-Δ^5-11-dihomo-IsoF.
(VI) docosapentaenoic acid (C22:5 n6, n6-DPA) derived 4(*R,S*)-4-F_{3t}-$NeuroP_{n6}$.

the transition reported previously corresponding to the fragment with the highest abundance was selected [51]. Regarding 4(*R,S*)-ST-Δ^5-8-NeuroF the fragment used in previous methods (*m/z* 123) [52] showed poor intensity, thus the fragment (*m/z* 187) with the highest abundance was selected (SI, Fig. S1 D(iv)).

3.2. Chromatographic separation

The chromatographic separation was optimized in order to obtain an efficient separation of the isobaric isomers in a reasonable time. The method covers 25 F-ring IsoP comprising 12 diastereomeric (epimeric) pairs and one single stereoisomer derived

from ALA, ARA, EPA, n6-DPA, DHA and AdA, one B- and one L-ring PhytoP and 4 epimeric pairs of IsoF derived from ALA, DHA and AdA. Using a C18 column with sub 2 μm particles and an optimized gradient of acidified water and ACN as well as MeOH, separation of the analytes could be achieved within 12 min (Fig. 3A). The ALA derived PhytoF and F_{1t}-PhytoP elute first, followed by the polar β-oxidation metabolites 15(*R,S*)-2,3-dinor-15-F_{2t}-IsoP from ARA and the IsoP from EPA and ARA. B- and L-ring PhytoP and DHA derived F_{4t}-NeuroP and NeuroF elute in the middle part of the chromatogram followed by AdA derived F_{2t}-dihomo-IsoP and dihomo-IsoF as well as n6-DPA derived 4(*R,S*)-4-F_{3t}-$NeuroP_{n6}$ (Fig. 3).

The initial gradient conditions were adjusted in order to achieve separation from the void volume (1.5 min), i.e. sufficient retention of the early eluting analytes, which is characterized by a retention factor k of at least 2. The first analytes (PhytoF) elute at 4.19 and 4.30 min (after more than two void volumes), which corresponds to a retention factor of $k \geq 1.8$, showing a sufficient separation from the unretained void volume. The slope of the gradient was optimized in order to yield a high separation efficiency of most epimeric pairs.

A short isocratic step (1 min) with 25% organic at the beginning of the gradient was included to focus the analytes at the front end of the column. This led to narrow peaks over the whole separation time (exemplary shown in SI, Fig. S2) characterized by a full width at half maximum (FWHM) of about 3.3–4.2 s for almost all analytes (Table 1). Some epimeric pairs, e.g. 14(*R,S*)-14-F_{4t}-NeuroP and *ent*-7(*R,S*)-7-F_{2t}-dihomo-IsoP (Table 1, Fig. 3B), showed a broader FWHM due to incomplete separation of the epimers.

The chromatographic separation showed a high stability regarding retention time with an interbatch RSD of ≤ 0.25%, i.e. < 0.02 min (n = 360) or < 0.01 min within one batch (n = 50).

The gradient allows an efficient separation of 7 critical epimeric pairs of IsoP and IsoF characterized by a resolution of R > 1.5. With exception of the *ent*-16(*R,S*)-13-*epi*-ST-Δ^{14}-9-PhytoF, which is the first eluting epimeric pair showing a resolution of R = 1.4, the resolution of the other separated epimers is R ≥ 1.7. However, 3 epimeric pairs (14(*R,S*)-14-F_{4t}-NeuroP, *ent*-7(*R,S*)-7-F_{2t}-dihomo-IsoP and 7(*R,S*)-ST-Δ^{8}-11-dihomo-IsoF) show an incomplete separation and 6 epimeric pairs coelute (Fig. 3B). The use of a shallower gradient with an increase of 0.5% B/min instead of 2.7% B/min or isocratic separation (data not shown) only slightly improved the separation of the incompletely separated and coeluting stereoisomers while further prolonging the analysis time. Thus, only the use of a different column or mobile phase thereby changing the selectivity of the chromatographic system could solve this separation problem. However, we regarded these parameters as fixed during method development because the analytical procedure should be integrated in an existing method, already established in our lab for the analysis of enzymatically formed oxylipins [45,48,49]. This combination enables to determine 129 oxylipins in addition to the covered IsoP and IsoF, thus allowing the detection of a total of 164 oxylipins formed enzymatically and via autoxidation together with 17 IS within 30.5 min. The mass-spectrometric and chromatographic performance parameters for all analytes are summarized in the SI, Table S1.

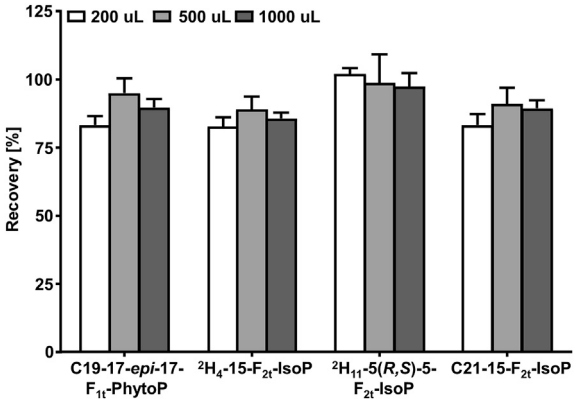

Fig. 4. Recovery of internal standards added to 200 μL, 500 μL and 1000 μL human plasma at the beginning of sample preparation followed by protein precipitation with MeOH and solid phase extraction. Shown are mean ± SD (n = 4).

3.3. Method performance

Quantification of the analytes was carried out based on the analyte to corresponding IS area ratio using the calibration curves. For the IsoP and IsoF two deuterated IsoP ($^2H_{11}$-5(*R,S*)-5-F_{2t}-IsoP and $^2H_4$-15-F_{2t}-IsoP) and two odd-chain unlabeled IsoP (C19-17-*epi*-17-F_{1t}-PhytoP and C21-15-F_{2t}-IsoP) that are eluted over the analytical time (Fig. 3A) were used as IS. For 5(*R,S*)-5-F_{2t}-IsoP and 15-F_{2t}-IsoP their respective isotopologs were used as IS. For the other analytes the assignment of the IS was based on retention time (Table 1).

Characterization of the method performance was oriented on the guideline on bioanalytical method validation of the European Medicines Agency [47]. The sensitivity of the method was assessed by determining the LOD and the LLOQ based on the signal to noise ratio (Table 1). The concentration leading to an S/N ≥ 3 was defined as LOD (exemplary shown for 2,3-dinor-15-F_{2t}-IsoP, Fig. S3). Almost all analytes showed a comparable LOD ranging from 0.15 to 2 pg on column. However 14(*R,S*)-14-F_{4t}-NeuroP and 4(*R,S*)-ST-Δ^5-8-NeuroF showed a considerably higher LOD with 19 pg and 39 pg on column, respectively. Since the same differences in the signal intensity were observed in SIM mode (data not shown), these higher LOD could either be explained by different ionization behavior of the compounds or by impure standard stock solutions of the two compounds. Similar to the LOD, the LLOQ (i.e. the concentration with a S/N ≥ 5 and an accuracy within 80–120% of the calibration curve) ranged from 0.25 to 2 nM for almost all IsoP and IsoF except 14(*R,S*)-14-F_{4t}-NeuroP and 4(*R,S*)-ST-Δ^5-8-NeuroF. The sensitivity was also reflected by the slope of the calibration curves. Comparing the slopes of all covered IsoP and IsoF normalized to the same IS revealed that 14(*R,S*)-14-F_{4t}-NeuroP and 4(*R,S*)-ST-Δ^5-8-NeuroF showed a remarkably lower slope compared to the other analytes (factor 10 and 50 lower, respectively, compared to the mean of normalized slopes) which is consistent with the observed higher LLOQ and LOD (Table 1). Interestingly this higher LLOQ for 14(*R,S*)-14-F_{4t}-NeuroP was also observed previously [33]. Remarkably, 5(*R,S*)-5-F_{3t}-IsoP with an LLOQ of 2 nM, showed a comparatively low slope. Compared to other IsoP, a slightly higher LLOQ for 5(*R,S*)-5-F_{3t}-IsoP was also reported previously [33].

The obtained LOD and LLOQ are in a similar range as reported previously for other oxylipins [45] and in comparison with previous reports for isoprostanes the obtained sensitivity was comparable or slightly better [30,33]. Noteworthy, two methods which were focused only on F_{2t}-IsoP [41] and PhytoP and PhytoF [34] reported LLOQs one to two orders of magnitude lower despite using a comparable triple quadrupole mass spectrometer. This may be in part explained by the high injection volume of 50 μL as well as the use of a micro-HPLC instrumentation [34,41]. In our method, using a higher injection volume led to peak splitting and inacceptable peak shape (SI, Fig. S4). This is caused by the high elution power of the methanol which is used to reconstitute the samples after SPE. Using a more polar solvent leads to an insufficient solution of less polar hydroxy- and epoxy fatty acids which are also covered by our method and thus the amount of sample injected cannot be further

Table 2
Intra- and interday accuracy (acc.) as well as precision (prec.) of the extraction of all IsoP and IsoF comprised by the method from human plasma (500 μL). For the determination of accuracy and precision, IsoP and IsoF were spiked in four concentration levels to the plasma samples (3, 10, 30, 100 nM) at the beginning of the sample preparation. Accuracy was determined from the calculated concentration following SPE in comparison to the spiking standard solution and precision was calculated as relative standard deviation of the sample sets (n = 4 for intra- and n = 3 for interday). *) For IsoP and IsoF which were available as isomeric mixtures, the spiking level correspond to the sum concentration of both isomers in the mixture and individual spiking level were calculated based on the isomeric ratio of the substances.

	Analyte	conc [nM]	INTRADAY		INTERDAY			Analyte	conc [nM]	INTRADAY		INTERDAY	
			acc.[%]	prec.[%]	acc.[%]	prec.[%]				acc.[%]	prec.[%]	acc.[%]	prec.[%]
ARA	5(*R,S*)-5-F_{2t}-IsoP	3	91	4	91	4	**ALA**	*ent*-9-F_{1t}-PhytoP	3	103	6	111	4
		10	84	6	81	3			10	96	4	98	6
		30	82	3	78	4			30	96	3	96	2
		100	87	8	83	3			100	99	7	93	1
	15-F_{2t}-IsoP (8-*iso*-PGF_{2a})	3	102	4	108	7		*ent*-9-*epi*-9-F_{1t}-PhytoP	3	98	8	109	2
		10	94	1	94	3			10	93	2	85	7
		30	101	6	93	2			30	93	4	91	4
		100	97	7	95	0			100	94	3	87	2
	15(*R,S*)-2,3-dinor-15-F_{2t}-IsoP	3	88	4	101	7		*ent*-16-*epi*-16-F_{1t}-PhytoP	3	112	6	115	9
		10	89	7	93	2			10	99	2	100	4
		30	87	7	80	2			30	98	3	102	2
		100	96	7	90	3			100	100	6	96	5
AdA	ent-7(*R,S*)-7-F_{2t}-dihomo-IsoP	3	95	12	105	3		*ent*-16-F_{1t}-PhytoP	3	121	4	125	2
		10	80	7	103	4			10	99	2	99	4
		30	92	9	91	6			30	96	4	101	3
		100	96	13	90	8			100	100	6	96	8
	17(*R,S*)-17-F_{2t}-dihomo-IsoP 1 *)	2	100	10	119	19		9-L_1-PhytoP	3	99	13	93	1
		6	100	7	116	2			10	98	10	91	3
		19	98	4	100	6			30	103	18	124	1
		63	102	12	94	6			100	95	6	94	5
	17(*R,S*)-17-F_{2t}-dihomo-IsoP 2 *)	1	106	14	65	15		16-B_1-PhytoP	3	101	13	127	8
		4	77	5	97	21			10	102	10	100	3
		11	85	15	77	8			30	108	16	133	1
		37	97	14	89	7			100	100	5	99	1
	7(*R,S*)-ST-Δ^8-11-dihomo-IsoF	3	93	13	92	32		*ent*-16(*R,S*)-13-*epi*-ST-Δ^{14}-9-PhytoF 1 *)	1	89	9	94	4
		10	97	10	104	11			5	89	6	88	3
		30	99	9	101	2			14	91	2	92	1
		100	100	12	96	7			47	93	6	86	1
	17(*R,S*)-10-epi-SC-Δ^{15}-11-dihomo-IsoF 1 *)	2	109	7	90	15		*ent*-16(*R,S*)-13-*epi*-ST-Δ^{14}-9-PhytoF 2 *)	2	104	6	100	4
		5	93	7	103	2			5	91	2	92	4
		16	107	9	122	8			16	94	4	97	2
		52	105	8	97	9			53	97	7	93	5
	17(*R,S*)-10-*epi*-SC-Δ^{15}-11-dihomo-IsoF 2 *)	1	96	6	96	13	**DHA**	4(*R,S*)-4-F_{4t}-NeuroP	3	92	16	114	5
		5	96	6	108	1			10	83	7	98	3
		14	103	11	124	10			30	85	16	74	9
		48	101	9	97	10			100	95	15	84	3
EPA	5(*R,S*)-5-F_{3t}-IsoP	3	110	11	150	2		10-F_{4t}-NeuroP	3	113	4	124	3
		10	104	3	102	7			10	109	2	112	3
		30	96	6	92	2			30	119	8	108	2
		100	103	5	89	0			100	113	12	103	1
	8-F_{3t}-IsoP	3	103	5	97	3		10-*epi*-10-F_{4t}-NeuroP	3	105	9	118	12
		10	97	3	94	4			10	99	5	100	2
		30	96	4	94	3			30	106	10	87	3
		100	99	8	93	3			100	102	10	97	4
	8-*epi*-8-F_{3t}-IsoP	3	98	5	107	1		14(*R,S*)-14-F_{4t}-NeuroP	3	< LLOQ		< LLOQ	
		10	91	3	96	3			10	< LLOQ		< LLOQ	
		30	88	4	86	2			30	103	5	100	12
		100	95	5	91	4			100	101	7	97	17
n6-DPA	4(*R,S*)-4-F_{3t}-$NeuroP_{n6}$	3	93	11	105	22		4(*R,S*)-ST-Δ^5-8-NeuroF	3	< LLOQ		< LLOQ	
		10	77	13	94	1			10	< LLOQ		< LLOQ	
		30	78	22	63	9			30	< LLOQ		< LLOQ	
		100	84	17	79	11			100	93	22	78	6

increased. Nevertheless, our approach is still one of the three most sensitive methods described so far for the detection of IsoP. Moreover, it is the most comprehensive approach for the simultaneous quantification of prostanoid-like autoxidation products and covers more analytes than all previous methods.

Matching between method sensitivity and expected concentration in biological samples one should take into account that the baseline levels of IsoP and IsoF are very low, e.g. the commonly analyzed 15(*R,S*)-15-F_{2t}-IsoP is in the range of 40–170 pg/mL human plasma (total, i.e. free and esterified) of healthy subjects [53], corresponding to 0.1–0.5 nM. Sufficient sample preparation including a pre-concentration step as carried out in the presented method by an optimized SPE procedure is therefore needed to determine these compounds in biological samples.

For quantification, calibration curves at 10 concentration levels covering a concentration range from 0.1 to 500 nM for each analyte were prepared. With linear least square regression based on $1/x^2$ weighting correlation coefficients $\geq$ 0.994 were achieved for all analytes indicating linearity for the covered concentration range (Table 1). The highest calibration level was set as upper limit of quantification (ULOQ), however does not represent the end of the linear detector response. Taking the low physiological

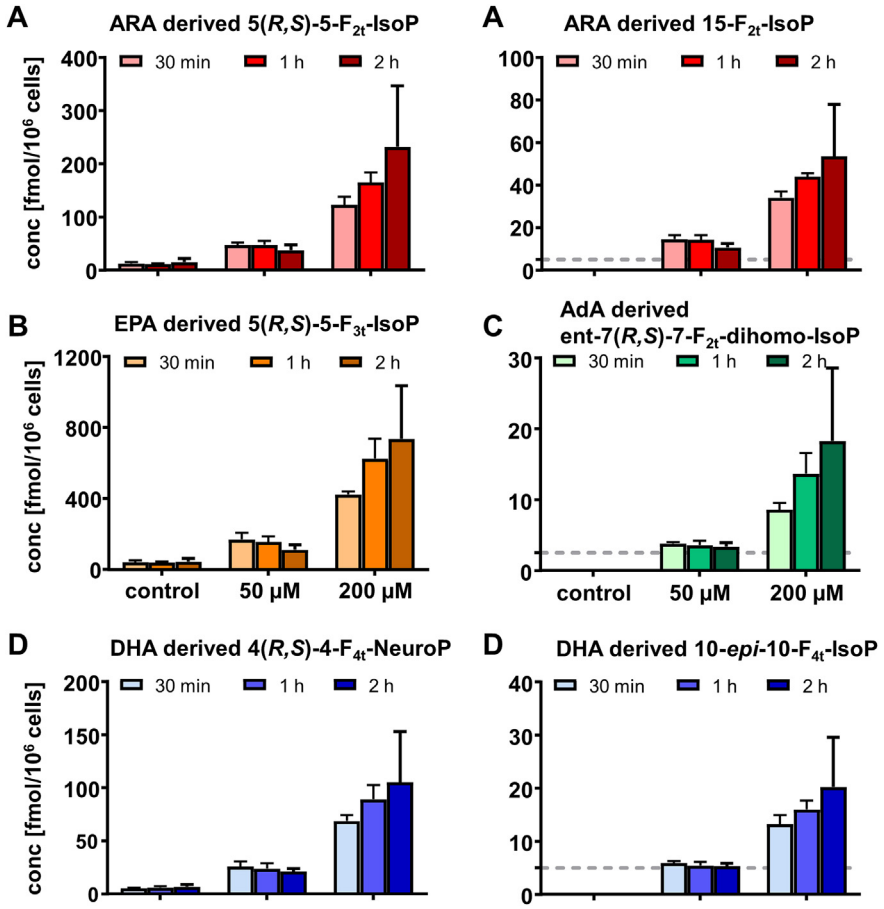

Fig. 5. Application of the method on the analysis of HTC116 cells. IsoP were quantified following incubation with 50 µM and 200 µM *t*-butyl hydroperoxide for 30 min, 1 h and 2 h. Shown are representative IsoP derived from **(A)** ARA, **(B)** EPA, **(C)** AdA, **(D)** DHA. All results are mean ± SD (n = 3) and the grey dashed line indicates the lower limit of quantification (LLOQ).

concentration of IsoP and IsoF into account the calibration of higher concentration as carried out in other methods [30–33] was for the intended application not necessary.

3.4. Extraction efficiency

The extraction efficiency from biological samples was characterized based on the recovery of IS spiked to the sample prior extraction. For the evaluation of the extraction efficiency of the used sample preparation procedure different volumes (200 µL, 500 µL, 1000 µL) of plasma from healthy volunteers were extracted by SPE. As shown in Fig. 4, recoveries in the range of 80–100% for all IS independent from the used plasma volume indicate a sufficient extraction for quantitative determination.

Regarding all IsoP and IsoF covered by the method, no IsoF and only ARA derived F_{2t}-IsoP were detected in the analyzed human plasma from healthy subjects. The most abundant regioisomer was 5(*R,S*)-5-F_{2t}-IsoP with comparable concentration for all investigated volumes (128 ± 13; 138 ± 6 and 132 ± 6 pM for 200 µL, 500 µL and 1000 µL respectively) indicating a good accuracy and precision regardless of the amount of sample/matrix injected. For 15-F_{2t}-IsoP, which is the most studied regioisomer, lower levels were detected (48 ± 1 and 38 ± 1 pM for 500 µL and 1000 µL respectively). This is consistent with previous findings reporting concentrations for 15(*R,S*)-15-F_{2t}-IsoP in the range of 16–48 pg/mL (45–135 pM) [19] and 3–25 pg/mL (8–71 pM) [54] in human plasma of healthy subjects.

3.5. Intra- and interday accuracy and precision

Intra- and interday accuracy and precision were characterized oriented on the guideline on bioanalytical method validation of the European Medicines Agency. In order to evaluate the accuracy and precision of the analytical procedure, human plasma samples spiked at four concentration levels prior extraction were analyzed in four replicates. The intraday accuracy ranged for all analytes from 77 to 121% indicating low interference of plasma matrix and good extraction efficiency of the analytes using the presented SPE procedure. Intraday precision calculated as RSD was < 15% for almost all analytes at all spiking levels with few exceptions being, however, below 22% (Table 2). Interday precision was better, below 11% for 10, 30 and 100 nM spiking levels, thus indicating a stable method which allows the analysis of large sample batches. However, at the low concentration level (3 nM), which is close to LLOQ, RSDs showed a trend towards higher values, but were still < 22% for almost all analytes, except 7(*R,S*)-ST-Δ^8-11-dihomo-IsoF (LLOQ of 2 nM, RSD = 32%, Table 2).

3.6. Formation of IsoP in cell culture

The developed method was applied to investigate the formation of IsoP and IsoF in HCT116 cells during oxidative stress caused by *t*-BOOH. First, the viability of HCT116 cells treated with increasing doses of *t*-BOOH for 2 h was determined with the MTS assay, revealing no effects at a dose of 50 µM and a moderate reduction of

the viability to 84% in cells incubated with 200 μM *t*-BOOH (SI, Fig S5). Following incubation a large number of IsoP were detected in the cells, i.e. 5(*R,S*)-5-F_{2t}-IsoP, 15-F_{2t}-IsoP, *ent*-7(*R,S*)-7-F_{2t}-dihomo-IsoP, 17(*R,S*)-17-F_{2t}-dihomo-IsoP 2, 5(*R,S*)-5-F_{3t}-IsoP, 4(*R,S*)-4-F_{4t}-NeuroP, 10-F_{4t}-NeuroP, 10-*epi*-10-F_{4t}-IsoP (Fig. 5, Table S3). In control incubations the levels of the detected IsoP were low or below the LLOQ (Table S3, Fig. 5), with EPA derived 5(*R,S*)-5-F_{3t}-IsoP being most abundant.

Regarding distribution of the different IsoP, a dominant formation of regioisomers carrying the side chain hydroxyl group in proximity to the carboxy terminus was observed for the IsoP formed from all different PUFA: 5(*R,S*)-5-F_{2t}-IsoP, 5(*R,S*)-5-F_{3t}-IsoP, *ent*-7(*R,S*)-7-F_{2t}-dihomo-IsoP and 4(*R,S*)-4-F_{4t}-NeuroP. At high concentrations of *t*-BOOH also other regiosomers were formed and the IsoP concentration increased dose dependently with the *t*-BOOH concentration. IsoP levels after 30 min with 200 μM were generally higher than after 2 h of incubation with 50 μM *t*-BOOH. Moreover, with 200 μM *t*-BOOH, even if not statistically significant, a trend towards higher levels of IsoP with increasing incubation time was observed while in incubations with 50 μM *t*-BOOH similar concentrations of IsoP were found for the different time points. This may indicate a cellular defense mechanism against ROS and thus IsoP formation decreased. It is also remarkable that with higher *t*-BOOH concentration the regioisomers with the side chain hydroxyl group in proximity to the carboxy terminus were stronger elevated than other regiosomers (Fig. 5), which may indicate not only differences in formation but also in the metabolism rates of the different regioisomers. This becomes particularly evident for the ARA derived IsoP. Here, 3–4 fold higher levels of 5(*R,S*)-5-F_{2t}-IsoP were found compared to 15-F_{2t}-IsoP while in livers of CCl_4 exposed rats a ratio of 1.5:1 was found [12]. However, it should be noted that these differences might also indicate species specific formation and metabolism rates of different regioisomers. The metabolism of the F_2-IsoPs, particularly 15-F_{2t}-IsoP has been well described [55,56]. By contrast the metabolism of the NeuroPs is not yet well understood, except an earlier investigation reported by Lawson et al. who showed that 7-F_{4t}-NeuroP is readily beta-oxidized to 5-F_{3t}-IsoP (an isoprostanoid metabolite from EPA oxidation) and excreted [57] whereas certain NeuroPs like 4-F_{4t}-NeuroP are probably more stable due to the presence of the side chain hydroxyl group at C4, which can limit access of the enzymes involved in beta-oxidation as it is the case for 5-hydroxyeicosanoids [58].

These results indicate that either the cellular formation is cell specific or the products are metabolized at different rates. The cellular formation of IsoP in response to oxidative stress and especially the resulting IsoP pattern warrants further investigation. In particular, application of different cell types and cell lines, e.g. deficient in different ROS defense mechanisms, should be used to understand the intracellular formation and the metabolic fate of IsoP. This investigation will allow gaining more insights into the role of IsoP in biology and help to identify specific biomarkers for distinct physiological states. With the developed method described herein, we provide the ideal tool to comprehensively quantify IsoP derived from all biologically relevant PUFA.

Acknowledgement

Our work is supported by a grant (01EA1702) of the Federal Ministry of Education and Research of Germany (BMBF) in the framework of the Joint Program Initiative ERA-HDHL to NHS, in part by the German Research Foundation (DFG, Grant SCHE 1801 to NHS) and by the Fonds der Chemischen Industrie in form of a PhD scholarship to KR. TD thanks his two colleagues, Dr Valérie Bultel-Poncé and Dr Alexandre Guy, for having synthesized the two unlabeled odd-chain IS.

Appendix A. Supplementary data

Supplementary data related to this article can be found at https://doi.org/10.1016/j.aca.2017.11.002.

References

[1] A. Weidinger, A. Kozlov, Biological activities of reactive oxygen and nitrogen species: oxidative stress versus signal transduction, Biomolecules 5 (2015) 472.
[2] H. Sies, 1-Oxidative Stress: Introductory Remarks, Oxidative Stress, Academic Press, London, 1985, pp. 1–8.
[3] D.P. Jones, H. Sies, The redox code, Antioxidants Redox Signal. 23 (2015) 734–746.
[4] H. Sies, Biochemistry of oxidative stress, Angewandte Chemie Int. Ed. Engl. 25 (1986) 1058–1071.
[5] G. Stark, Functional consequences of oxidative membrane damage, J. Membr. Biol. 205 (2005) 1–16.
[6] H. Yin, L. Xu, N.A. Porter, Free radical lipid peroxidation: mechanisms and analysis, Chem. Rev. 111 (2011) 5944–5972.
[7] D. Giustarini, I. Dalle-Donne, D. Tsikas, R. Rossi, Oxidative stress and human diseases: origin, link, measurement, mechanisms, and biomarkers, Crit. Rev. Clin. Lab. Sci. 46 (2009) 241–281.
[8] M.B. Kadiiska, B.C. Gladen, D.D. Baird, D. Germolec, L.B. Graham, C.E. Parker, A. Nyska, J.T. Wachsman, B.N. Ames, S. Basu, N. Brot, G.A. Fitzgerald, R.A. Floyd, M. George, J.W. Heinecke, G.E. Hatch, K. Hensley, J.A. Lawson, L.J. Marnett, J.D. Morrow, D.M. Murray, J. Plastaras, L.J. Roberts 2nd, J. Rokach, M.K. Shigenaga, R.S. Sohal, J. Sun, R.R. Tice, D.H. Van Thiel, D. Wellner, P.B. Walter, K.B. Tomer, R.P. Mason, J.C. Barrett, Biomarkers of oxidative stress study II: are oxidation products of lipids, proteins, and DNA markers of CCl4 poisoning? Free Radic. Biol. Med. 38 (2005) 698–710.
[9] J.D. Morrow, J.A. Awad, H.J. Boss, I.A. Blair, L.J. Roberts 2nd, Non-cyclooxygenase-derived prostanoids (F2-isoprostanes) are formed in situ on phospholipids, Proc. Natl. Acad. Sci. U. S. A. 89 (1992) 10721–10725.
[10] J.D. Morrow, L.J. Roberts, V.C. Daniel, J.A. Awad, O. Mirochnitchenko, L.L. Swift, R.F. Burk, Comparison of formation of D2/E2-isoprostanes and F2-isoprostanes in vitro and in vivo–effects of oxygen tension and glutathione, Archives Biochem. Biophysics 353 (1998) 160–171.
[11] R.J. Waugh, R.C. Murphy, Mass spectrometric analysis of four regioisomers of F2-isoprostanes formed by free radical oxidation of arachidonic acid, J. Am. Soc. Mass Spectrom. 7 (1996) 490–499.
[12] R.J. Waugh, J.D. Morrow, L.J. Roberts Ii, R.C. Murphy, Identification and relative quantitation of F2-Isoprostane regioisomers formed in vivo in the rat, Free Radic. Biol. Med. 23 (1997) 943–954.
[13] J.P. Fessel, N.A. Porter, K.P. Moore, J.R. Sheller, L.J. Roberts 2nd, Discovery of lipid peroxidation products formed in vivo with a substituted tetrahydrofuran ring (isofurans) that are favored by increased oxygen tension, Proc. Natl. Acad. Sci. U. S. A. 99 (2002) 16713–16718.
[14] C. Cuyamendous, K.S. Leung, T. Durand, J.C.-Y. Lee, C. Oger, J.-M. Galano, Synthesis and discovery of phytofurans: metabolites of α-linolenic acid peroxidation, Chem. Commun. 51 (2015) 15696–15699.
[15] K.S. Leung, V. Bultel-Poncé, A. Guy, T. Durand, J.M. Galano, C.Y. Lee, C. Oger, Total syntheses and in vivo quantitation of novel Phytofurans derived from alpha-linolenic acid, Eur. J. Org. Chem. (2017) 2486–2490.
[16] E.R. Skinner, C. Watt, J.A. Besson, P.V. Best, Differences in the fatty acid composition of the grey and white matter of different regions of the brains of patients with Alzheimer's disease and control subjects, Brain a J. Neurol. 116 (Pt 3) (1993) 717–725.
[17] M. VanRollins, R.L. Woltjer, H. Yin, J.D. Morrow, T.J. Montine, F2-dihomo-isoprostanes arise from free radical attack on adrenic acid, J. Lipid Res. 49 (2008) 995–1005.
[18] H. Schweer, B. Watzer, H.W. Seyberth, R.M. Nusing, Improved quantification of 8-epi-prostaglandin F2 alpha and F2-isoprostanes by gas chromatography/triple-stage quadrupole mass spectrometry: partial cyclooxygenase-dependent formation of 8-epi-prostaglandin F2 alpha in humans, J. Mass Spectrom. JMS 32 (1997) 1362–1370.
[19] C. Signorini, M. Comporti, G. Giorgi, Ion trap tandem mass spectrometric determination of F2-isoprostanes, J. Mass Spectrom. JMS 38 (2003) 1067–1074.
[20] E.S. Musiek, J.K. Cha, H. Yin, W.E. Zackert, E.S. Terry, N.A. Porter, T.J. Montine, J.D. Morrow, Quantification of F-ring isoprostane-like compounds (F4-neuroprostanes) derived from docosahexaenoic acid in vivo in humans by a stable isotope dilution mass spectrometric assay, J. Chromatogr. B, Anal. Technol. Biomed. Life Sci. 799 (2004) 95–102.
[21] C.Y. Lee, A.M. Jenner, B. Halliwell, Rapid preparation of human urine and plasma samples for analysis of F2-isoprostanes by gas chromatography-mass spectrometry, Biochem. Biophysical Res. Commun. 320 (2004) 696–702.
[22] C.Y. Lee, S.H. Huang, A.M. Jenner, B. Halliwell, Measurement of F2-isoprostanes, hydroxyeicosatetraenoic products, and oxysterols from a single plasma sample, Free Radic. Biol. Med. 44 (2008) 1314–1322.
[23] C. Signorini, L. Ciccoli, S. Leoncini, S. Carloni, S. Perrone, M. Comporti, W. Balduini, G. Buonocore, Free iron, total F-isoprostanes and total F-neuroprostanes in a model of neonatal hypoxic-ischemic encephalopathy:

neuroprotective effect of melatonin, J. Pineal Res. 46 (2009) 148–154.
[24] G.L. Milne, B. Gao, E.S. Terry, W.E. Zackert, S.C. Sanchez, Measurement of F2-isoprostanes and isofurans using gas chromatography–mass spectrometry, Free Radic. Biol. Med. 59 (2013) 36–44.
[25] D.R. Briskey, G.R. Wilson, R.G. Fassett, J.S. Coombes, Optimized method for quantification of total F2-isoprostanes using gas chromatography–tandem mass spectrometry, J. Pharm. Biomed. Anal. 90 (2014) 161–166.
[26] W. Yan, G.D. Byrd, M.W. Ogden, Quantitation of isoprostane isomers in human urine from smokers and nonsmokers by LC-MS/MS, J. Lipid Res. 48 (2007) 1607–1617.
[27] S. Medina, R. Dominguez-Perles, J.I. Gil, F. Ferreres, C. Garcia-Viguera, J.M. Martinez-Sanz, A. Gil-Izquierdo, A ultra-pressure liquid chromatography/triple quadrupole tandem mass spectrometry method for the analysis of 13 eicosanoids in human urine and quantitative 24 hour values in healthy volunteers in a controlled constant diet, Rapid Commun. Mass Spectrom. RCM 26 (2012) 1249–1257.
[28] J.K. Prasain, A. Arabshahi, P.R. Taub, S. Sweeney, R. Moore, J.D. Sharer, S. Barnes, Simultaneous quantification of F2-isoprostanes and prostaglandins in human urine by liquid chromatography tandem-mass spectrometry, J. Chromatogr. B 913–914 (2013) 161–168.
[29] J. Larose, P. Julien, J.F. Bilodeau, Analysis of F2-isoprostanes in plasma of pregnant women by HPLC-MS/MS using a column packed with core-shell particles, J. Lipid Res. 54 (2013) 1505–1511.
[30] S. Medina, I.D. Miguel-Elizaga, C. Oger, J.M. Galano, T. Durand, M. Martinez-Villanueva, M.L. Castillo, I. Villegas-Martinez, F. Ferreres, P. Martinez-Hernandez, A. Gil-Izquierdo, Dihomo-isoprostanes-nonenzymatic metabolites of AdA-are higher in epileptic patients compared to healthy individuals by a new ultrahigh pressure liquid chromatography-triple quadrupole-tandem mass spectrometry method, Free Radic. Biol. Med. 79 (2015) 154–163.
[31] J. Collado-Gonzalez, S. Medina, T. Durand, A. Guy, J.M. Galano, A. Torrecillas, F. Ferreres, A. Gil-Izquierdo, New UHPLC-QqQ-MS/MS method for quantitative and qualitative determination of free phytoprostanes in foodstuffs of commercial olive and sunflower oils, Food Chem. 178 (2015) 212–220.
[32] C. Chafer-Pericas, L. Rahkonen, A. Sanchez-Illana, J. Kuligowski, I. Torres-Cuevas, M. Cernada, E. Cubells, A. Nunez-Ramiro, S. Andersson, M. Vento, J. Escobar, Ultra high performance liquid chromatography coupled to tandem mass spectrometry determination of lipid peroxidation biomarkers in newborn serum samples, Anal. Chim. Acta 886 (2015) 214–220.
[33] A. Dupuy, P. Le Faouder, C. Vigor, C. Oger, J.M. Galano, C. Dray, J.C. Lee, P. Valet, C. Gladine, T. Durand, J. Bertrand-Michel, Simultaneous quantitative profiling of 20 isoprostanoids from omega-3 and omega-6 polyunsaturated fatty acids by LC-MS/MS in various biological samples, Anal. Chim. Acta 921 (2016) 46–58.
[34] M.E. Yonny, A. Rodríguez Torresi, C. Cuyamendous, G. Réversat, C. Oger, J.-M. Galano, T. Durand, C. Vigor, M.A. Nazareno, Thermal stress in melon plants: phytoprostanes and phytofurans as oxidative stress biomarkers and the effect of antioxidant supplementation, J. Agric. Food Chem. 64 (2016) 8296–8304.
[35] Z. Wang, G. Ciabattoni, C. Creminon, J. Lawson, G.A. Fitzgerald, C. Patrono, J. Maclouf, Immunological characterization of urinary 8-epi-prostaglandin F2 alpha excretion in man, J. Pharmacol. Exp. Ther. 275 (1995) 94–100.
[36] S. Basu, Radioimmunoassay of 8-iso-prostaglandin F2alpha: an index for oxidative injury via free radical catalysed lipid peroxidation, Prostagl. Leukot. Essent. Fat. Acids 58 (1998) 319–325.
[37] D. Il'yasova, J.D. Morrow, A. Ivanova, L.E. Wagenknecht, Epidemiological marker for oxidant status: comparison of the ELISA and the gas chromatography/mass spectrometry assay for urine 2,3-dinor-5,6-dihydro-15-F2t-isoprostane, Ann. Epidemiol. 14 (2004) 793–797.
[38] J. Klawitter, M. Haschke, T. Shokati, J. Klawitter, U. Christians, Quantification of 15-F2t-isoprostane in human plasma and urine: results from enzyme-linked immunoassay and liquid chromatography/tandem mass spectrometry cannot be compared, Rapid Commun. Mass Spectrom. RCM 25 (2011) 463–468.
[39] D. Il'yasova, J.D. Morrow, A. Ivanova, L.E. Wagenknecht, Epidemiological marker for oxidant status: comparison of the ELISA and the gas chromatography/mass spectrometry assay for urine 2,3-dinor-5,6-dihydro-15-F2t-isoprostane, Ann. Epidemiol. 14 (2004) 793–797.
[40] C.F. Labuschagne, E.C. Stigter, M.M. Hendriks, R. Berger, J. Rokach, H.C. Korswagen, A.B. Brenkman, Quantification of in vivo oxidative damage in Caenorhabditis elegans during aging by endogenous F3-isoprostane measurement, Aging Cell 12 (2013) 214–223.
[41] J. Aszyk, J. Kot, Y. Tkachenko, M. Woźniak, A. Bogucka-Kocka, A. Kot-Wasik, Novel liquid chromatography method based on linear weighted regression for the fast determination of isoprostane isomers in plasma samples using sensitive tandem mass spectrometry detection, J. Chromatogr. B 1051 (2017) 17–23.
[42] M.L. Chung, K.Y. Lee, C.Y. Lee, Profiling of oxidized lipid products of marine fish under acute oxidative stress, Food Chem. Toxicol. Int. J. Publ. Br. Ind. Biol. Res. Assoc. 53 (2013) 205–213.
[43] C. Oger, Y. Brinkmann, S. Bouazzaoui, T. Durand, J.M. Galano, Stereocontrolled access to isoprostanes via a Bicyclo[3.3.0]octene framework, Org. Lett. 10 (2008) 5087–5090.
[44] M. Mimmler, S. Peter, A. Kraus, S. Stroh, T. Nikolova, N. Seiwert, S. Hasselwander, C. Neitzel, J. Haub, B.H. Monien, P. Nicken, P. Steinberg, J.W. Shay, B. Kaina, J. Fahrer, DNA damage response curtails detrimental replication stress and chromosomal instability induced by the dietary carcinogen PhIP, Nucleic Acids Res. 44 (2016) 10259–10276.
[45] A.I. Ostermann, I. Willenberg, N.H. Schebb, Comparison of sample preparation methods for the quantitative analysis of eicosanoids and other oxylipins in plasma by means of LC-MS/MS, Anal. Bioanal. Chem. 407 (2015) 1403–1414.
[46] S.H. Hwang, H.-J. Tsai, J.-Y. Liu, C. Morisseau, B.D. Hammock, Orally bioavailable potent soluble epoxide hydrolase inhibitors, J. Med. Chem. 50 (2007) 3825–3840.
[47] EMEA/CHMP/EWP/192217/2009 Rev. 1Corr. 2, Guideline on Bioanalytical Method Validation, European Medicines Agency, 2011.
[48] I. Willenberg, A.K. Meschede, F. Gueler, M.S. Jang, N. Shushakova, N.H. Schebb, Food polyphenols fail to cause a biologically relevant reduction of COX-2 activity, PLoS One 10 (2015) e0139147.
[49] I. Willenberg, K. Rund, S. Rong, N. Shushakova, F. Gueler, N.H. Schebb, Characterization of changes in plasma and tissue oxylipin levels in LPS and CLP induced murine sepsis, Inflamm. Res. Offic. J. Eur. Histamine Res. Soc. 65 (2016) 133–142 [et al.].
[50] R.C. Murphy, R.M. Barkley, K. Zemski Berry, J. Hankin, K. Harrison, C. Johnson, J. Krank, A. McAnoy, C. Uhlson, S. Zarini, Electrospray ionization and tandem mass spectrometry of eicosanoids, Anal. Biochem. 346 (2005) 1–42.
[51] A. de La Torre, Y.Y. Lee, C. Oger, P.T. Sangild, T. Durand, J.C.-Y. Lee, J.-M. Galano, Synthesis, discovery, and quantitation of dihomo-isofurans: biomarkers for in vivo adrenic acid peroxidation, Angew. Chem. Int. Ed. 53 (2014) 6249–6252.
[52] A. de la Torre, Y.Y. Lee, A. Mazzoni, A. Guy, V. Bultel-Poncé, T. Durand, C. Oger, J.C.-Y. Lee, J.-M. Galano, Total syntheses and in vivo quantitation of novel neurofuran and dihomo-isofuran derived from docosahexaenoic acid and adrenic acid, Chem. – A Eur. J. 21 (2015) 2442–2446.
[53] N.E. Bastani, T.E. Gundersen, R. Blomhoff, Determination of 8-epi PGF(2alpha) concentrations as a biomarker of oxidative stress using triple-stage liquid chromatography/tandem mass spectrometry, Rapid Commun. Mass Spectrom. RCM 23 (2009) 2885–2890.
[54] M. Haschke, Y.L. Zhang, C. Kahle, J. Klawitter, M. Korecka, L.M. Shaw, U. Christians, HPLC-atmospheric pressure chemical ionization MS/MS for quantification of 15-F2t-isoprostane in human urine and plasma, Clin. Chem. 53 (2007) 489–497.
[55] C. Chiabrando, A. Valagussa, C. Rivalta, T. Durand, A. Guy, E. Zuccato, P. Villa, J.C. Rossi, R. Fanelli, Identification and measurement of endogenous beta-oxidation metabolites of 8-epi-Prostaglandin F2alpha, J. Biol. Chem. 274 (1999) 1313–1319.
[56] L.J. Roberts, K.P. Moore, W.E. Zackert, J.A. Oates, J.D. Morrow, Identification of the major urinary metabolite of the F-2-isoprostane 8-iso-prostaglandin F-2 alpha in humans, J. Biol. Chem. 271 (1996) 20617–20620.
[57] J.A. Lawson, S. Kim, W.S. Powell, G.A. FitzGerald, J. Rokach, Oxidized derivatives of omega-3 fatty acids: identification of IPF3 alpha-VI in human urine, J. Lipid Res. 47 (2006) 2515–2524.
[58] D.O. Stene, R.C. Murphy, Metabolism of leukotriene E4 in isolated rat hepatocytes. Identification of beta-oxidation products of sulfidopeptide leukotrienes, J. Biol. Chem. 263 (1988) 2773–2778.

Supplementary information

Development of an LC-ESI(-)-MS/MS method for the simultaneous quantification of 35 isoprostanes and isofurans derived from the major n3- and n6-PUFAs

K. M. Rund, A. I. Ostermann, L. Kutzner, J.-M. Galano, C. Oger,
C. Vigor, S. Wecklein, N. Seiwert, T. Durand, N. H. Schebb

Tab. S1: Parameters of the LC-ESI(-)-MS/MS method for the quantification of oxylipins. Shown are all analytes covered by the method with their mass transitions for quantification in scheduled SRM mode, electronical MS parameters (declustering potential (DP), entrance potential (EP), collision energy (CE), collision exit potential (CXP)), the assigned internal standards (IS), retention time (t_R), full peak width at half maximum (FWHM), limit of detection (LOD) and the calibration range (lower limit of quantification (LLOQ), upper limit of quantification (ULOQ)) and correlation coefficient of the calibration curve (r).

Analyte	Mass transition		MS parameters				Internal standard	t_R [1]	FWHM [2]	LOD [3]		Calibration range		r^2 [6]
												LLOQ [4]	ULOQ [5]	
	Q1	Q3	DP	EP	CE	CXP		[min]	[sec]	[nM]	[pg on column]	[nM]		
20-OH-PGE_2	367.2	189.1	-30	-10	-25	-8	$^2H_4$-PGE_2	3.68	3.4	0.10	0.18	0.25	500	0.9986
ent-16(*R,S*)-13-*epi*-ST-Δ^{14}-9-PhytoF 1	343.1	200.9	-80	-10	-33	-8	C19-17-*epi*-17-F_{1t}-PhytoP	4.19	3.4	0.12	0.20	0.24	235	0.9993
ent-16(*R,S*)-13-*epi*-ST-Δ^{14}-9-PhytoF 2	343.1	200.9	-80	-10	-33	-8	C19-17-*epi*-17-F_{1t}-PhytoP	4.30	3.4	0.13	0.23	0.26	265	0.9995
ent-16-*epi*-16-F_{1t}-PhytoP	327.3	225.0	-70	-10	-34	-8	C19-17-*epi*-17-F_{1t}-PhytoP	4.72	3.3	0.25	0.41	0.5	500	0.9983
ent-16-F_{1t}-PhytoP	327.3	225.0	-70	-10	-34	-8	C19-17-*epi*-17-F_{1t}-PhytoP	4.89	3.4	0.50	0.82	1.0	500	0.9997
ent-9-F_{1t}-PhytoP	327.3	170.9	-40	-10	-31	-8	C19-17-*epi*-17-F_{1t}-PhytoP	4.81	3.3	0.10	0.16	0.25	500	0.9991
ent-9-*epi*-9-F_{1t}-PhytoP	327.3	170.9	-40	-10	-31	-8	C19-17-*epi*-17-F_{1t}-PhytoP	4.98	3.3	0.25	0.41	0.5	500	0.9990
Δ^{17}-6-keto-$PGF_{1\alpha}$	367.2	163.2	-40	-10	-36	-10	$^2H_4$-6-keto-$PGF_{1\alpha}$	4.99	21	0.50	0.92	1.0	500	0.9938
2,3-dinor-TxB_1	343.0	142.9	-30	-10	-19	-8	$^2H_4$-TxB_2	5.11	4.1	2.0	3.4	5.0	500	0.9961
15(*R,S*)-2,3-dinor-15-F_{2t}-IsoP	325.2	237.0	-40	-10	-18	-8	C19-17-*epi*-17-F_{1t}-PhytoP	5.41	3.3	0.25	0.41	0.5	500	0.9995
2,3-dinor-TxB_2	341.2	167.0	-40	-10	-15	-8	$^2H_4$-TxB_2	5.59	3.8	0.50	0.86	1.0	500	0.9971
6-keto-PGF_{1a}	369.3	163.2	-70	-10	-36	-6	$^2H_4$-6-keto-$PGF_{1\alpha}$	6.10	24	0.90	1.7	1.8	500	0.9937
8-F_{3t}-IsoP	351.1	155.0	-60	-10	-27	-8	C19-17-*epi*-17-F_{1t}-PhytoP	6.15	3.6	0.50	0.88	1.0	500	0.9980
8-*epi*-8-F_{3t}-IsoP	351.1	155.0	-60	-10	-27	-8	C19-17-*epi*-17-F_{1t}-PhytoP	6.51	3.3	0.50	0.88	1.0	500	0.9992
RvE1	349.3	195.0	-65	-10	-22	-10	$^2H_4$-TxB_2	6.21	3.5	0.60	1.1	1.2	480	0.9947
20-COOH-LTB_4	365.2	347.2	-80	-10	-25	-8	$^2H_4$-TxB_2	6.25	3.8	0.50	0.92	1.0	40	0.9619
TxB_3	367.3	169.3	-70	-10	-34	-8	$^2H_4$-TxB_2	6.51	3.5	0.10	0.18	0.25	100	0.9976
20-OH-LTB_4	351.2	195.2	-80	-10	-25	-8	$^2H_4$-PGD_2	6.52	3.3	0.10	0.18	0.25	40	0.9984
5(*R,S*)-5-F_{3t}-IsoP	351.2	114.9	-50	-10	-27	-8	C19-17-*epi*-17-F_{1t}-PhytoP	6.53	3.4	1.0	1.8	2.0	500	0.9962
13,14-dihydro-15-keto-tetranor-PGE_2	296.9	109.0	-30	-10	-19	-8	$^2H_4$-PGE_2	7.29	3.9	0.10	0.15	0.25	500	0.9992
TxB_1	371.3	171.2	-70	-10	-34	-10	$^2H_4$-TxB_2	7.36	3.9	0.25	0.47	0.5	100	0.9982
15-F_{2t}-IsoP (8-*iso*-$PGF_{2\alpha}$)	353.1	193.1	-70	-6	-33	-8	$^2H_4$-15-F_{2t}-IsoP	7.56	3.7	0.25	0.44	0.5	500	0.9989
TXB_2	369.2	169.1	-60	-10	-25	-7	$^2H_4$-TxB_2	7.68	3.8	0.25	0.46	1.3	500	0.9949
11-dehydro-TxB_3	365.3	161.2	-30	-10	-25	-8	$^2H_4$-TxB_2	7.75	3.6	0.50	0.92	1.0	100	0.9969
PGE_3	349.3	269.2	-60	-10	-22	-6	$^2H_4$-PGE_2	7.76	3.5	0.15	0.26	0.3	120	0.9995

Tab. S1: Continued.

Analyte	Mass transition		MS parameters				Internal standard	t_R [1]	FWHM [2]	LOD [3]		Calibration range LLOQ [4] ULOQ [5]		r^2 [6]
	Q1	Q3	DP	EP	CE	CXP		[min]	[sec]	[nM]	[pg on column]	[nM]		
11β-$PGF_{2\alpha}$	353.3	193.1	-30	-12	-36	-12	$^2H_4$-PGE_2	7.84	3.3	0.25	0.44	0.5	500	0.9952
10-F_{4t}-NeuroP	377.2	153.0	-40	-10	-25	-8	$^2H_4$-15-F_{2t}-IsoP	8.04	3.3	0.25	0.47	0.5	500	0.9989
10-*epi*-10-F_{4t}-NeuroP	377.2	153.0	-40	-10	-25	-8	$^2H_4$-15-F_{2t}-IsoP	8.37	3.5	0.50	0.95	1.0	500	0.9990
5(*R,S*)-5-F_{2t}-IsoP (5-i$PF_{2\alpha}$-VI)	353.2	114.8	-60	-10	-26	-8	$^2H_{11}$-5(*R,S*)-5-F_{2t}-IsoP	8.07	3.5	0.25	0.44	0.5	500	0.9959
PGD_3	349.3	269.2	-60	-10	-22	-6	$^2H_4$-PGD_2	8.15	3.4	0.50	0.88	1.0	40	0.9992
16-B_1-PhytoP	307.3	235.0	-60	-10	-27	-8	$^2H_{11}$-5(*R,S*)-5-F_{2t}-IsoP	8.26	3.7	0.10	0.15	0.25	500	0.9994
9-L_1-PhytoP	307.3	185.1	-60	-10	-27	-8	$^2H_{11}$-5(*R,S*)-5-F_{2t}-IsoP	8.33	3.7	0.10	0.15	0.25	500	0.9986
$PGF_{2\alpha}$	353.2	309.2	-80	-10	-26	-7	$^2H_4$-PGE_2	8.59	3.5	0.35	0.62	0.70	281	0.9991
14(*R,S*)-14-F_{4t}-NeuroP	377.2	205.1	-50	-10	-27	-8	C21-15-F_{2t}-IsoP	8.62	6.5	10	19	20	500	0.9998
$PGF_{1\alpha}$	355.4	293.2	-90	-12	-36	-6	$^2H_4$-PGE_2	8.63	3.5	0.10	0.18	0.25	500	0.9985
PGE_2	351.2	271.3	-60	-10	-24	-6	$^2H_4$-PGE_2	8.98	3.5	0.10	0.18	0.25	500	0.9982
11-dehydro-TxB_2	367.0	161.1	-50	-10	-27	-8	$^2H_4$-TxB_2	9.08	3.7	0.25	0.46	0.50	100	0.9988
PGE_1	353.3	317.2	-60	-10	-20	-6	$^2H_4$-PGE_2	9.27	3.6	0.13	0.23	0.33	260	0.9984
4(*R,S*)-4-F_{4t}-NeuroP	377.1	101.3	-60	-10	-26	-8	C21-15-F_{2t}-IsoP	9.35	3.8	0.50	0.95	1.0	500	0.9982
PGD_1	353.3	317.2	-60	-10	-20	-6	$^2H_4$-PGD_2	9.45	3.6	0.25	0.44	0.50	40	0.9956
PGD_2	351.2	271.3	-60	-10	-24	-6	$^2H_4$-PGD_2	9.46	3.6	0.50	0.88	1.0	500	0.9960
15-keto-$PGF_{1\alpha}$	353.3	193.1	-40	-12	-38	-6	$^2H_4$-PGE_2	9.54	3.7	0.10	0.18	0.25	500	0.9970
4(*R,S*)-ST-Δ^5-8-NeuroF	393.3	187.2	-40	-10	-29	-8	C21-15-F_{2t}-IsoP	9.59	4.2	20	39	40	500	0.9941
17(*R,S*)-17-F_{2t}-dihomo-IsoP 1	381.3	263.2	-90	-10	-31	-8	C21-15-F_{2t}-IsoP	9.78	3.6	0.63	1.2	1.3	314	0.9967
17(*R,S*)-17-F_{2t}-dihomo-IsoP 2	381.3	263.2	-90	-10	-31	-8	C21-15-F_{2t}-IsoP	9.95	3.2	0.37	0.71	0.75	186	0.9980
7(*R,S*)-ST-Δ^8-11-dihomo-IsoF	397.3	245.1	-50	-10	-31	-8	C21-15-F_{2t}-IsoP	9.81	3.8	1.0	2.0	2.0	500	0.9993
ent-7(*R,S*)-7-F_{2t}-dihomo-IsoP	381.3	143.0	-50	-10	-31	-8	C21-15-F_{2t}-IsoP	9.86	5.7	0.25	0.48	0.50	500	0.9972
11,12,15-TriHETrE	353.2	167.1	-80	-10	-28	-10	$^2H_4$-PGE_2	10.20	3.4	0.25	0.44	0.50	100	0.9988
LXA_4	351.2	115.2	-60	-10	-21	-8	$^2H_4$-PGE_2	10.23	3.7	0.088	0.15	0.18	70	0.9985
RvD1	375.3	141.0	-50	-10	-20	-8	$^2H_4$-PGE_2	10.35	3.6	0.10	0.19	0.25	100	0.9993
13,14-dihydro-15-keto-$PGF_{2\alpha}$	353.3	183.3	-80	-10	-36	-10	$^2H_4$-PGE_2	10.41	3.6	0.25	0.44	0.50	500	0.9990
13,14-dihydro-15-keto-PGE_1	353.3	221.2	-40	-6	-30	-6	$^2H_4$-PGE_2	10.97	4.5	0.25	0.44	0.50	500	0.9989
dihomo-$PGF_{2\alpha}$	381.4	221.1	-60	-10	-38	-10	$^2H_4$-PGE_2	11.01	3.8	0.025	0.048	0.10	500	0.9977
4*(R,S)*-4-F_{3t}-$NeuroP_{n6}$	379.2	273.0	-50	-10	-27	-8	C21-15-F_{2t}-IsoP	11.03	4.1	0.50	0.95	1.0	500	0.9971

Tab. S1: Continued.

Analyte	Mass transition		MS parameters				Internal standard	t_R [1]	FWHM [2]	LOD [3]		Calibration range LLOQ [4] ULOQ [5]		r^2 [6]
	Q1	Q3	DP	EP	CE	CXP		[min]	[sec]	[nM]	[pg on column]	[nM]		
17(*R,S*)-10-*epi*-SC-Δ^{15}-11-dihomo-IsoF	397.1	221.0	-90	-10	-31	-8	C21-15-F_{2t}-IsoP	11.26	3.7	0.52	1.0	1.0	260	0.9992
17(*R,S*)-10-*epi*-SC-Δ^{15}-11-dihomo-IsoF	397.1	221.0	-90	-10	-31	-8	C21-15-F_{2t}-IsoP	11.44	3.7	0.48	0.96	0.96	240	0.9982
RvE2	333.2	253.3	-60	-10	-20	-9	$^2H_4$-PGE_2	11.42	3.7	1.0	1.7	2.0	100	0.9991
PGJ_2	333.3	189.2	-60	-10	-25	-8	$^2H_4$-PGE_2	12.02	3.8	0.80	1.3	1.6	160	0.9957
Δ^{12}-PGJ_2	333.1	189.0	-40	-10	-22	-8	$^2H_4$-PGE_2	12.09	4.0	0.50	0.84	1.0	500	0.9986
LTB_5	333.3	195.2	-65	-10	-22	-8	$^2H_4$-LTB_4	12.11	4.0	0.050	0.084	0.10	200	0.9992
PGB_2	333.3	175.1	-60	-10	-28	-8	$^2H_4$-PGE_2	12.13	4.0	0.20	0.33	0.40	800	0.9982
THF diol	353.2	127.1	-80	-10	-32	-8	$^2H_4$-LTB_4	12.27	4.0	0.13	0.22	0.25	100	0.9987
18(*S*)-RvE3	333.2	201.3	-60	-10	-20	-9	$^2H_4$-PGE_2	12.78	4.1	0.50	0.84	1.0	100	0.9976
12-OH-17(18)-EpETE	333.1	179.3	-65	-10	-20	-6	$^2H_4$-9,10-DiHOME	12.85	4.3	0.25	0.42	0.50	100	0.9992
15,16-DiHODE	311.2	223.2	-80	-10	-29	-10	$^2H_4$-9,10-DiHOME	12.99	4.3	0.50	0.78	1.0	80	0.9992
9,10-DiHODE	311.2	201.2	-65	-10	-27	-10	$^2H_4$-9,10-DiHOME	13.05	4.2	0.10	0.16	0.20	80	0.9998
12,13-DiHODE	311.2	183.1	-80	-10	-30	-8	$^2H_4$-9,10-DiHOME	13.15	4.3	0.50	0.78	1.0	80	0.9990
8,15-DiHETE	335.2	235.2	-65	-10	-22	-4	$^2H_{11}$-14,15-DiHETrE	13.17	4.0	0.40	0.67	0.80	80	0.9981
10(S),17(S)diH n3 DPA	361.3	262.9	-40	-10	-23	-8	$^2H_4$-9,10-DiHOME	13.36	4.3	0.50	0.91	1.0	500	0.9991
18(*R*)-RvE3	333.2	201.3	-60	-10	-20	-9	$^2H_4$-PGE_2	13.45	4.2	0.25	0.42	0.50	100	0.9960
NPD1	359.0	153.0	-50	-10	-21	-8	$^2H_4$-9,10-DiHOME	13.49	4.2	0.25	0.45	0.50	500	0.9985
6-*trans*-LTB_4	335.2	195.1	-65	-10	-23	-9	$^2H_4$-LTB_4	13.58	4.2	0.25	0.42	0.50	200	0.9984
5,15-DiHETE	335.3	173.2	-60	-10	-21	-8	$^2H_{11}$-14,15-DiHETrE	13.60	4.0	0.13	0.21	0.25	100	0.9984
17,18-DiHETE	335.3	247.2	-65	-10	-24	-8	$^2H_{11}$-14,15-DiHETrE	13.71	4.3	0.13	0.21	0.25	100	0.9978
LTB_4	335.2	195.1	-65	-10	-23	-9	$^2H_4$-LTB_4	14.07	4.3	0.10	0.17	0.25	200	0.9996
7(S),17(S)-diH n3 DPA	361.5	263.3	-65	-10	-20	-4	$^2H_4$-9,10-DiHOME	14.29	3.8	0.30	0.54	0.75	500	0.9989
14,15-DiHETE	335.3	207.2	-65	-10	-25	-10	$^2H_{11}$-14,15-DiHETrE	14.34	4.5	0.13	0.21	0.25	100	0.9992
11,12-DiHETE	335.2	167.1	-65	-10	-26	-5	$^2H_{11}$-14,15-DiHETrE	14.57	4.6	0.13	0.21	0.25	100	0.9977
12,13-DiHOME	313.2	183.2	-80	-10	-30	-8	$^2H_4$-9,10-DiHOME	14.76	4.7	0.25	0.39	0.50	200	0.9986
8,9-DiHETE	335.2	127.1	-65	-10	-26	-5	$^2H_{11}$-14,15-DiHETrE	14.98	4.7	0.25	0.42	0.50	100	0.9962
10(*S*),17(*S*)diH n6 DPA	361.2	153.1	-50	-10	-21	-8	$^2H_{11}$-14,15-DiHETrE	15.14	4.5	0.10	0.18	0.25	500	0.9987
9,10-DiHOME	313.2	201.2	-80	-10	-29	-8	$^2H_4$-9,10-DiHOME	15.24	4.7	0.25	0.39	0.50	200	0.9991
10(*S*),17(*S*)diH AdA	363.4	263.2	-80	-10	-23	-8	$^2H_{11}$-14,15-DiHETrE	15.90	4.6	0.50	0.91	1.0	500	0.9993

Tab. S1: Continued.

Analyte	Mass transition		MS parameters				Internal standard	t_R [1]	FWHM [2]	LOD [3]		Calibration range LLOQ [4] ULOQ [5]		r^2 [6]
	Q1	Q3	DP	EP	CE	CXP		[min]	[sec]	[nM]	[pg on column]	[nM]		
12(*S*)-HHTrE	279.1	179.0	-50	-10	-17	-8	$^2H_{11}$-14,15-DiHETrE	15.96	4.9	0.25	0.35	0.50	500	0.9977
14,15-DiHETrE	337.2	207.1	-65	-10	-25	-10	$^2H_{11}$-14,15-DiHETrE	16.00	4.8	0.050	0.085	0.10	200	0.9985
19,20-DiHDPE	361.2	273.2	-65	-10	-24	-6	$^2H_{11}$-14,15-DiHETrE	16.05	4.8	0.25	0.45	0.50	100	0.9972
LTB_3	337.2	195.2	-65	-10	-22	-8	$^2H_4$-LTB_4	16.27	5.0	0.25	0.42	0.50	200	0.9995
9,10-diH-stearic acid	315.0	170.8	-60	-10	-36	-9	$^2H_4$-9,10-DiHOME	16.61	5.1	1.0	1.6	2.0	500	0.9994
16,17-DiHDPE	361.2	233.2	-65	-10	-24	-6	$^2H_{11}$-14,15-DiHETrE	16.69	4.7	0.25	0.45	0.50	100	0.9984
11,12-DiHETrE	337.2	167.1	-65	-10	-26	-8	$^2H_{11}$-14,15-DiHETrE	16.82	5.0	0.10	0.17	0.25	200	0.9980
19-HEPE	317.2	229.3	-50	-10	-18	-8	$^2H_8$-12-HETE	16.98	-	0.30	0.48	0.71		#
13,14-DiHDPE	361.2	193.2	-65	-10	-24	-6	$^2H_{11}$-14,15-DiHETrE	16.99	4.8	0.13	0.23	0.25	100	0.9985
20-HEPE	317.2	287.3	-50	-10	-20	-8	$^2H_8$-12-HETE	17.11	5.0	0.50	0.80	1.0	100	0.9985
9-HOTrE	293.2	171.2	-65	-10	-22	-8	$^2H_4$-9-HODE	17.23	5.2	0.25	0.37	0.50	500	0.9994
10,11-DiHDPE	361.2	153.2	-65	-10	-24	-6	$^2H_{11}$-14,15-DiHETrE	17.37	4.8	0.13	0.23	0.25	100	0.9987
8,9-DiHETrE	337.2	127.1	-70	-10	-30	-8	$^2H_{11}$-14,15-DiHETrE	17.48	5.1	0.25	0.42	0.50	200	0.9993
13-HOTrE	293.2	195.1	-70	-10	-24	-8	$^2H_4$-9-HODE	17.60	4.6	0.30	0.44	0.60	12	0.9961
18-HEPE	317.2	259.2	-55	-10	-17	-7	$^2H_8$-12-HETE	17.67	4.9	0.50	0.80	1.0	500	0.9972
15-deoxy-PGJ_2	315.2	271.2	-65	-10	-20	-6	$^2H_{11}$-14,15-DiHETrE	18.09	6.1	0.20	0.32	0.50	400	0.9989
19-HETE	319.3	230.9	-50	-10	-21	-6	$^2H_4$-9-HODE	18.15	5.3	5.0	8.0	10	500	0.9981
7,8-DiHDPE	361.2	113.1	-65	-10	-24	-6	$^2H_{11}$-14,15-DiHETrE	18.22	5.3	0.50	0.91	1.0	100	0.9988
20-HETE	319.2	289.1	-80	-10	-24	-6	$^2H_6$-20-HETE	18.40	5.1	0.50	0.80	1.0	500	0.9983
15-HEPE	317.2	219.2	-60	-10	-20	-10	$^2H_8$-12-HETE	18.43	5.1	0.63	0.99	1.3	500	0.9991
5,6-DiHETrE	337.2	145.1	-70	-10	-26	-10	$^2H_{11}$-14,15-DiHETrE	18.44	5.4	0.25	0.42	0.50	200	0.9989
11-HEPE	317.0	167.0	-40	-10	-21	-8	$^2H_8$-12-HETE	18.52	4.5	0.25	0.40	0.50	500	0.9962
8-HEPE	317.2	155.2	-60	-10	-20	-8	$^2H_8$-12-HETE	18.77	5.1	0.25	0.40	0.63	500	0.9986
12-HEPE	317.2	179.2	-65	-10	-20	-8	$^2H_8$-12-HETE	18.96	5.0	0.25	0.40	0.63	500	0.9989
9-HEPE	317.2	166.9	-40	-10	-19	-8	$^2H_8$-12-HETE	19.11	4.4	0.25	0.40	0.50	500	0.9970
21-HDHA	343.0	255.0	-60	-10	-18	-7	$^2H_8$-12-HETE	19.38	-	1.3	2.24	1.65		#
5-HEPE	317.2	115.1	-60	-10	-20	-6	$^2H_8$-12-HETE	19.49	5.2	0.20	0.32	0.50	500	0.9988
22-HDHA	343.2	313.2	-65	-10	-20	-7	$^2H_8$-12-HETE	19.49	-	1.40	2.41	2.80		#
4,5-DiHDPE	361.2	229.3	-65	-10	-24	-6	$^2H_{11}$-14,15-DiHETrE	19.51	4.7	1.0	1.8	2.0	100	0.9940

Tab. S1: Continued.

Analyte	Mass transition		MS parameters				Internal standard	t_R [1]	FWHM [2]	LOD [3]		Calibration range LLOQ [4] ULOQ [5]		r^2 [6]
	Q1	Q3	DP	EP	CE	CXP		[min]	[sec]	[nM]	[pg on column]	[nM]		
13-HODE	295.2	195.2	-80	-10	-26	-9	$^2H_4$-9-HODE	19.70	5.3	2.5	3.7	5.0	400	0.9985
9-HODE	295.2	171.1	-80	-10	-26	-7	$^2H_4$-9-HODE	19.81	5.2	2.5	3.7	5.0	400	0.9995
20-HDHA	343.2	241.2	-55	-10	-19	-7	$^2H_8$-12-HETE	20.07	4.9	0.25	0.43	0.50	20	0.9975
15(16)-EpODE	293.3	235.2	-65	-10	-20	-4	$^2H_4$-9(10)-EpOME	20.34	5.5	0.25	0.37	0.50	20	0.9973
15-HETE	319.2	219.2	-60	-10	-20	-8	$^2H_8$-12-HETE	20.45	5.0	0.50	0.80	1.3	500	0.9996
9(10)-EpODE	293.3	171.2	-65	-10	-20	-8	$^2H_4$-9(10)-EpOME	20.51	5.4	0.20	0.29	0.40	16	0.9953
17(18)-EpETE	317.2	215.2	-65	-10	-20	-6	$^2H_{11}$-14(15)-EpETrE	20.58	5.2	0.50	0.80	1.0	20	0.9994
16-HDHA	343.2	233.2	-55	-10	-19	-7	$^2H_8$-12-HETE	20.61	4.6	0.10	0.17	0.25	20	0.9993
17-HDHA	343.2	201.2	-60	-10	-20	-6	$^2H_8$-12-HETE	20.73	4.7	1.0	1.7	2.0	500	0.9990
13-HDHA	343.2	193.1	-55	-10	-19	-7	$^2H_8$-12-HETE	20.91	4.5	0.25	0.43	0.50	20	0.9985
12(13)-EpODE	293.2	183.1	-65	-10	-24	-8	$^2H_4$-9(10)-EpOME	20.93	5.1	0.25	0.37	0.50	20	0.9960
13-oxo-ODE	293.2	195.1	-75	-10	-20	-8	$^2H_4$-9-HODE	20.93	4.8	0.50	0.74	1.0	20	0.9966
11-HETE	319.2	167.2	-60	-10	-23	-7	$^2H_8$-12-HETE	20.98	4.7	0.25	0.40	0.50	500	0.9995
10-HDHA	343.2	153.2	-45	-10	-21	-7	$^2H_8$-12-HETE	21.14	4.4	0.25	0.43	0.50	20	0.9994
14-HDHA	343.2	205.2	-50	-10	-19	-7	$^2H_8$-12-HETE	21.14	4.2	0.50	0.86	1.0	500	0.9979
9-oxo-ODE	293.2	185.1	-90	-10	-28	-8	$^2H_4$-9-HODE	21.17	5.0	0.50	0.74	1.0	20	0.9934
15-oxo-ETE	317.2	113.1	-65	-10	-25	-8	$^2H_8$-5-HETE	21.18	4.3	0.25	0.40	0.50	100	0.9981
14(15)-EpETE	317.2	207.2	-65	-10	-20	-6	$^2H_{11}$-14(15)-EpETrE	21.25	4.8	0.25	0.40	0.50	20	0.9952
8-HETE	319.2	155.2	-60	-10	-22	-6	$^2H_8$-12-HETE	21.33	4.5	0.50	0.80	1.3	500	0.9989
12-HETE	319.2	179.2	-60	-10	-20	-8	$^2H_8$-12-HETE	21.36	4.4	0.25	0.40	0.50	500	0.9970
11(12)-EpETE	317.2	167.2	-65	-10	-20	-6	$^2H_{11}$-14(15)-EpETrE	21.40	4.3	0.25	0.40	0.50	20	0.9970
11-HDHA	343.2	121.1	-45	-10	-20	-7	$^2H_8$-5-HETE	21.41	4.0	0.10	0.17	0.25	20	0.9992
7-HDHA	343.2	141.2	-55	-10	-19	-7	$^2H_8$-5-HETE	21.54	4.2	0.50	0.86	1.0	500	0.9984
8(9)-EpETE	317.2	127.2	-65	-10	-20	-6	$^2H_{11}$-14(15)-EpETrE	21.55	4.9	0.50	0.80	1.0	20	0.9969
9-HETE	319.2	167.2	-60	-10	-23	-7	$^2H_8$-5-HETE	21.64	4.2	1.3	2.0	2.5	1000	0.9987
15(S)-HETrE	321.2	221.2	-70	-10	-23	-10	$^2H_8$-5-HETE	21.68	4.3	0.25	0.40	0.50	200	0.9984
8-HDHA	343.2	189.2	-50	-10	-19	-7	$^2H_8$-5-HETE	21.73	3.8	0.50	0.86	0.50	20	0.9976
5-HETE	319.2	115.2	-60	-10	-21	-7	$^2H_8$-5-HETE	21.88	4.1	0.25	0.40	0.50	1000	0.9990
4-HDHA	343.2	101.1	-55	-10	-19	-7	$^2H_8$-5-HETE	22.31	3.7	0.25	0.43	0.25	500	0.9986

Tab. S1: Continued.

Analyte	Mass transition		MS parameters				Internal standard	t_R [1]	FWHM [2]	LOD [3]		Calibration range		r^2 [6]
												LLOQ [4]	ULOQ [5]	
	Q1	Q3	DP	EP	CE	CXP		[min]	[sec]	[nM]	[pg on column]	[nM]		
19(20)-EpDPE	343.2	241.2	-65	-10	-20	-7	$^2H_{11}$-14(15)-EpETrE	22.39	3.3	0.25	0.43	0.50	20	0.9994
12(13)-EpOME	295.3	195.2	-80	-10	-23	-8	$^2H_4$-9(10)-EpOME	22.45	3.8	0.10	0.15	0.25	40	0.9980
14(15)-EpETrE	319.2	219.3	-65	-10	-20	-4	$^2H_{11}$-14(15)-EpETrE	22.60	3.8	0.25	0.40	0.50	20	0.9985
9(10)-EpOME	295.3	171.1	-80	-10	-23	-8	$^2H_4$-9(10)-EpOME	22.64	3.8	0.10	0.15	0.25	40	0.9949
16(17)-EpDPE	343.2	233.2	-65	-10	-20	-7	$^2H_{11}$-14(15)-EpETrE	22.80	3.5	0.25	0.43	0.50	20	0.9978
13(14)-EpDPE	343.2	193.2	-65	-10	-20	-7	$^2H_{11}$-14(15)-EpETrE	22.88	3.4	0.25	0.43	0.50	20	0.9961
5-oxo-ETE	317.2	273.2	-65	-10	-22	-6	$^2H_4$-9(10)-EpOME	22.95	3.5	1.0	1.6	2.0	20	0.9998
10(11)-EpDPE	343.2	153.2	-65	-10	-20	-7	$^2H_{11}$-14(15)-EpETrE	22.98	3.4	0.13	0.22	0.25	20	0.9990
11(12)-EpETrE	319.3	167.2	-60	-10	-20	-7	$^2H_{11}$-14(15)-EpETrE	23.09	3.3	0.25	0.40	0.50	40	0.9965
8(9)-EpETrE	319.2	155.2	-65	-10	-20	-6	$^2H_{11}$-14(15)-EpETrE	23.24	3.3	0.50	0.80	1.0	20	0.9993
5(6)-EpETrE	319.2	191.1	-60	-10	-20	-7	$^2H_{11}$-14(15)-EpETrE	23.41	2.9	1.0	1.6	2.0	20	0.9974
5(S)-HETrE	321.2	115.1	-70	-10	-19	-9	$^2H_8$-5-HETE	23.55	3.0	0.1	0.2	0.2	500	0.9991
9(10)-ep-stearic acid	297.0	170.8	-100	-10	-28	-11	$^2H_4$-9(10)-EpOME	23.97	3.5	1.0	1.5	2.0	500	0.9953

1) Relative standard deviation for t_R within one batch was ≤ 0.18 % (± 0.01 min).
2) Full peak width at half maximum (FWHM) was determined as mean width of standards, concentration 1-200 nM.
3) LOD was set to the lowest concentration yielding a signal to noise ratio ≥ 3.
4) LLOQ was set to the lowest calibration standard yielding a signal to noise ratio ≥ 5 and an accuracy within the calibration curve of ± 20 %.
5) ULOQ concentration does not represent the end of the dynamic range, but is the highest calibration standard injected.
6) Calibration was performed as weighted regression using 1/x2 weighting.
#) 19-HEPE and 21- and 22 HDHA are quantified based on a response factor relative to 20-HEPE and 20-HDHA respectively.

Tab. S2: List of all internal standards used for the quantification of oxylipins with their LC-ESI(-)-MS/MS parameters. Shown are the mass transitions for quantification in scheduled SRM mode, electronical MS parameters (declustering potential (DP), entrance potential (EP), collision energy (CE), collision exit potential (CXP)), and retention time (t_R).

Analyte	Mass transition		MS parameters				t_R
	Q1	Q3	DP	EP	CE	CXP	[min]
C19-17-*epi*-17-F1t-PhytoP	341.3	239	-70	-10	-35	-8	6.02
^{2}H4-6-keto-PGF$_{1\alpha}$	373.3	167.1	-80	-10	-36	-8	6.10
$^2H_4$-15-F$_{2t}$-IsoP	357.2	196.8	-50	-6	-33	-8	7.54
$^2H_4$-TXB$_2$	373.3	173.2	-65	-10	-24	-8	7.64
$^2H_{11}$-5(*R,S*)-5-F$_{2t}$-IsoP	364.3	115.2	-40	-10	-29	-10	7.97
$^2H_4$-PGE$_2$	355.2	275.3	-60	-10	-25	-6	8.93
C21-15-F$_{2t}$-IsoP	367.2	193.1	-60	-10	-35	-8	9.18
$^2H_4$-PGD$_2$	355.2	275.3	-60	-10	-25	-6	9.43
$^2H_4$-LTB$_4$	339.2	197.2	-65	-10	-23	-9	14
$^2H_4$-9,10-DiHOME	317.2	203.4	-80	-10	-29	-8	15.13
$^2H_{11}$-14,15-DiHETrE	348.2	207.1	-65	-10	-25	-10	15.83
$^2H_6$-20-HETE	325.2	295.2	-70	-10	-24	-6	18.31
$^2H_4$-9-HODE	299.2	172.3	-80	-10	-26	-6	19.69
$^2H_8$-12-HETE	327.2	184.2	-65	-10	-22	-8	21.2
$^2H_8$-5-HETE	327.2	116.1	-60	-10	-21	-8	21.75
$^2H_{11}$-14(15)-EpETrE	330.2	219.3	-65	-10	-20	-4	22.48
$^2H_4$-9(10)-EpOME	299.2	172.2	-80	-10	-23	-8	22.54

Tab. S3: Total concentrations of IsoP (i.e. free and esterified) in HCT116 cells following incubation with 50 µM and 200 µM t-butylhydroperoxide for 30 min, 1 h and 2 h. Shown are the mean ± SD. For analytes below the limit of quantification the LLOQ is indicated.

			control		50µM		200 µM	
	analyte [fmol/10^6 cells]	incubation time	Mean	SD	Mean	SD	Mean	SD
AA	5(*R,S*)-F_{2t}-IsoP	30 min	12	3	47	5	123	16
		1h	11	2	47	8	165	19
		2 h	15	7	43	13	232	115
	15-F_{2t}-IsoP (8-*iso*-PGF_{2a})	30 min	< 5.0		15	2	34	3
		1h	< 5.0		14	2	44	2
		2 h	< 5.0		12	3	54	25
AdA	*ent*-7(*R,S*)-F_{2t}-dihomo-IsoP	30 min	< 2.5		4	0	9	1
		1h	< 2.5		4	1	14	3
		2 h	< 2.5		4	1	18	10
	17(*R,S*)-F_{2t}-dihomo-IsoP 2	30 min	< 3.7		< 3.7		4	0
		1h	< 3.7		< 3.7		5	1
		2 h	< 3.7		< 3.7		5	1
EPA	5(*R,S*)-F_{3t}-IsoP	30 min	40	11	167	39	424	17
		1h	39	4	155	30	625	113
		2 h	44	19	133	46	737	300
DHA	4(*R,S*)-F_{4t}-NeuroP	30 min	6	1	26	5	69	6
		1h	6	1	24	5	89	13
		2 h	7	2	22	3	105	48
	10-F_{4t}-NeuroP	30 min	< 2.5		< 2.5		6	1
		1h	< 2.5		< 2.5		7	1
		2 h	< 2.5		< 2.5		9	4
	10-*epi*-F_{4t}-NeuroP	30 min	< 5.0		6	0	13	2
		1h	< 5.0		5	1	16	2
		2 h	< 5.0		6	1	20	9

(A) α-Linolenic acid derived PhytoP and PhytoF

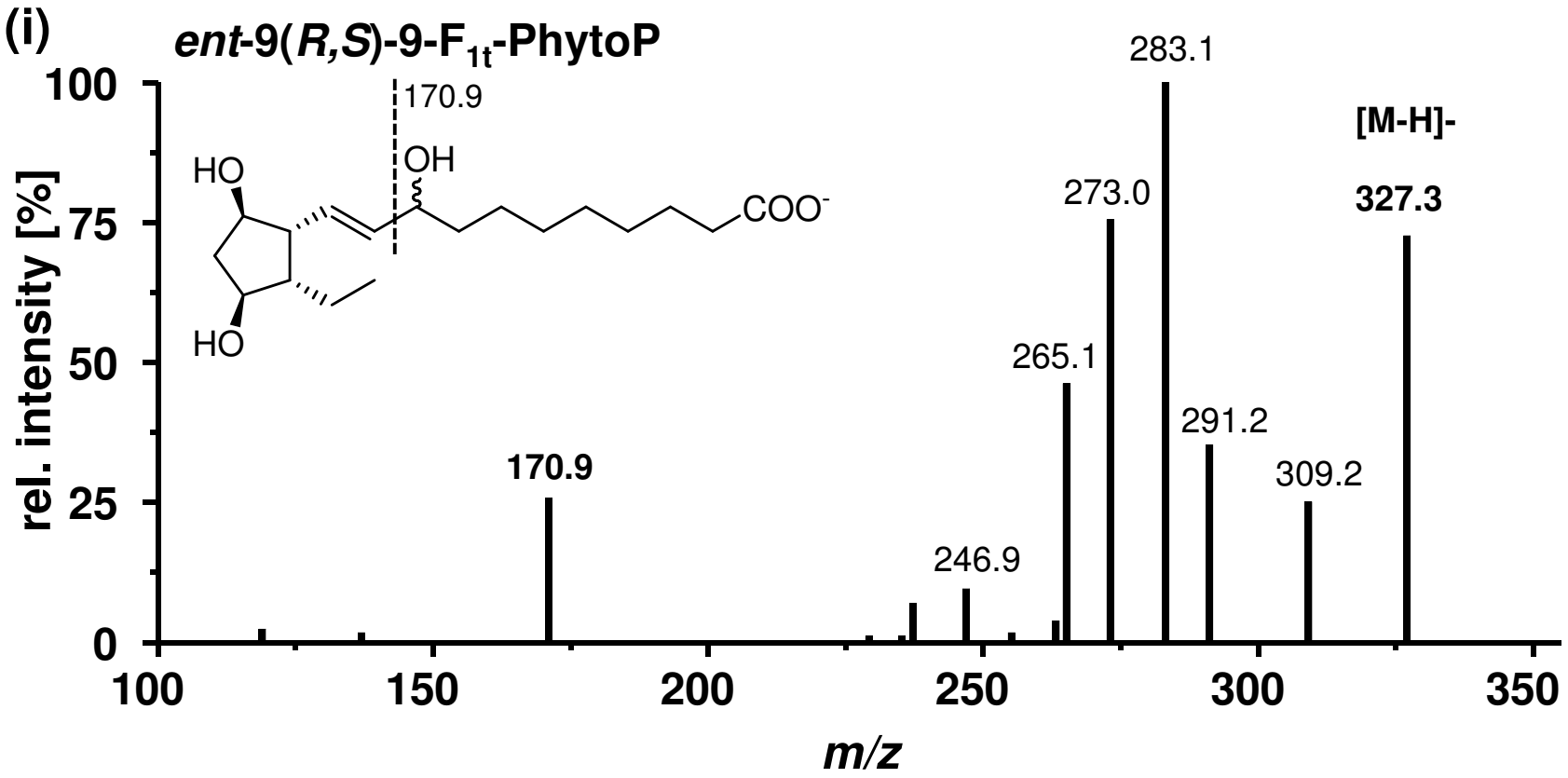

Fig. S1: Product ion spectra of isoprostanoids and isofurans derived from different PUFA. The spectra were aquired via CID of the ESI(-)-generated carboxylate-anion $[M-H]^-$ using a collision energy ramp from -17 to -30.
(A) (i)-(v) α-Linolenic acid derived PhytoP and PhytoF
(B) (i)-(iii) Arachidonic acid derived F_{2t}-IsoP
(C) (i)-(ii) Eicosapentaenoic acid derived F_{3t}-IsoP
(D) (i)-(iv) Docosahexaenoic acid derived F_{4t}-NeuroP and NeuroF
(E) (i)-(iv) Adrenic acid derived F_{2t}-dihomo-IsoP and dihomo-IsoF
(F) (i) Docosapentaenoic acid derived NeuroP
(G) (i)-(iv) Internal Standards

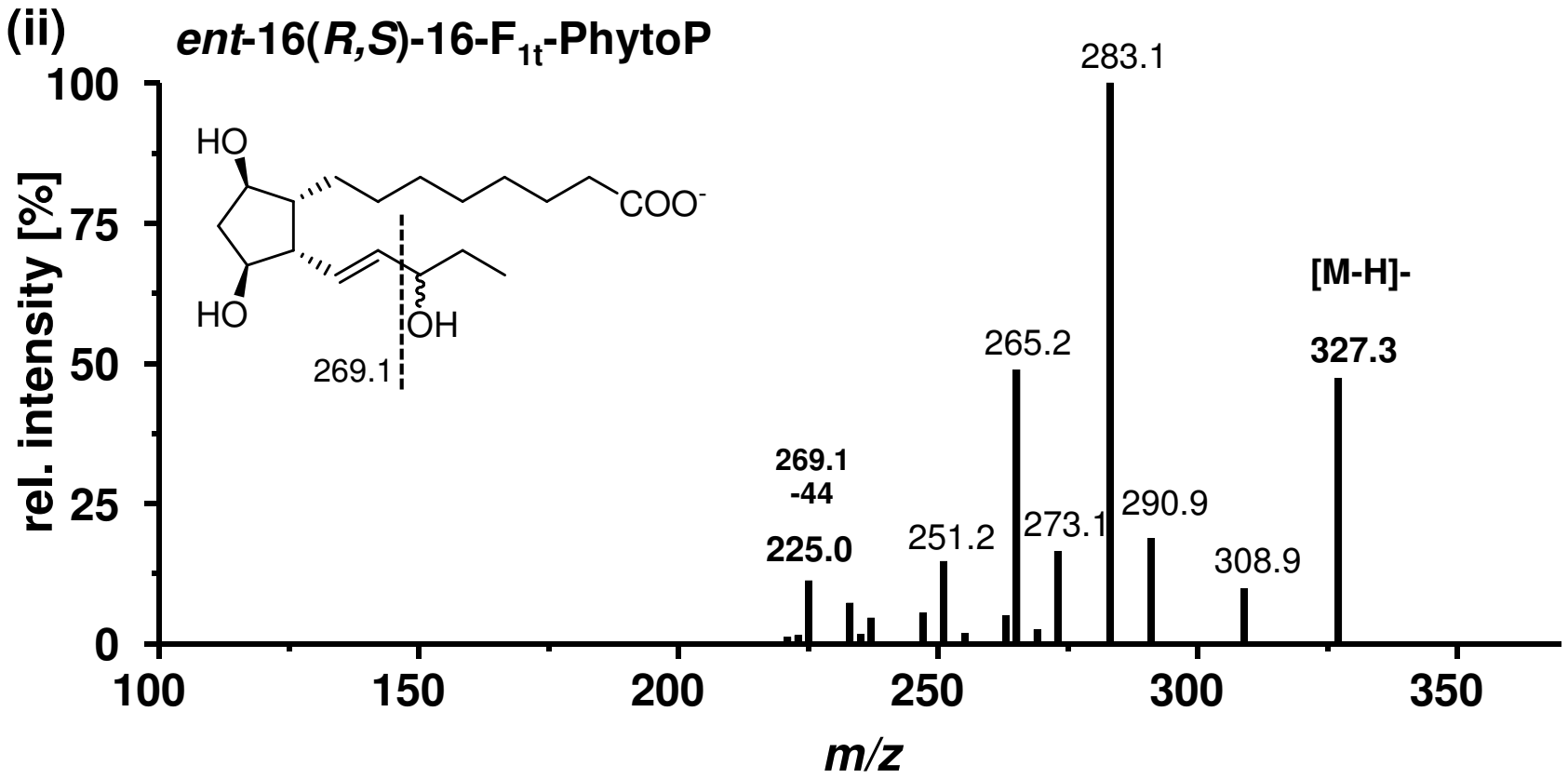

Fig. S1: Continued.

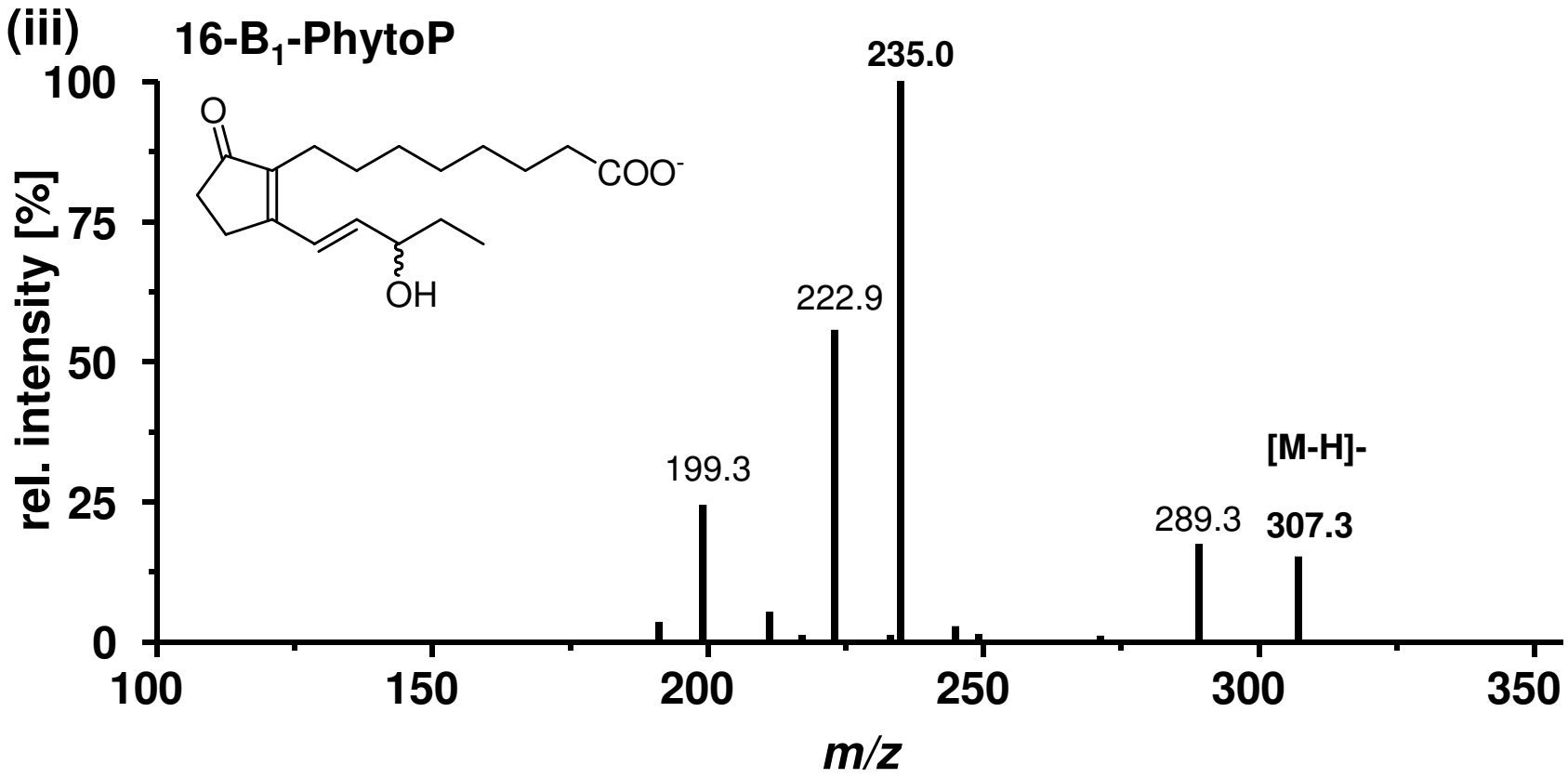

Fig. S1: Continued.

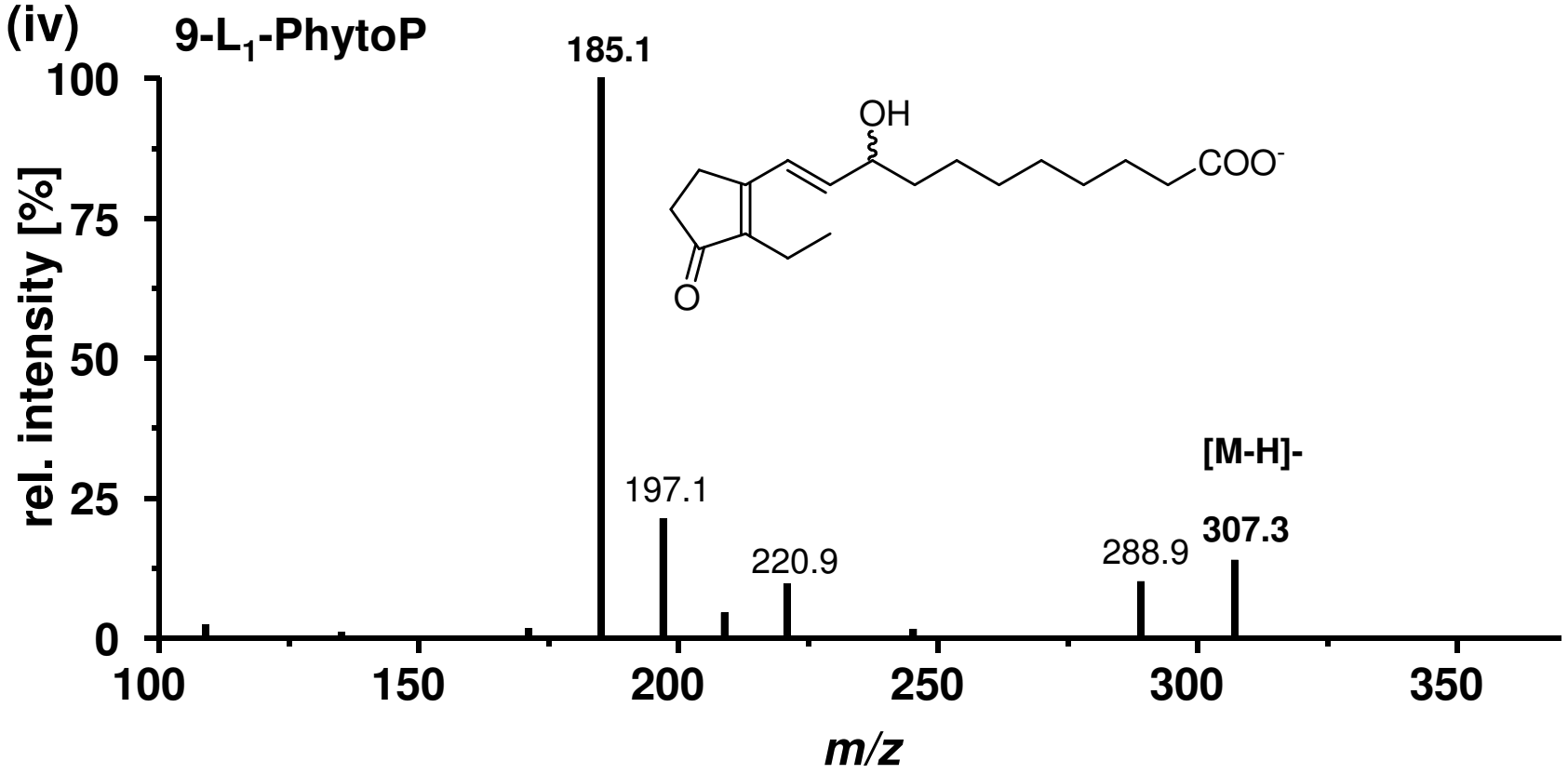

Fig. S1: Continued.

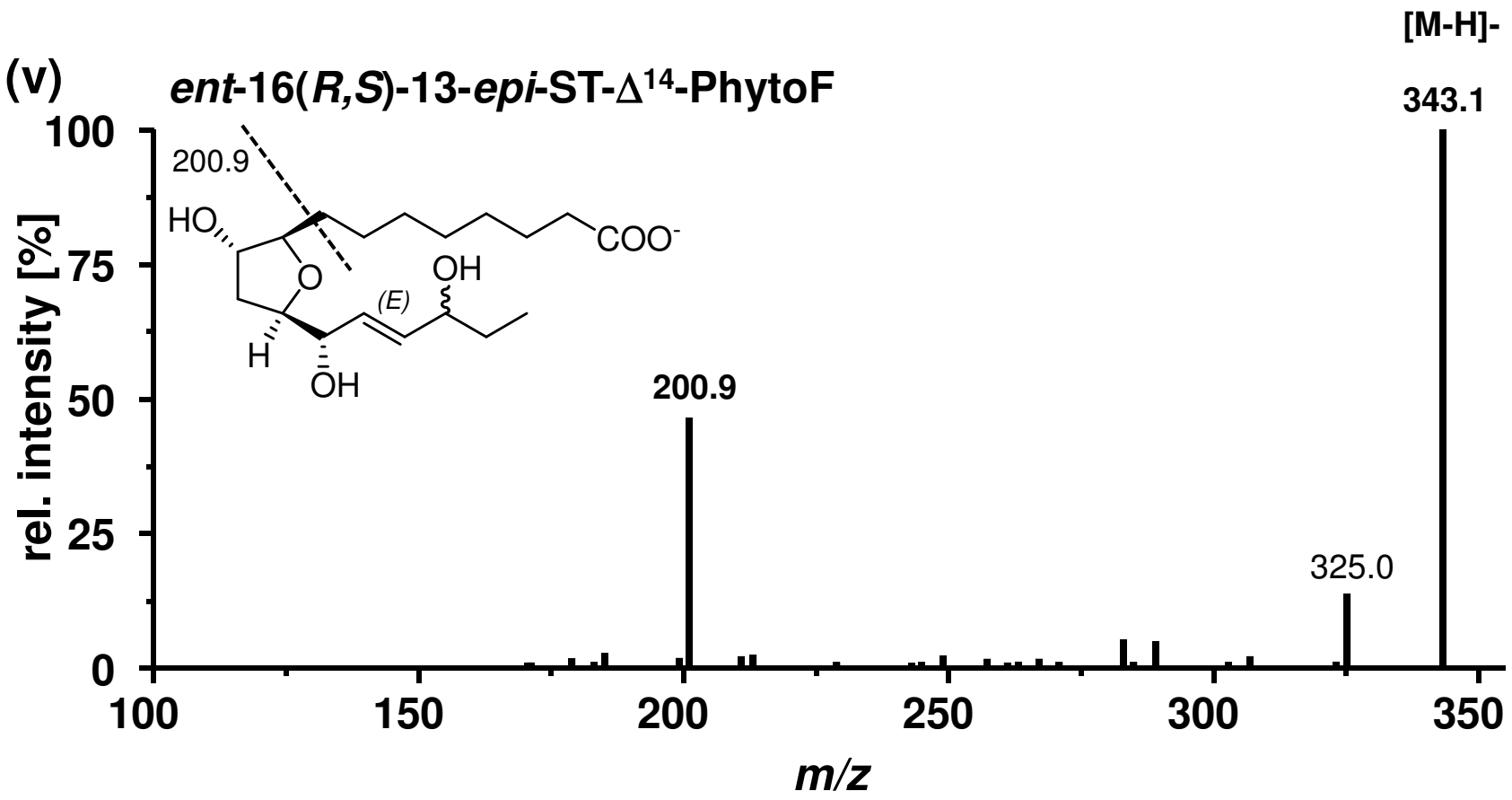

Fig. S1: Continued.

(B) Arachidonic acid derived IsoP

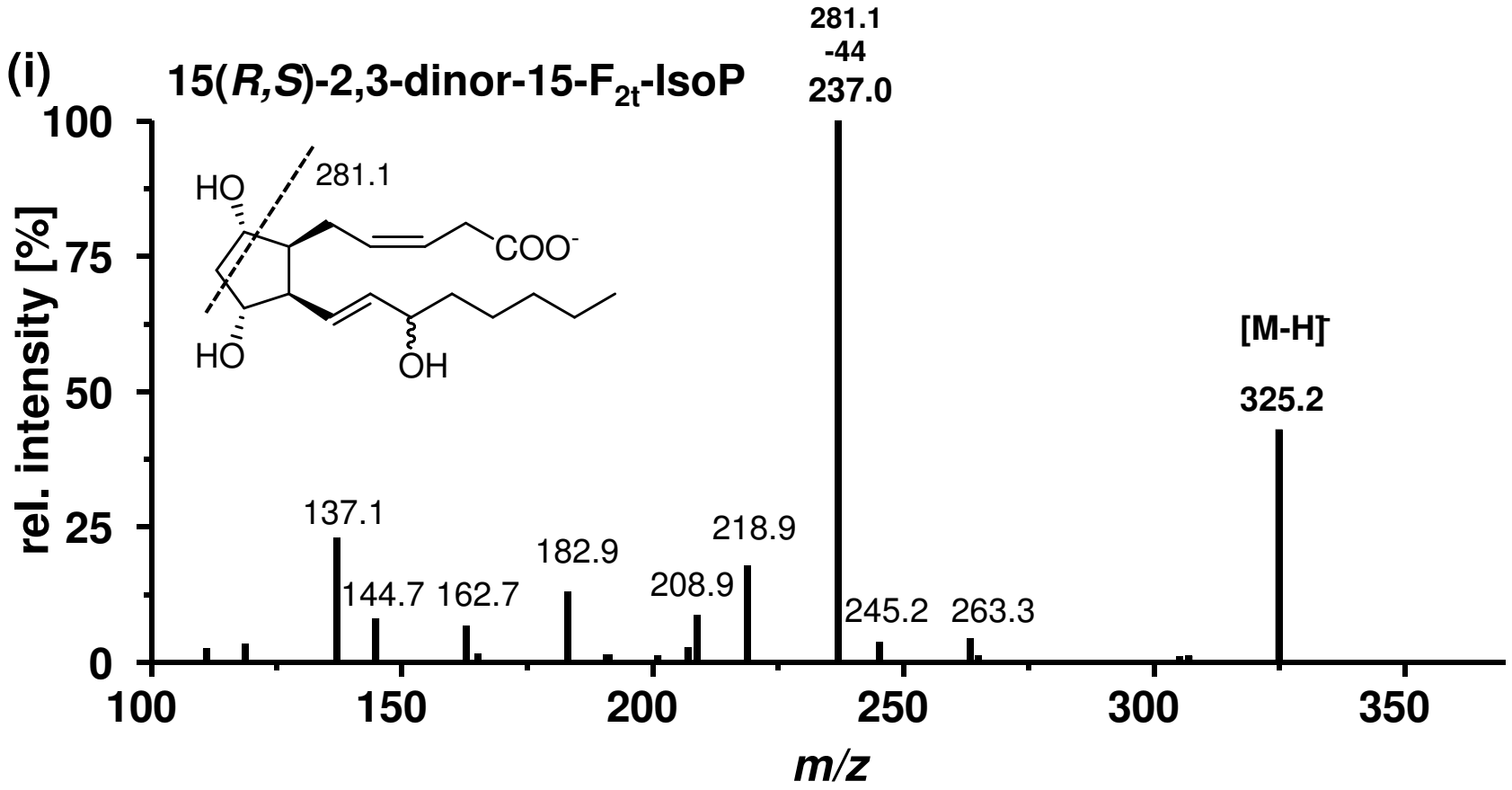

Fig. S1: Continued.

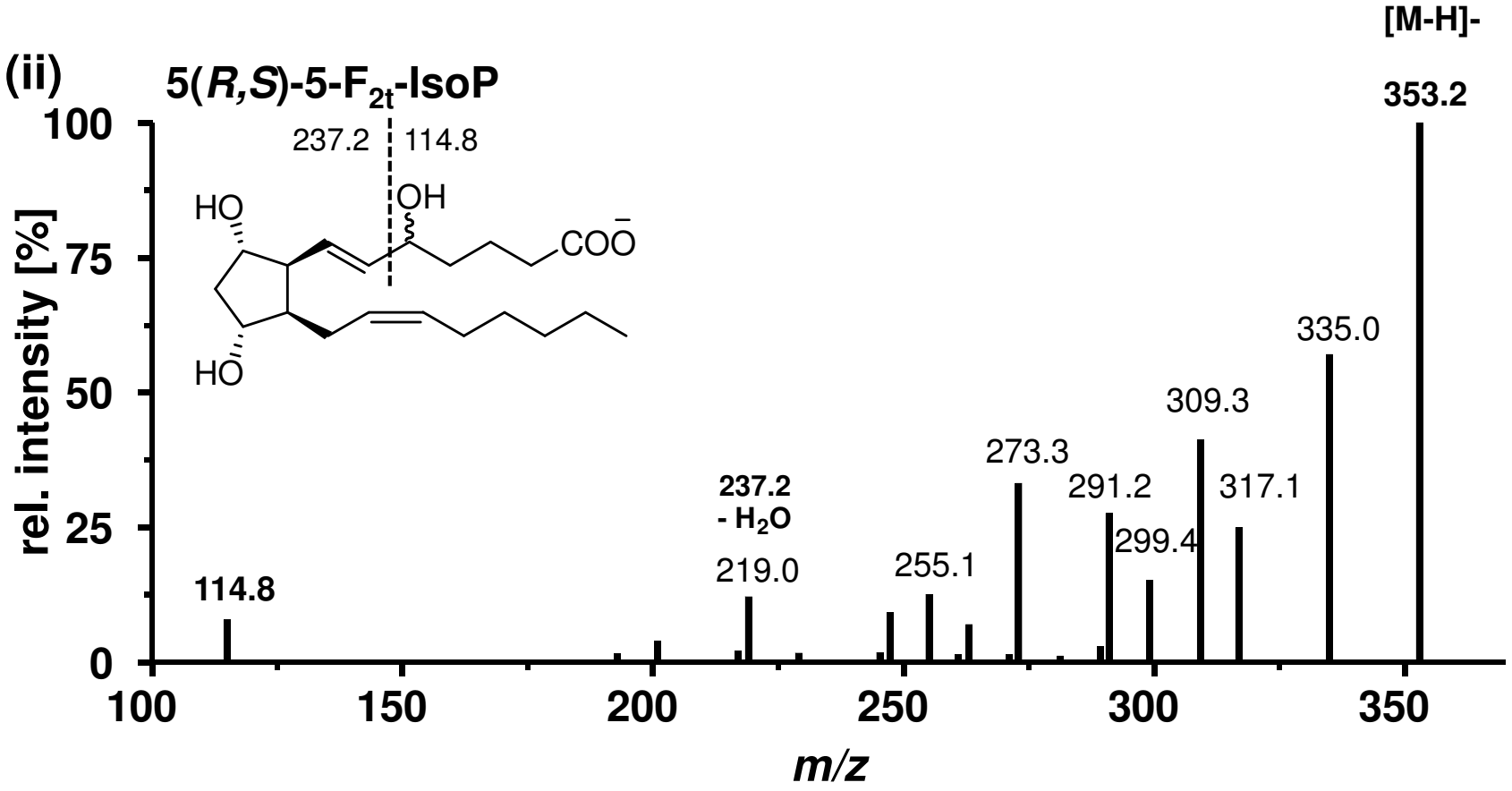

Fig. S1: Continued.

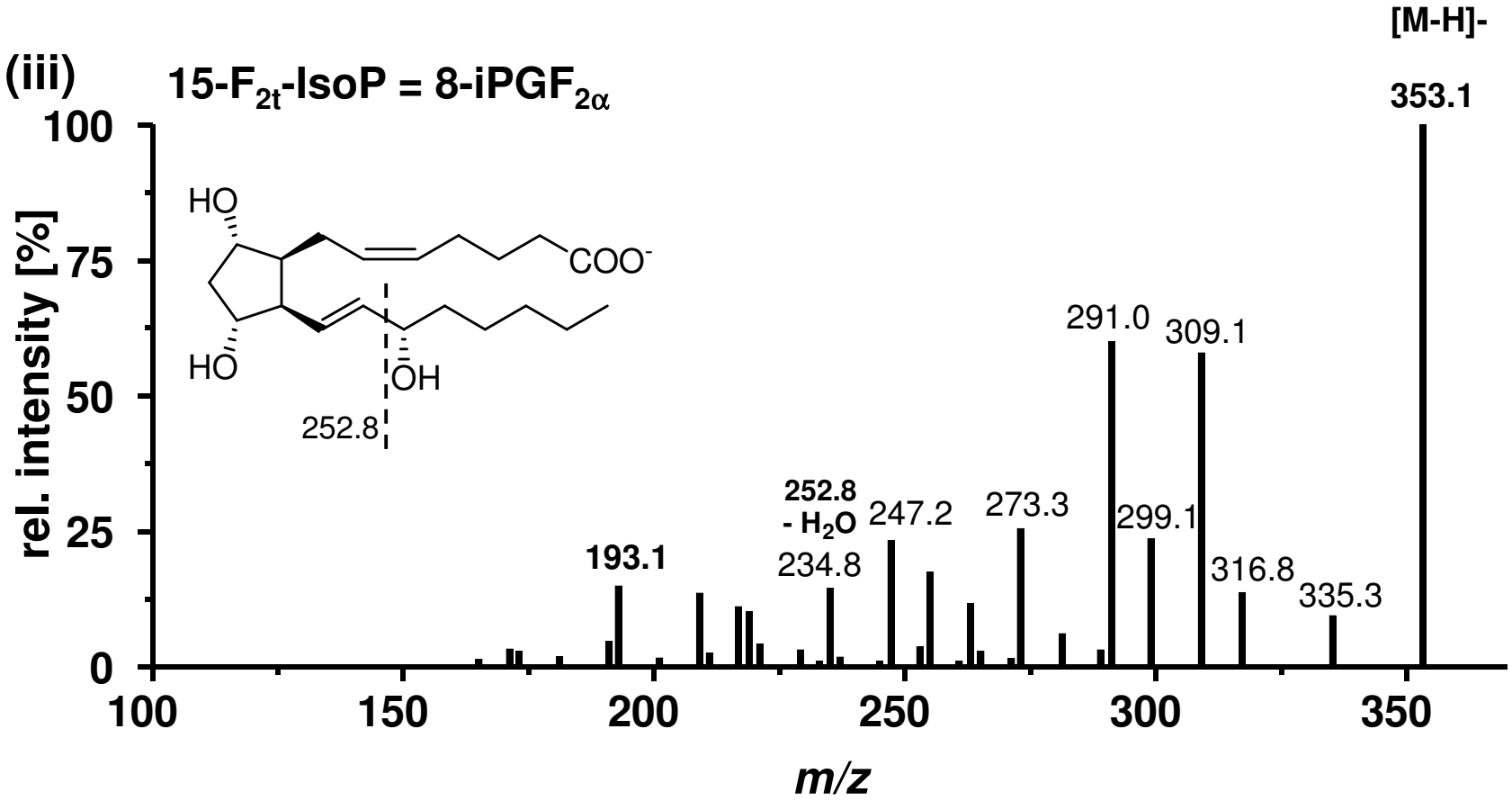

Fig. S1: Continued.

(C) Eicosapentaenoic acid derived IsoP

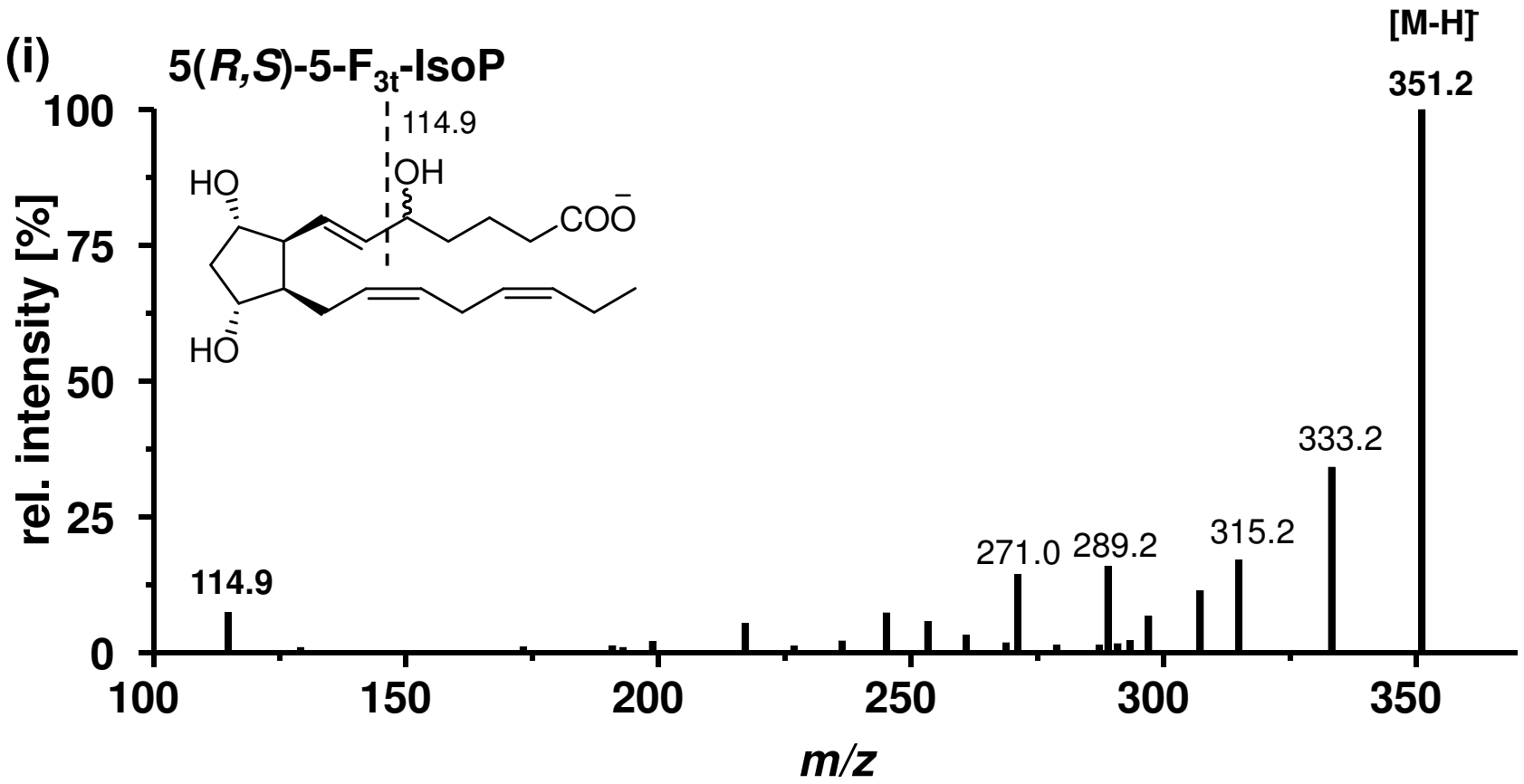

Fig. S1: Continued.

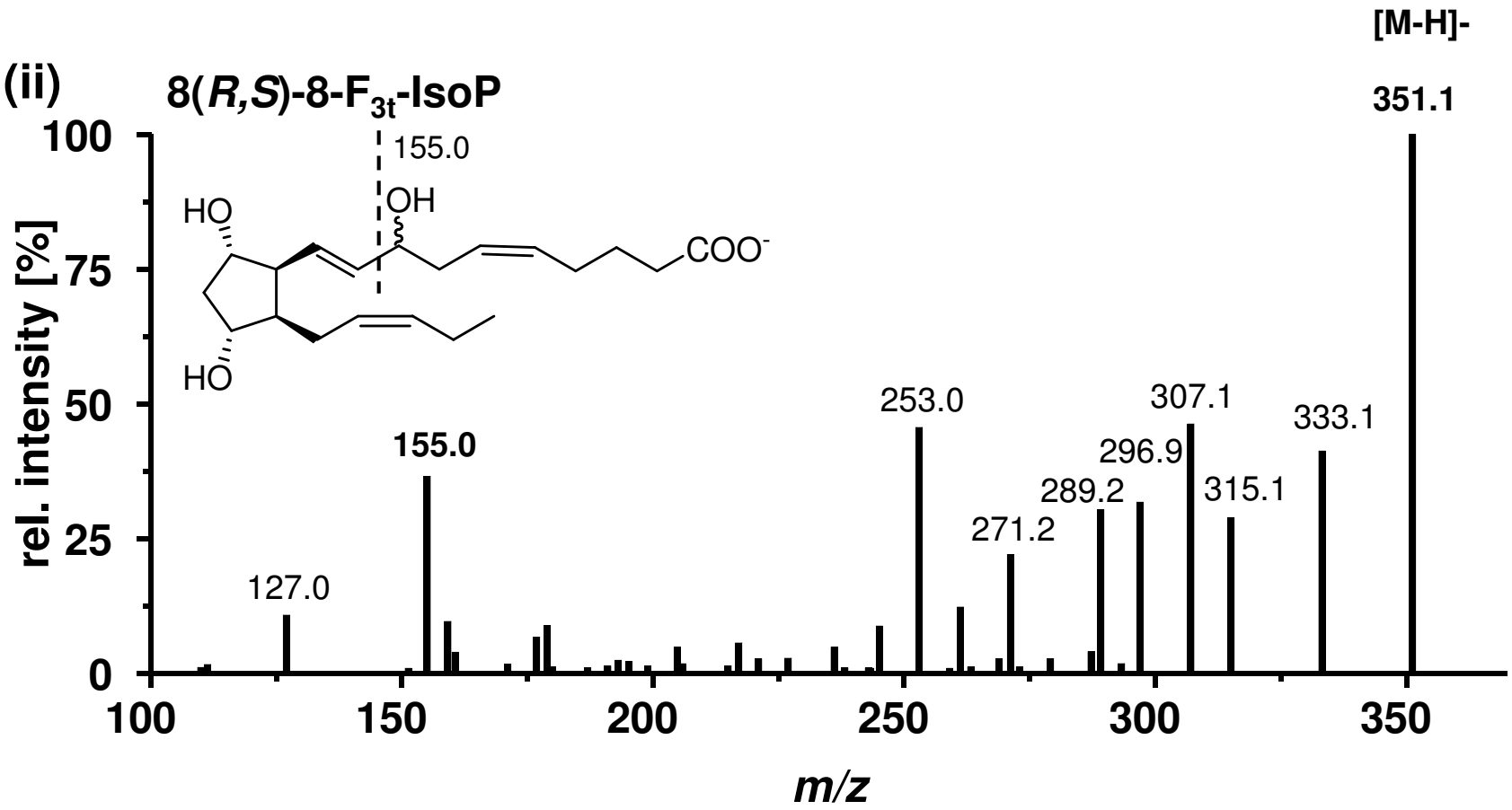

Fig. S1: Continued.

(D) Docosahexaenoic acid derived NeuroP and NeuroF

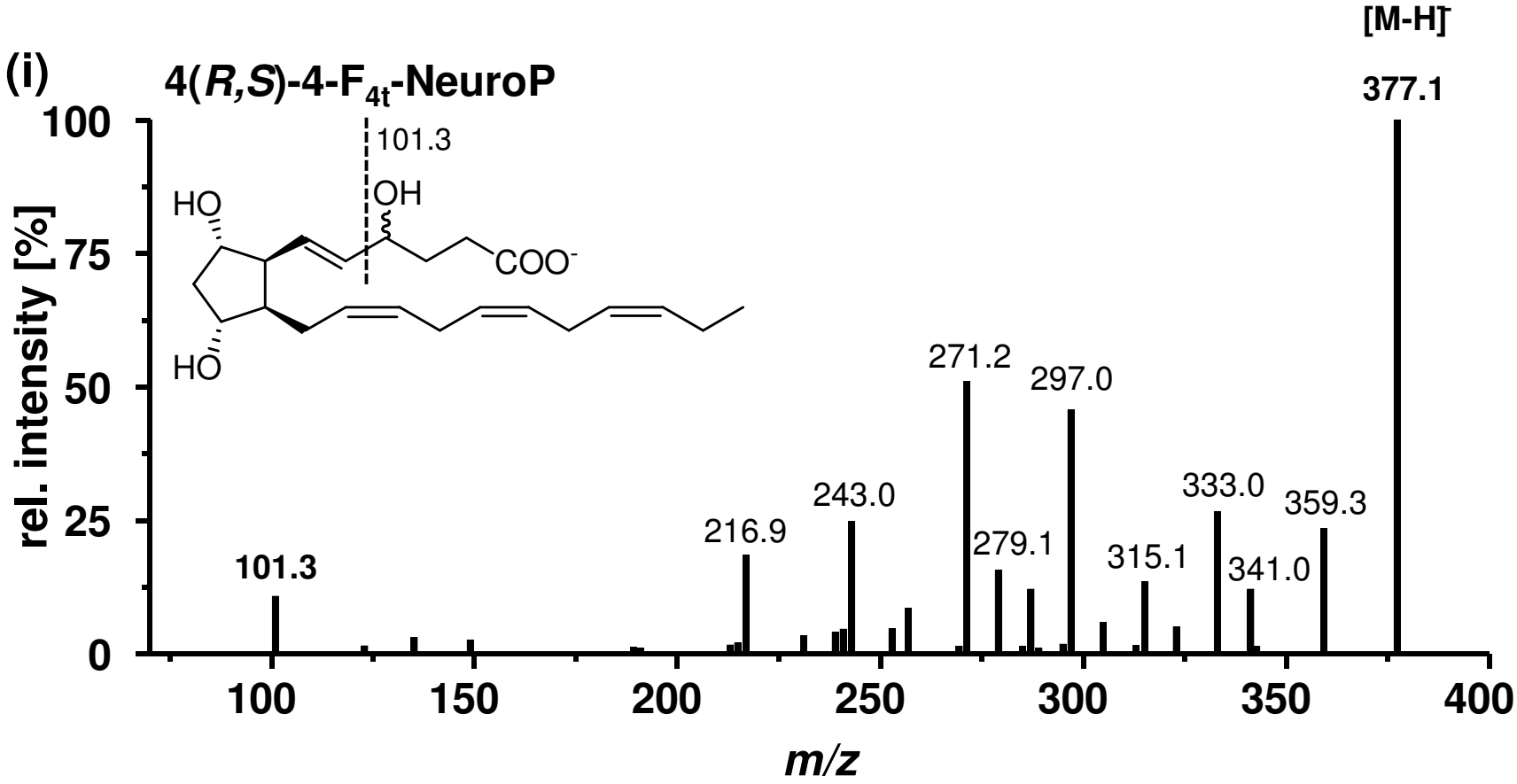

Fig. S1: Continued.

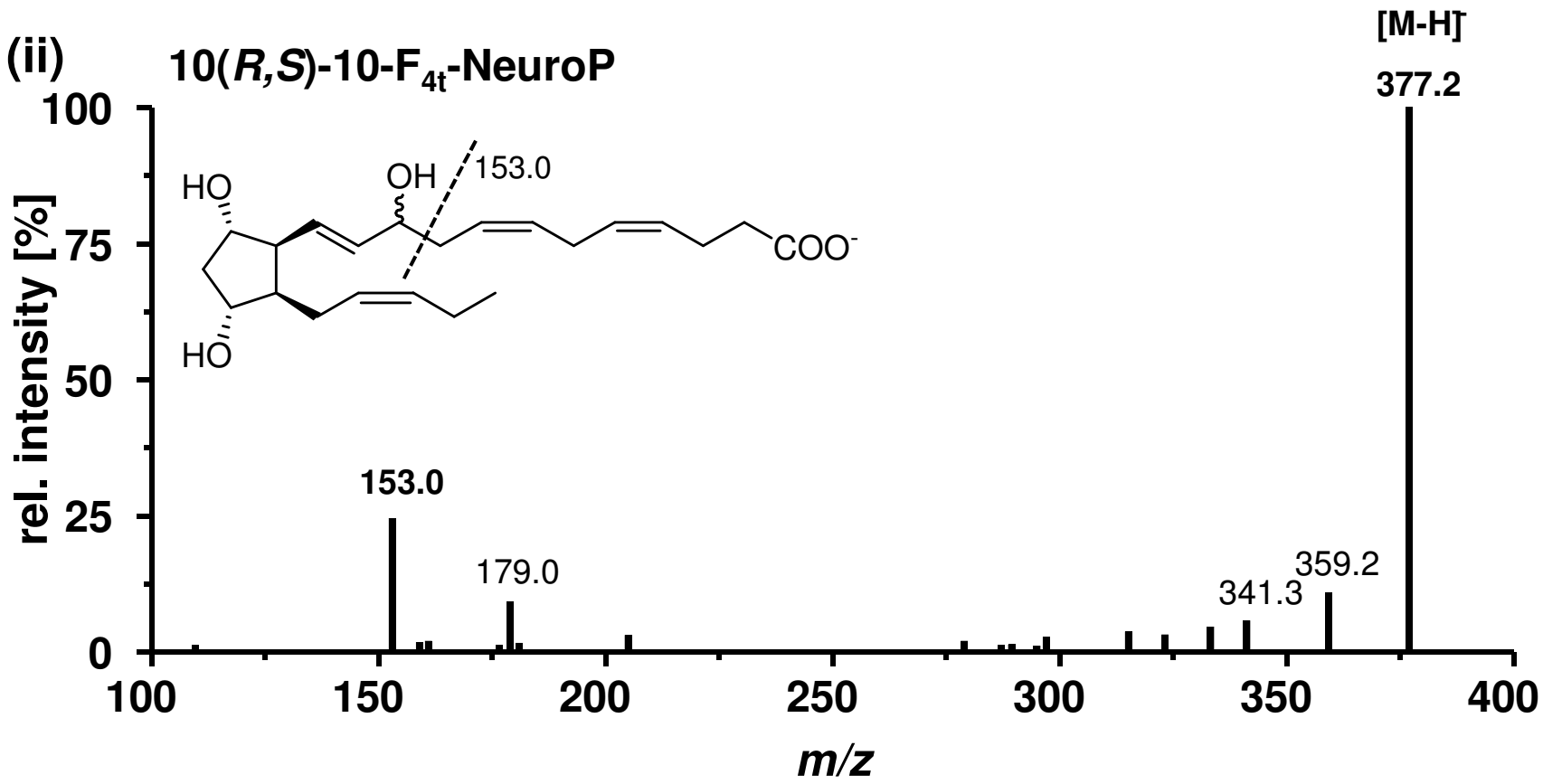

Fig. S1: Continued.

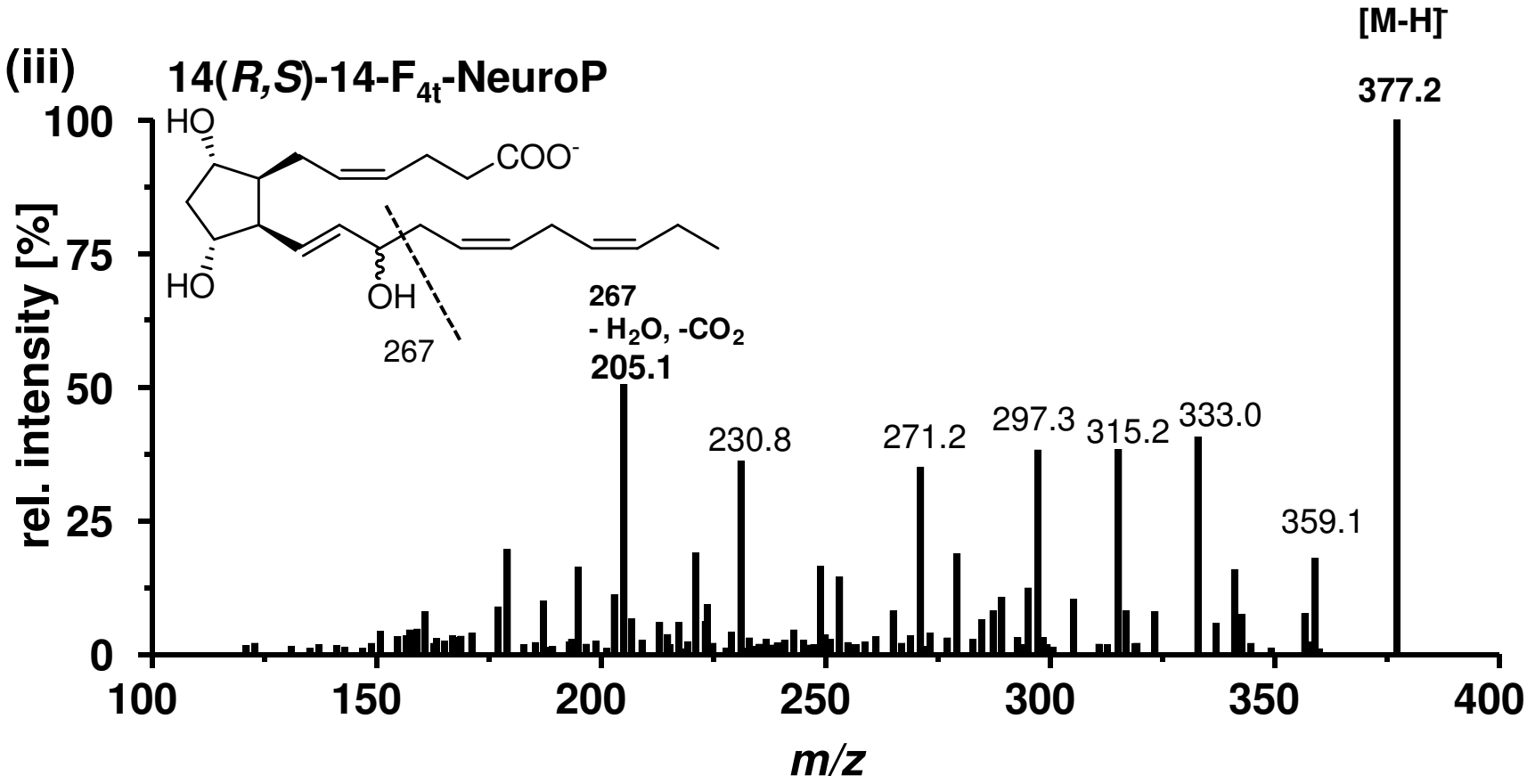

Fig. S1: Continued.

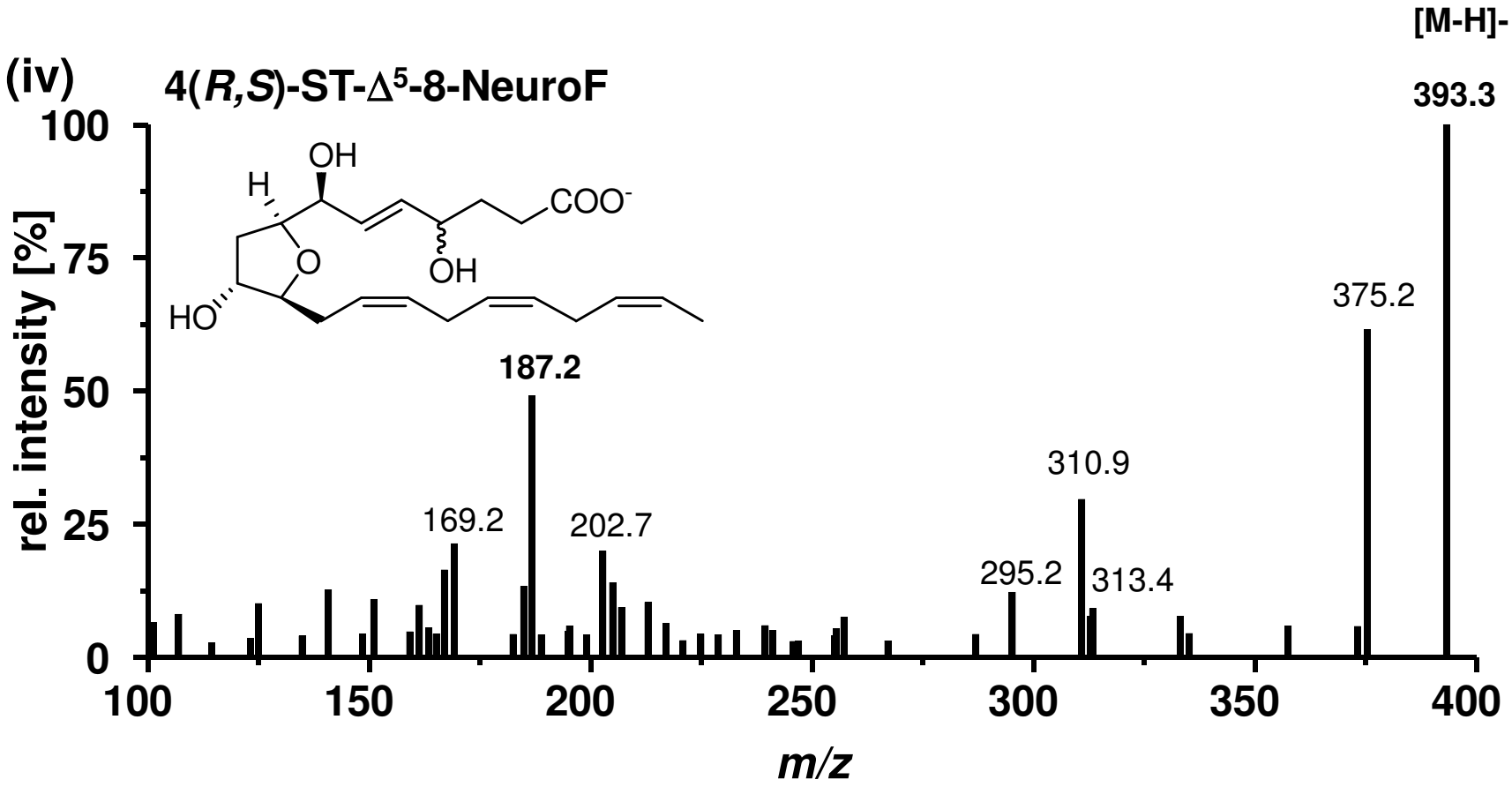

Fig. S1: Continued.

(E) Adrenic acid derived dihomo-IsoP and dihomo-IsoF

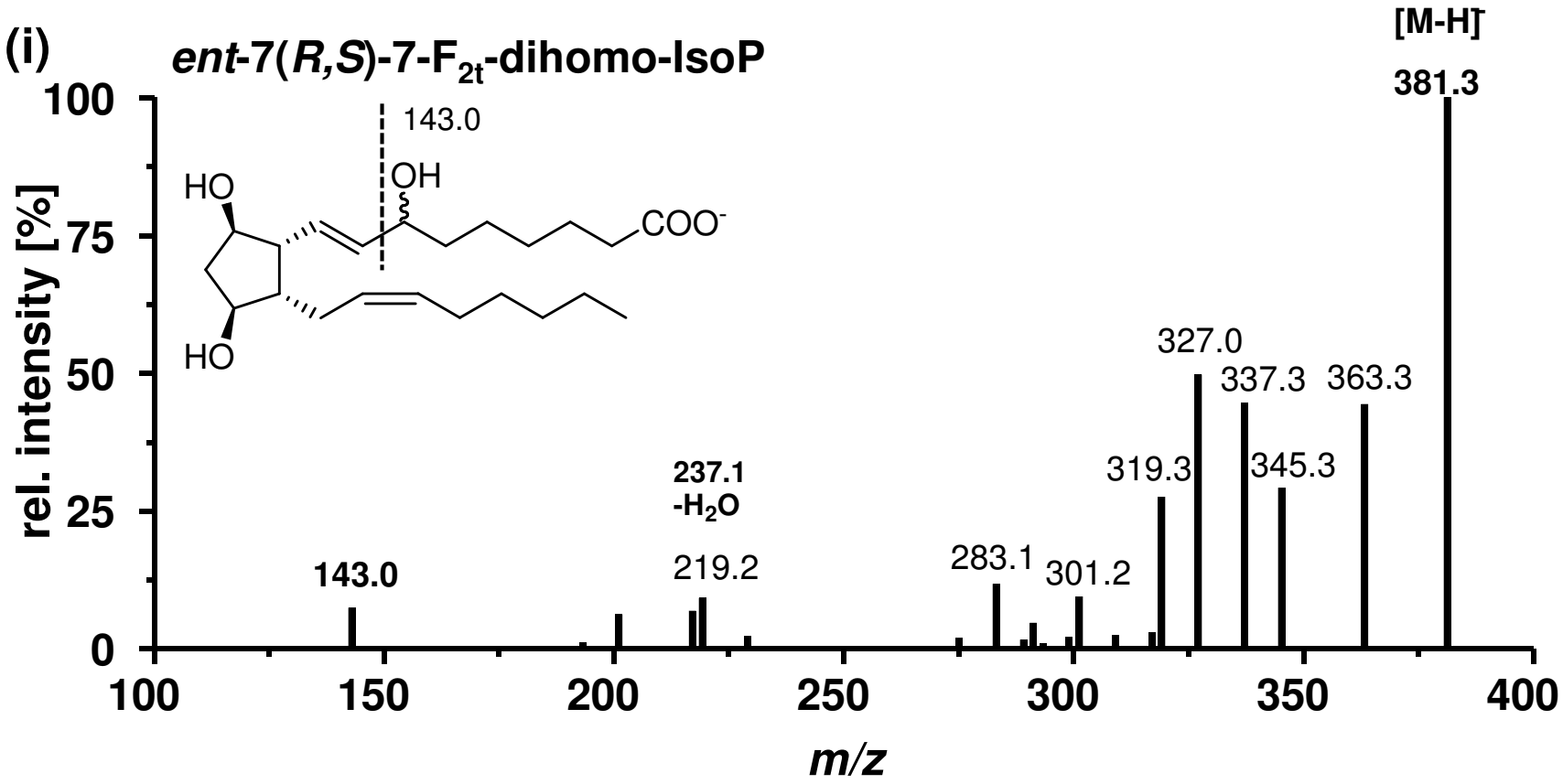

Fig. S1: Continued.

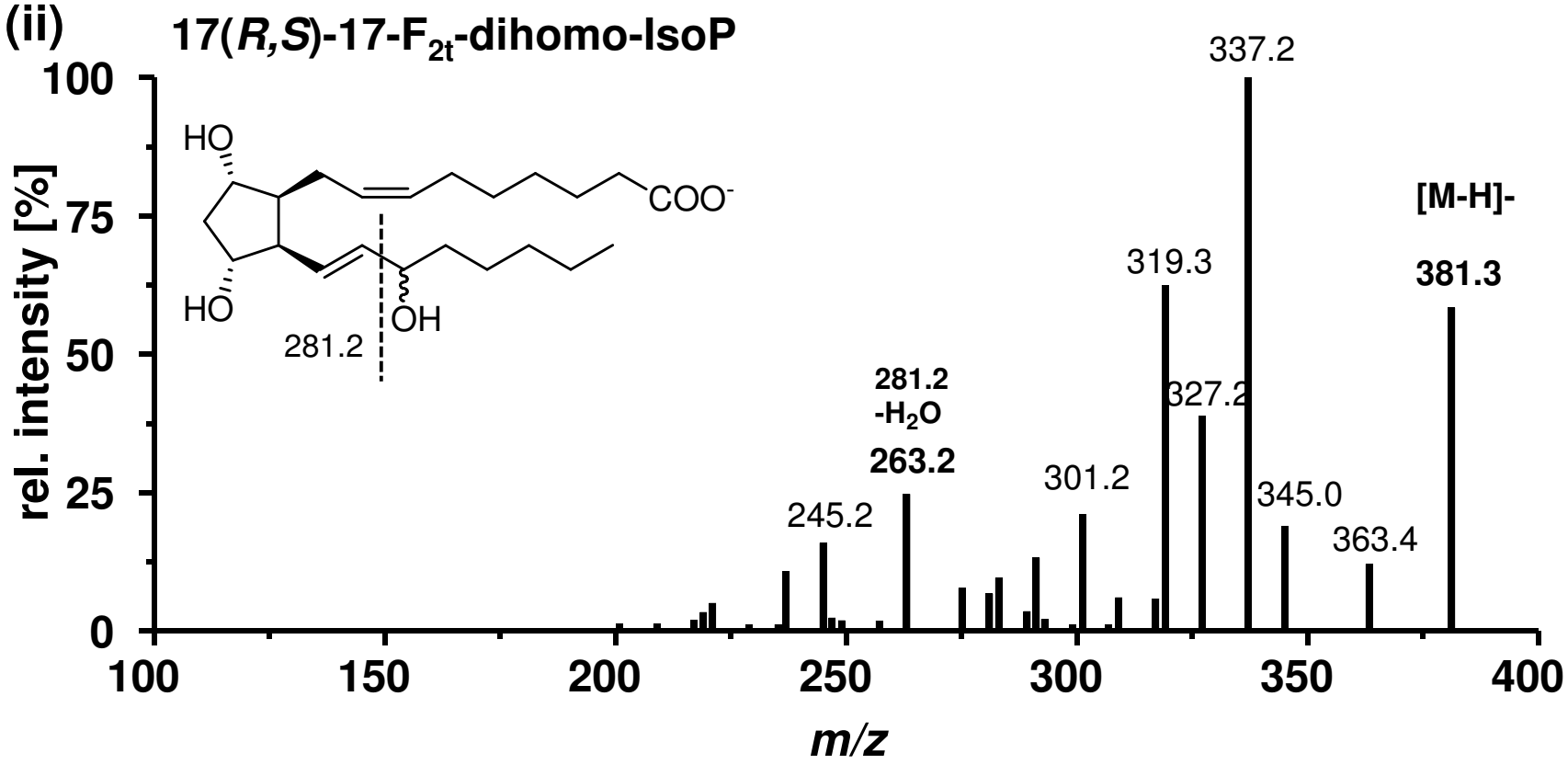

Fig. S1: Continued.

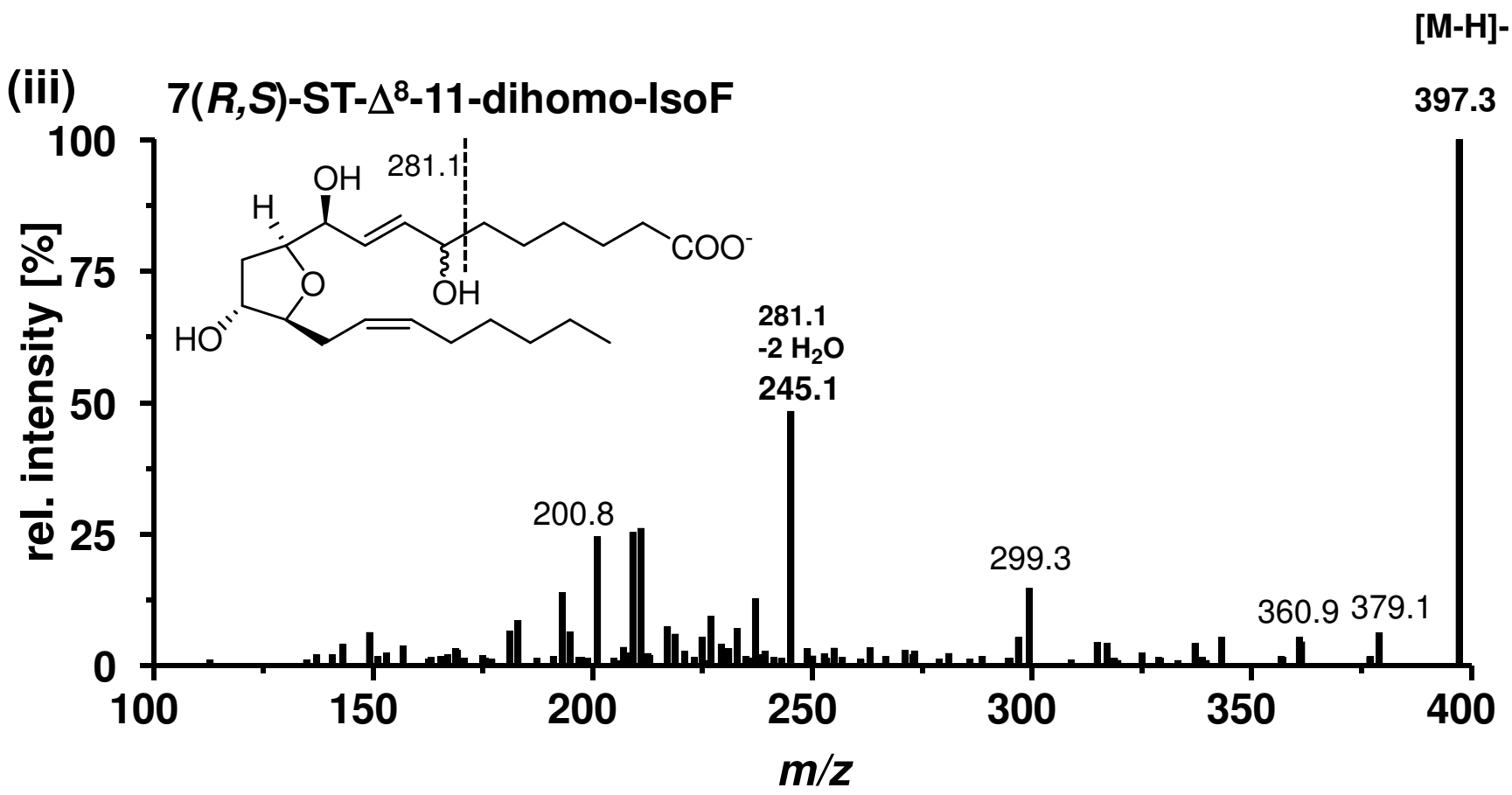

Fig. S1: Continued.

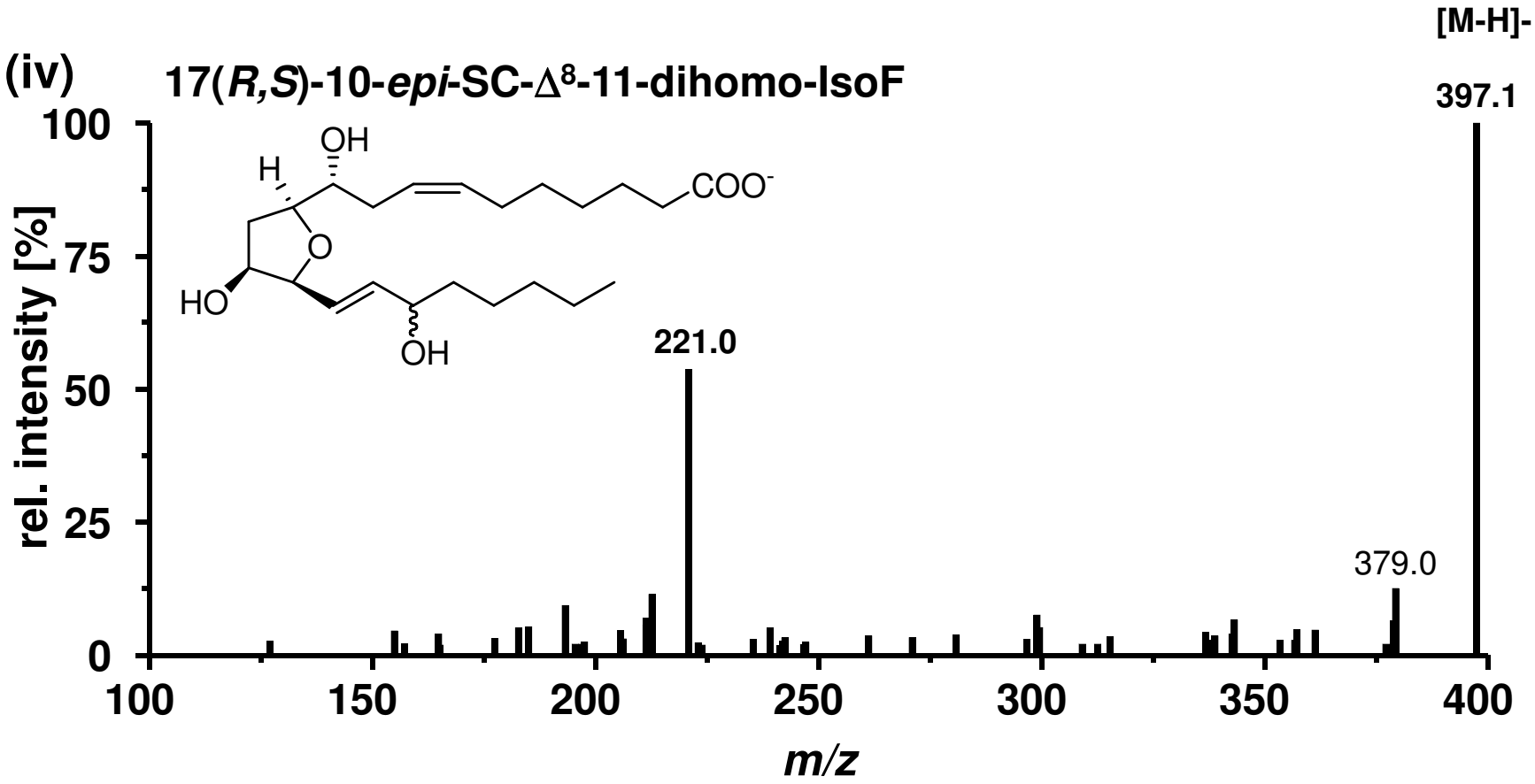

Fig. S1: Continued.

(F) Docosapentaenoic acid derived NeuroP

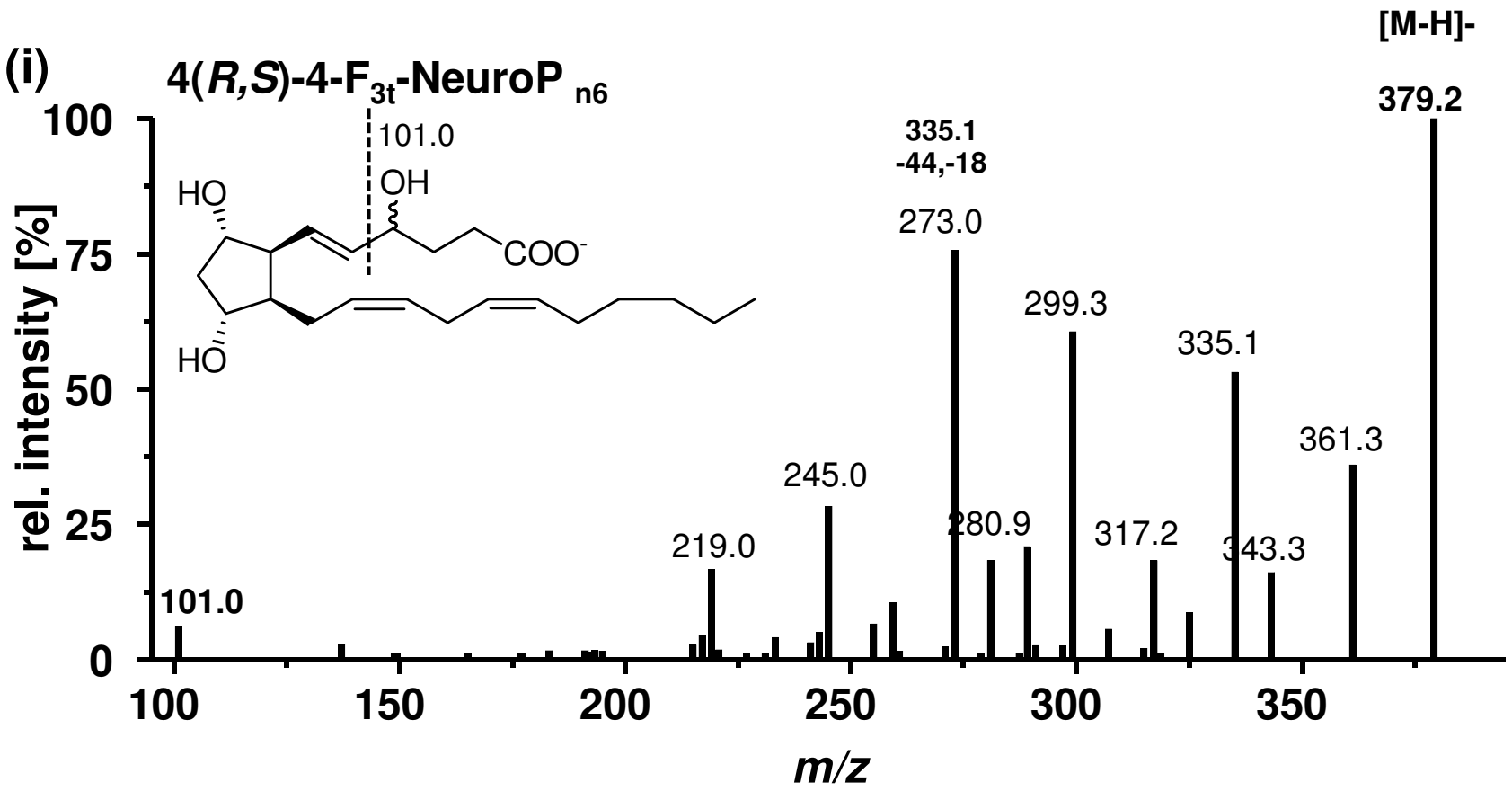

Fig. S1: Continued.

(G) Internal Standards

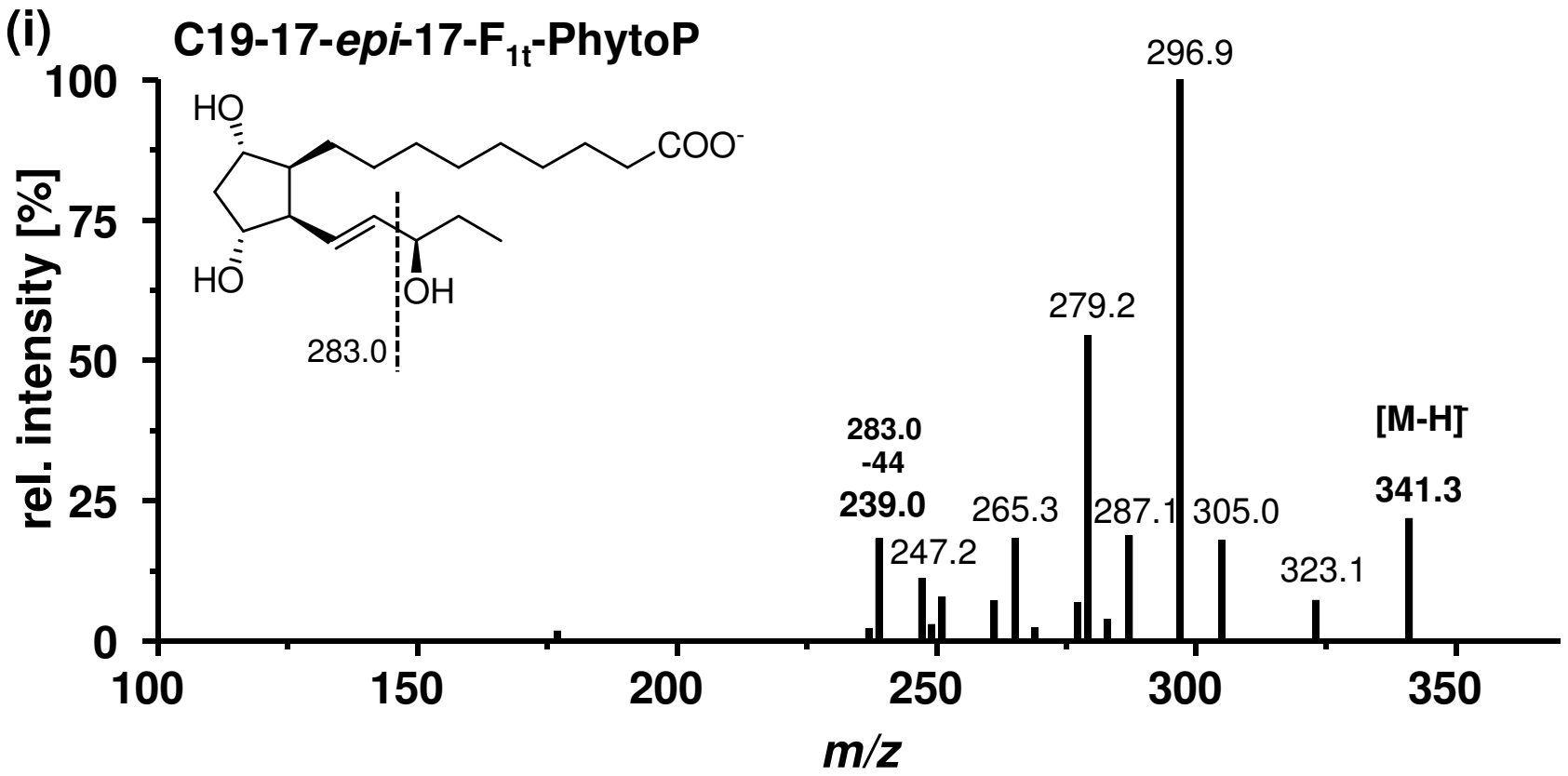

Fig. S1: Continued.

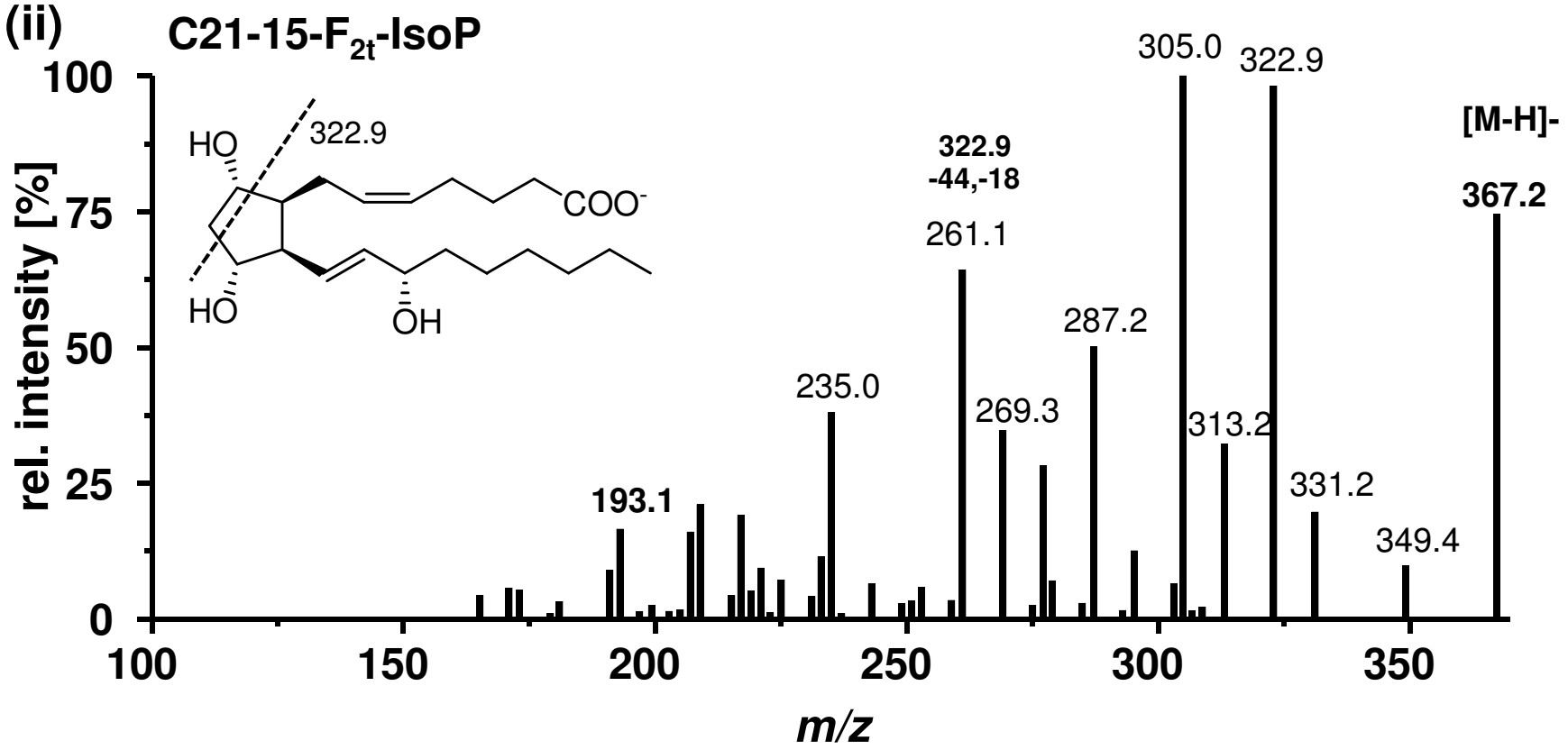

Fig. S1: Continued.

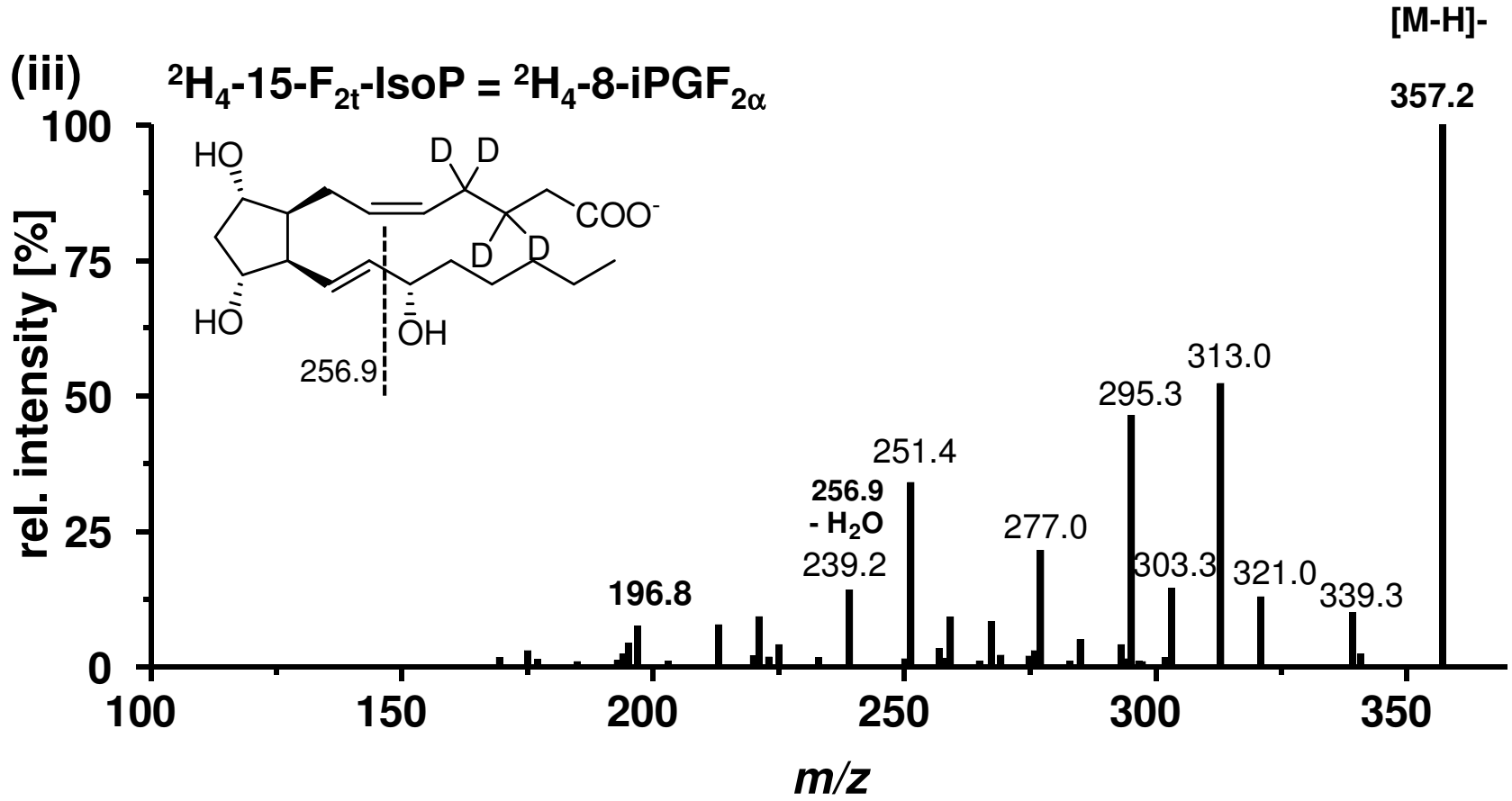

Fig. S1: Continued.

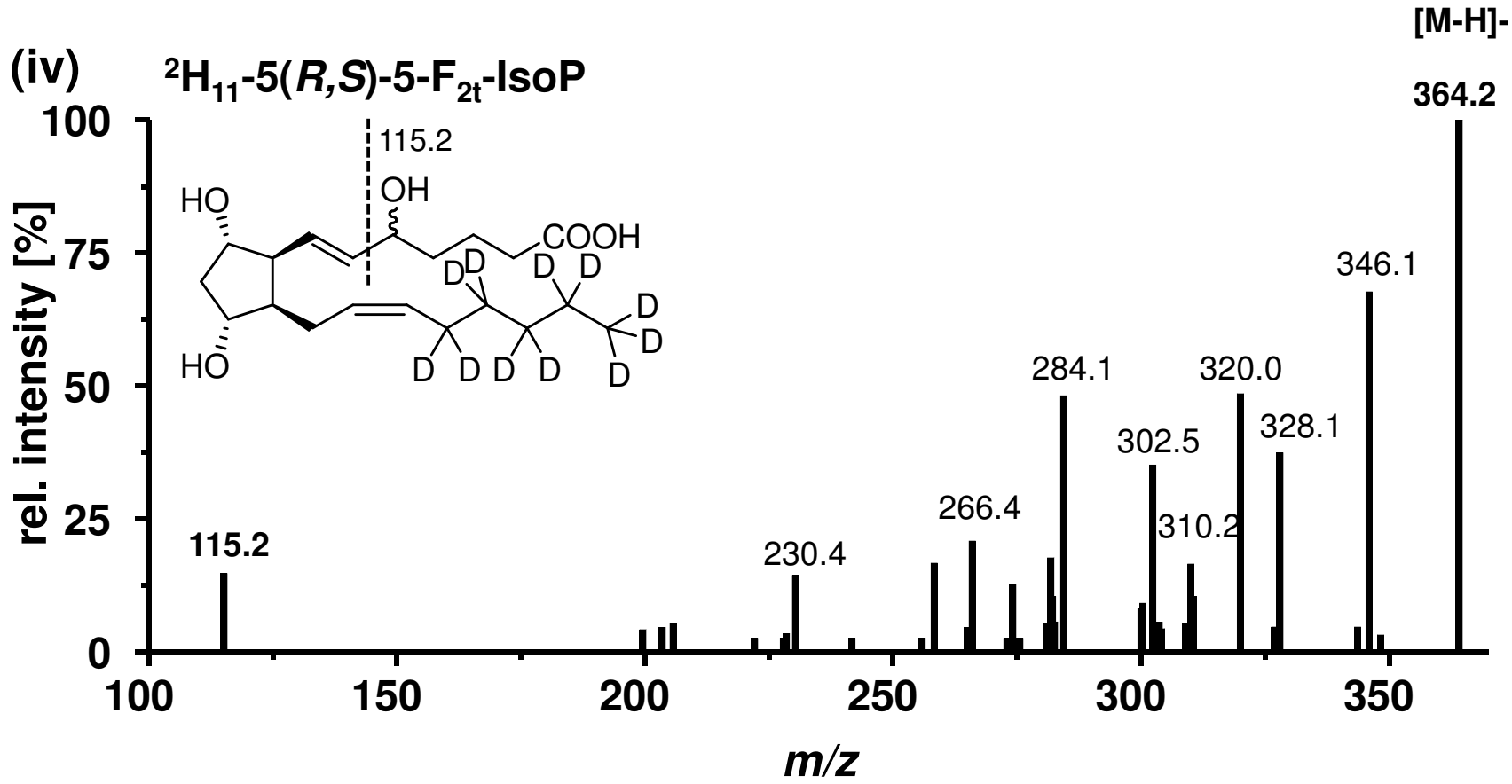

Fig. S1: Continued.

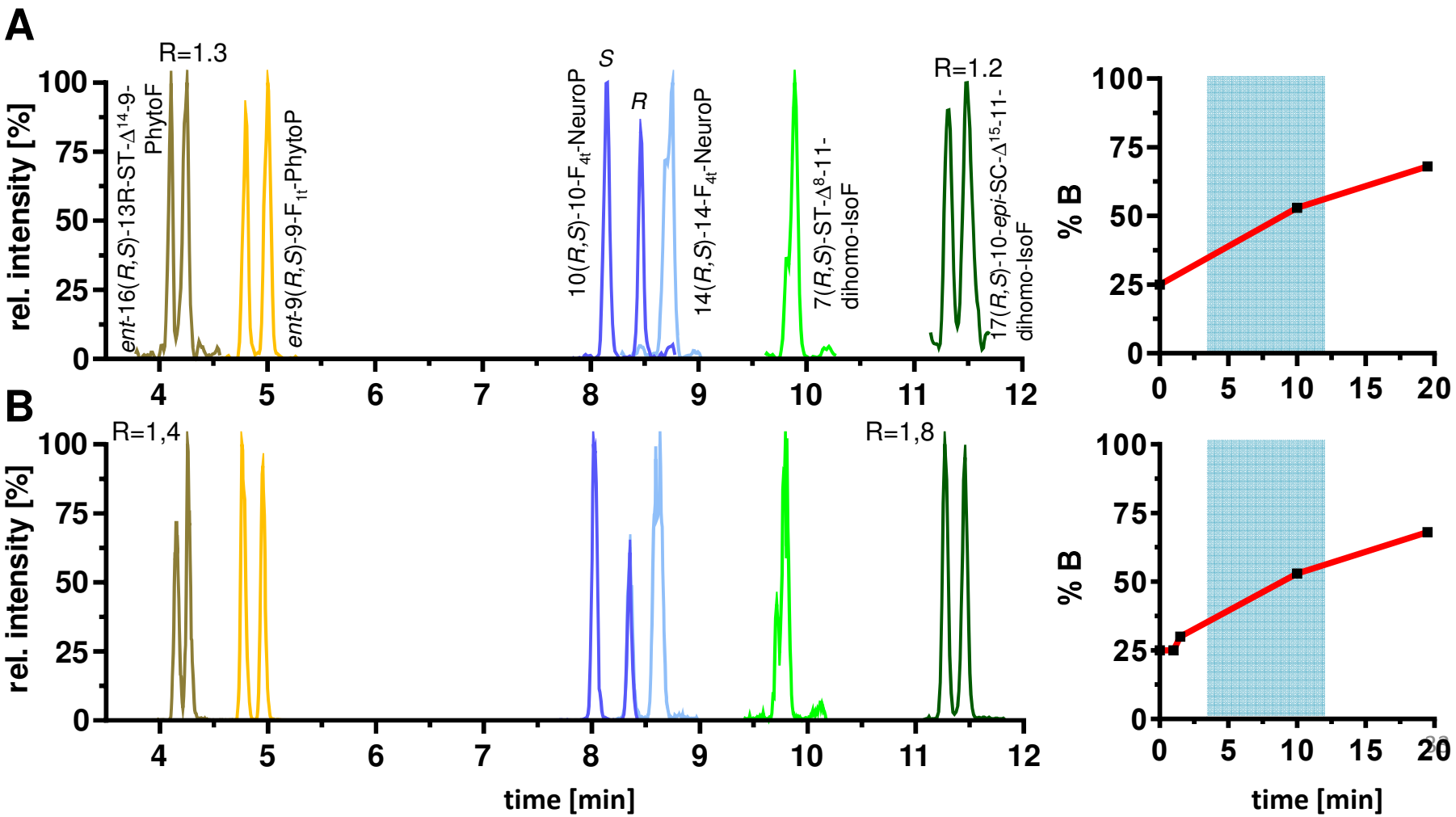

Fig. S2: Chromatographic separation efficiency of selected epimeric pairs using a gradient starting with 25% organic **(A)** without and **(B)** with inclusion of a short isocratic step (1 min) at the beginning of the gradient. The resolution (R) indicated for selected epimeric pairs.

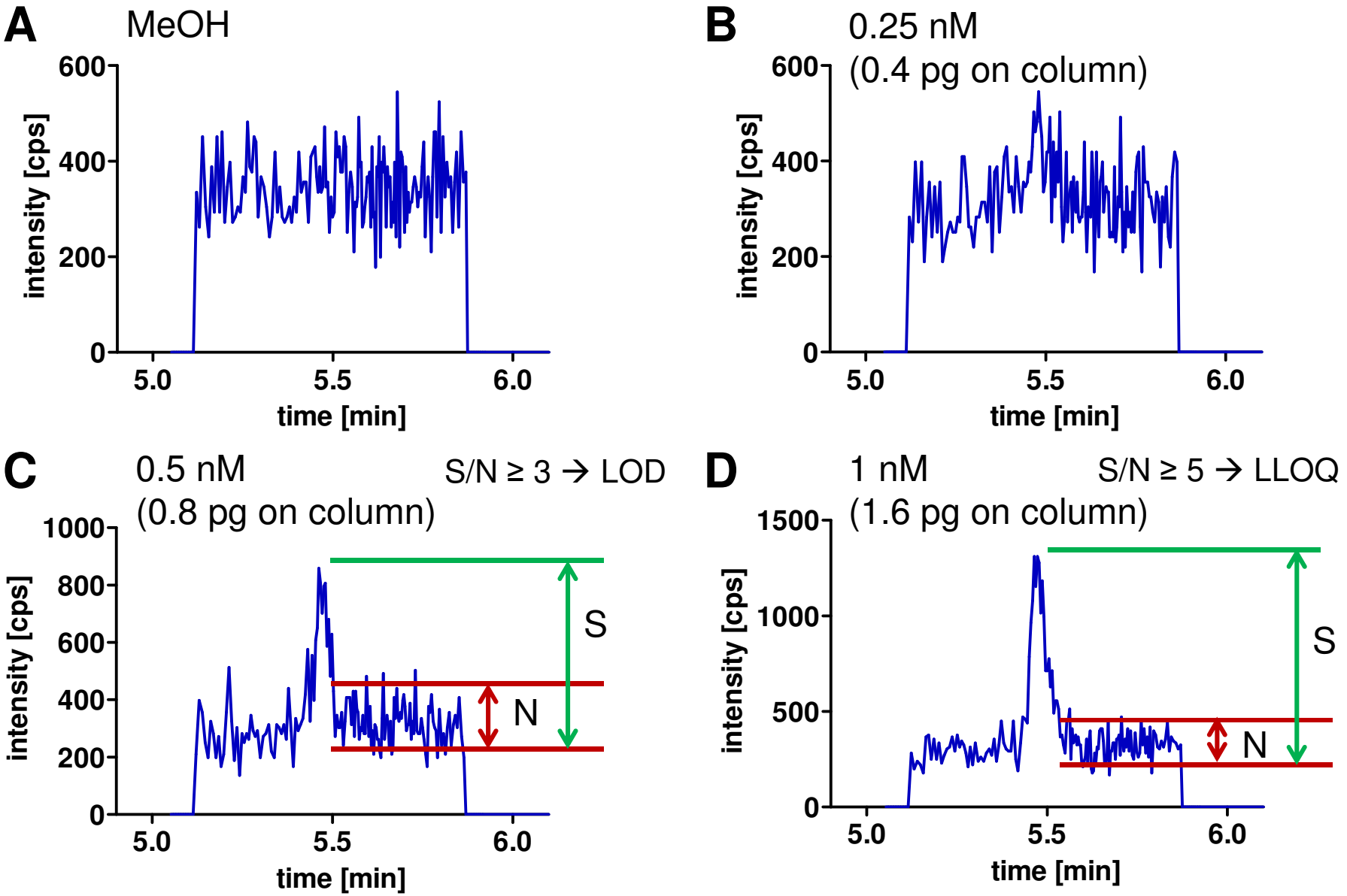

Fig. S3: Determination of the limit of detection (LOD) and lower limit of quantification (LLOQ) for 2,3-dinor-15-F_{2t}-IsoP based on the signal to noise (S/N) ratio. Starting from **(A)** blank (MeOH), successive standards **(B), (C), (D)** with increasing concentration of the analyte were injected. **(C)** The concentration yielding a S/N ≥ 3 was set as LOD. **(D)** The concentration with a S/N ≥ 5 and an accuracy within the calibration curve of ± 20% was defined as LLOQ.

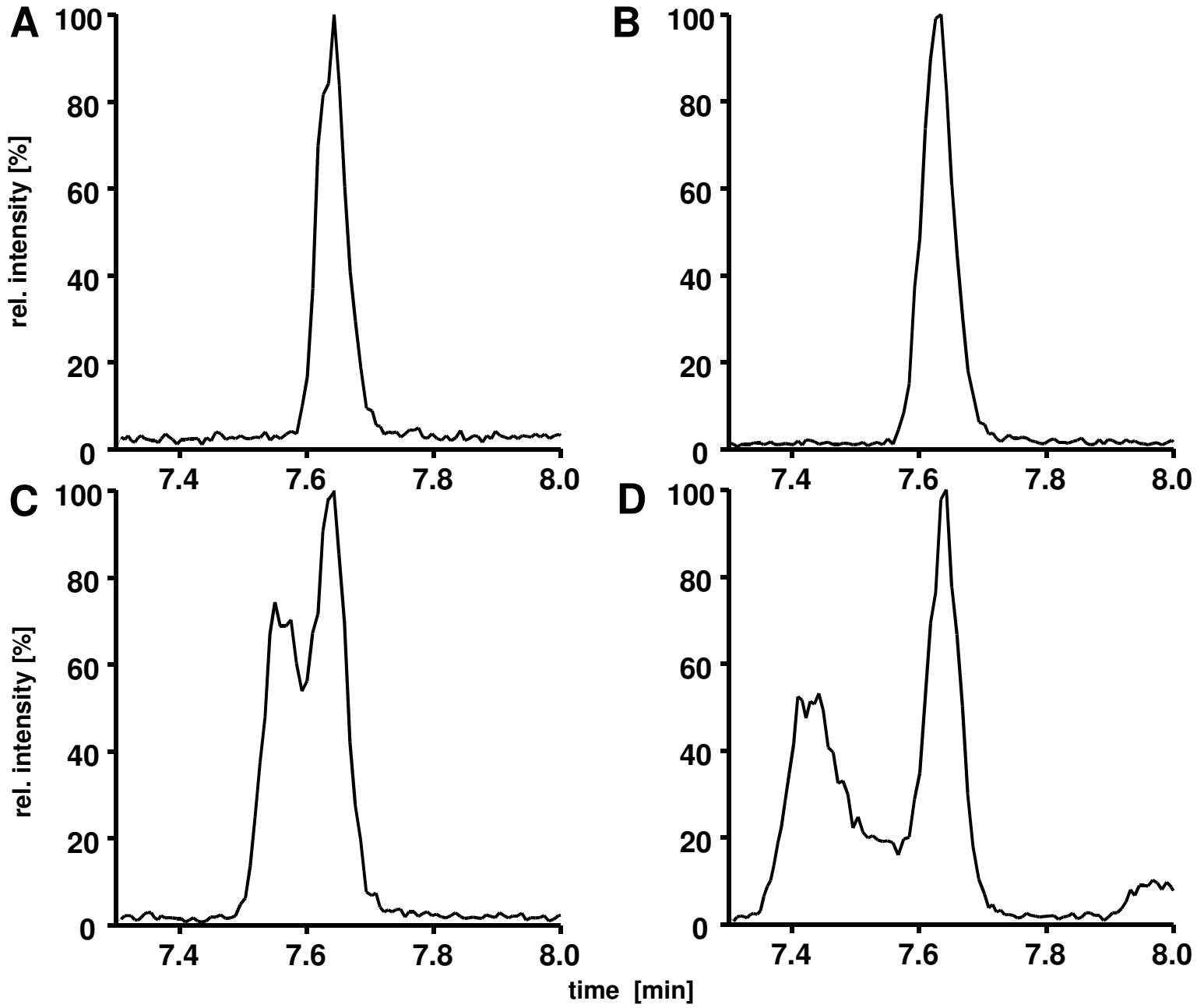

Fig. S4: Peak shape of 15-F_{2t}-IsoP (10 nM in methanol) with increasing injection volumes: **(A)** 5 µL, **(B)** 10 µL, **(C)** 15 µL, **(D)** 20 µL.

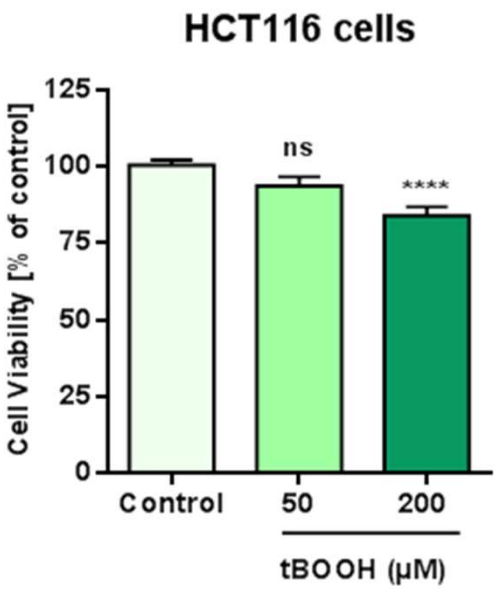

Fig. S5: Cell viability treated with increasing doses of t-BOOH for 2 h determined by MTS assay.